

भाभा परमाणु अनुसंधान केंद्र का आधिकारिक द्विमासिक प्रकाशन  
The official bi-monthly publication of Bhabha Atomic Research Centre



# भा.प.अ.के. न्यूज़लेटर BARC newsletter

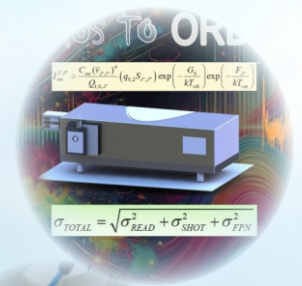
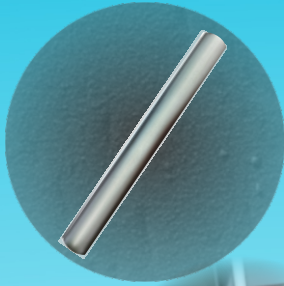
जनवरी-फरवरी 2025 January-February 2025

ISSN: 0976-2108

● Accident Tolerant Fuel Cladding

● Molecular Emission

● Cold Plasma Applications



**Multi-Disciplinary Pathways**  
Nuclear SciTech Leading Sustainable Development

## Editor

Manoj Singh

## Editorial Assistant

Madhav N

## Content Curation & Design

Dinesh J. Vaidya

Jyoti Panda

Madhav N

---

## Newsletter Committee

### Chairman

Dr. A.K. Dureja

### Members

Dr. L.M. Pant

Dr. B.K. Sapra

Dr. C.N. Patra

Dr. S. Santra

Dr. V.H. Patankar

Dr. S. Mukhopadhyay

Dr. J. Padma Nilaya

Manoj Singh

Dr. V. Sudarsan

Dr. Tessy Vincent

Dr. S.R. Shimjith

Dr. Sandip Basu

Dr. K.K. Singh

Dr. Kinshuk Dasgupta

Dr. I.A. Khan

Dr. Deepak Sharma

PPK. Venkat

Dr. K. Tirumalesh

Dr. Arnab Dasgupta

Dr. S. Banerjee

Dr. V.K. Kotak

### Member Secretary

Madhav N



**BARC Newsletter**  
**January-February 2025**  
**ISSN: 0976-2108**





EDITOR'S  
*message*

# Nuclear SciTech

## Leading Sustainable Development

**T**his edition of the BARC Newsletter showcases the latest breakthroughs in nuclear science and technology. Our feature articles highlight significant advancements across multiple disciplines, including developing accident-tolerant fuel coatings, innovative approaches in plasma spectroscopy, and enhanced used fuel management protocols. Recent research on cold atmospheric plasma for dental applications demonstrates the expanding potential of nuclear technologies in healthcare settings.

We are pleased to present a summary of research on natural isotope applications for groundwater management, underscoring our dedication to environmental stewardship. This issue also recognizes excellence through international acknowledgment of distinguished researchers in solid state physics subject.

National Science Day 2025 celebrations at BARC highlighted nuclear energy's vital role in India's self-reliance and sustainability while honoring Sir C.V. Raman's legacy. Led by the Materials Group with the theme "Transition to Clean, Green Viksit Bharat: Advanced Materials & Nuclear Technology", the three-day program attracted students from various schools. These young participants experienced hands-on demonstrations, engaged in interactive discussions with scientists, and guided tours to research facilities all designed to inspire them to pursue nuclear science and technology. The year's first Trombay Colloquium, delivered by Dr. Samir V. Kamat on defence sector R&D, articulated several key advancements and strategic initiatives undertaken by India in the defence sector and allied domains.

We invite you to explore these developments in shaping our mission of the clean & green energy future.

**Shri Manoj Singh**

Editor, BARC Newsletter &  
Head, Scientific Information Resource Division

- **EDITOR'S MESSAGE: Nuclear SciTech Leading Sustainable Development by Shri Manoj Singh, Head, SIRD** 3

## RESEARCH AND DEVELOPMENT

- **1 Development of Cr Coating on Zircaloy-4 as Accident Tolerant Fuel (ATF) Cladding under LOCA Conditions and Coating Thickness Dependent Impact on Reactivity of PHWRs** 7  
Subir Kumar Ghosh, Satish C. Mishra, V. S. V. Anantha Krishna, Vishal Singh, Supratik Roychoudhury, Anmol Singh, V. Harikrishnan, Usha Pal, R. Karthikeyan, K. K. Yadav, Alok Awasthi and Raghendra Tewari
- **2 From Noise to Knowledge: Harnessing Boron Molecular Emission Spectra in Laser-Induced Plasma** 17  
Anandhu Mohan, Anannya Banerjee, Rajesh V. Pai and Arnab Sarkar
- **3 Antimicrobial Efficacy of a Novel Cold Atmospheric Plasma Device (CAP) for Infection Control on Dental Surfaces** 21  
Vishakha Bende, Vandan Nagar, V. Saple, M. Doshi, C. Verma, R.L. Bhardwaj, Rajib Kar
- **4 Evaluation of Rate of Dissolution of UNF for Indian PHWR** 25  
Arya Das, K. Jayanarayanan
- **5 Physicochemical Characteristics of Solvent Production Plant Effluent & its Effluent Treatment Method** 31  
A. S. J. Hamilton, M. Srinivas, S. Sukumar and G. Venketesu

## RESEARCH HIGHLIGHTS

- **Tracing the Footprints of Contaminants in Water through Stable Isotope Techniques** 37  
Tirumalesh Keesari, Isotope and Radiation Applications Division, BARC

## NEWS & EVENTS

- **TROMBAY COLLOQUIUM: 'Accelerating India's Defence Innovation Ecosystem to 2047'** 38  
Excerpts of the talk by Dr. Samir V. Kamat, Secretary, DDR&D and Chairman, DRDO
- **Catalyzing Curiosity: BARC's National Science Day and the Path to Viksit Bharat** 39  
SIRD Newsletter Editorial Team

## AWARDS & HONORS

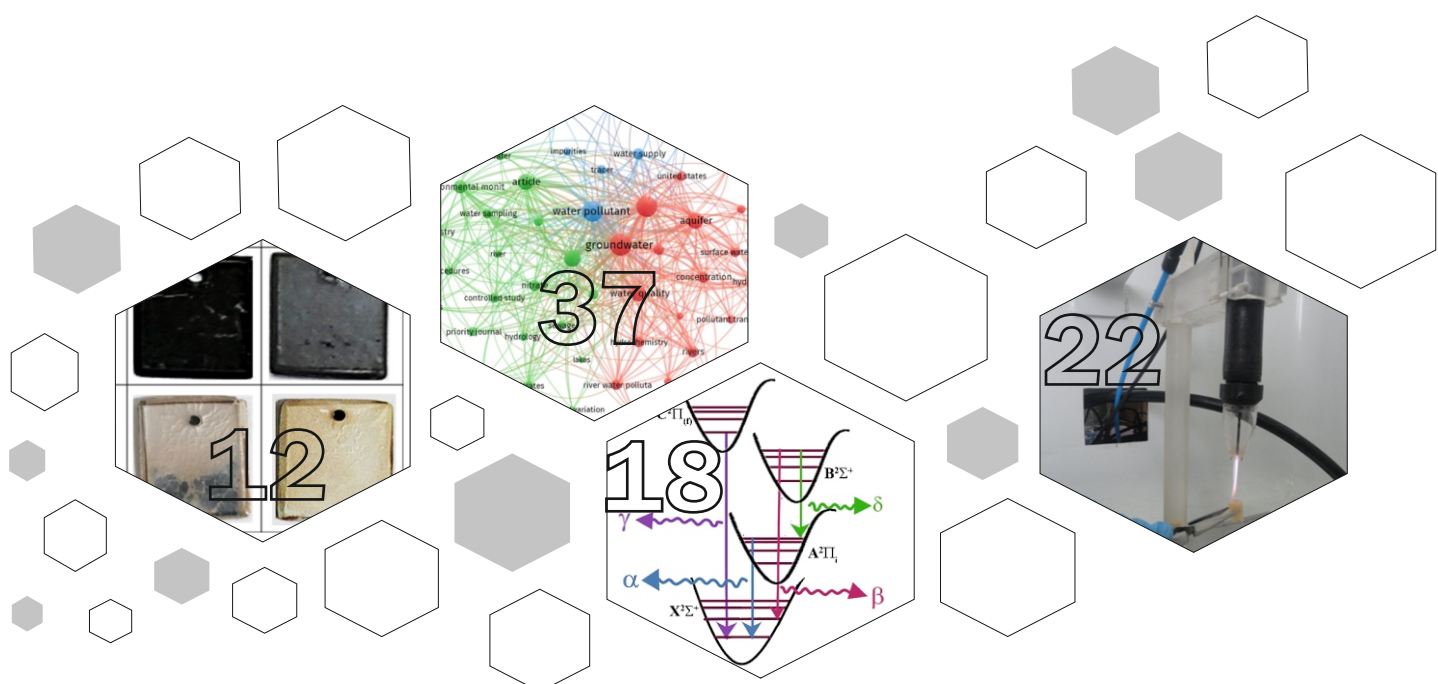
- **BARC scientist honored with the AONSA Science Award 2025** 40

## CONNECT

- **RPNST 2025: Conference on Recent Progress in Nuclear Science & Technology & Commemorating the Birth Centenary of Dr. Raja Ramanna** 41
- **Inspiring Young Minds: Outreach Programs by BARC in Madhya Pradesh** 42

## TECHNOLOGY MANAGEMENT

- **Industry beckons BARC's Nuclear Spin-off Technologies** 44  
Technology Transfer & Collaboration Division and SIRD Newsletter Editorial Team





# CONTENTS



## ARTICLES OF FORTHCOMING ISSUE

- Outcomes of Research & Development Activities in Applications of Natural Isotopes in Groundwater Management
- Interview of an eminent researcher in Groundwater Resources Management
- News and Events
- Proceedings of Conferences, Theme Meetings, Symposia and Outreach

**This page intentionally left blank**



# दुर्घटना सहिष्णु ईंधन आवरण

1

## एलओसीए स्थितियों के तहत जिर्केलॉय-4 पर दुर्घटना सहिष्णु ईंधन (एटीएफ) आवरण के रूप में Cr लेपन का विकास और पीएचडब्ल्यूआर की अभिक्रियाशीलता पर लेपन के मोटाई की निर्भरता का प्रभाव

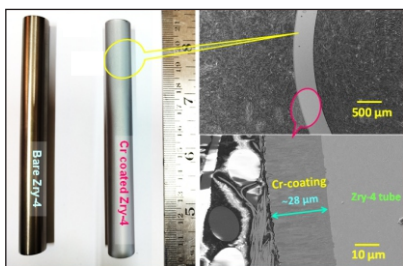
सुबीर कुमार घोष<sup>1\*</sup>, सतीश सी. मिश्रा<sup>1</sup>, वी.एस.वी. अनंथा कृष्णा<sup>2</sup>, विशाल सिंह<sup>2</sup>, सुप्रतिक रॉयचौधरी<sup>3</sup>, अनमोल सिंह<sup>3</sup>, वी. हरिकृष्णन<sup>3</sup>, उषा पाल<sup>3</sup>, आर. कार्तिकेयन<sup>3</sup>, के.के. यादव<sup>3</sup>, अलोक अवस्थि<sup>1</sup> एवं राघवेंद्र तिवारी<sup>4</sup>

<sup>1</sup>पदार्थ प्रक्रमण एवं संश्लेषण अभियांत्रिकी प्रभाग, भाभा परमाणु अनुसंधान केंद्र, ट्रांबे, मुंबई - 400 085, भारत

<sup>2</sup>पदार्थ विज्ञान प्रभाग, भाभा परमाणु अनुसंधान केंद्र, ट्रांबे, मुंबई - 400 085, भारत

<sup>3</sup>रिएक्टर भौतिकी अभिकल्पन प्रभाग, भाभा परमाणु अनुसंधान केंद्र, ट्रांबे, मुंबई - 400 085, भारत

<sup>4</sup>पदार्थ वर्ग, भाभा परमाणु अनुसंधान केंद्र, ट्रांबे, मुंबई - 400 085, भारत



अनावरित और Cr-लेपित Zry-4 ईंधन नलिकाओं की फोटोग्राफिक छायाचित्र और Cr लेपित ईंधन नलिका की एक्स-सेक्शन एफईएसईएम छायाचित्र

### सारांश

फुकुशिमा दुर्घटना ने मूल रूप से दुनिया भर के नाभिकीय समुदाय को शीतलक दुर्घटना (डीबीएलओसीए) की स्थिति के अभिकल्पन आधारित हानि को कम करने के लिए लंबे समय से अच्छी तरह से सिद्ध Zr-आधारित आवरण के विकल्पों की खोज करने के लिए मजबूर किया है। दो अलग-अलग अवधारणाएँ-या तो Zr-आधारित आवरण का पूर्ण प्रतिस्थापन या एक उपयुक्त लेपित Zr आधारित आवरण सबसे आशाजनक समाधान के रूप में उभरी है। इस संबंध में, डीसी मैग्नेट्रॉन स्पटरिंग का उपयोग करके जिर्केलॉय-4 (Zr-4) सबस्ट्रेट और ईंधन नलिकाओं पर मोटी (20-30 μm), छिद्र-मुक्त अत्यधिक घनी और सुसंगत Cr लेपन को सफलतापूर्वक विकसित किया गया। निक्षेपण के बाद, लेपनों को संरचना, क्रिस्टल संरचनाओं, क्रॉस-सेक्शन माइक्रोस्ट्रक्चर और Zry-4 सबस्ट्रेट के साथ आसंजन के संदर्भ में विस्तार से दर्शाया गया। विभिन्न अवधियों के साथ तापमान सीमा 700-1200°C में पूर्ण सतह के Cr लेपित Zry-4 कूपनों और अनावरित Zry-4 के भाप ऑक्सीकरण ने Zry-4 सबस्ट्रेट के नीचे के लिए Cr लेपन की उत्कृष्ट सुरक्षा क्षमता का प्रदर्शन किया। 700Mwe पीएचडब्ल्यूआर के 37 पिन समूह में नाभिकीय अभिक्रियाशीलता पर Cr लेपन मोटाई के प्रभाव का विश्लेषण करने के लिए एक सैद्धांतिक जांच की गई। Zry-4 पर 15 μm मोटी Cr लेपन के लिए, यह 7.15% के बर्नअप हानि की संभावना को दर्शाता है। यह अध्ययन इस बात पर प्रकाश डालता है कि डीबीएलओसीए की स्थिति के तहत Zry-4 आवरण की रक्षा के लिए 10-12 μm की सीमा में एक Cr लेपन मोटाई पर्याप्त हो सकती है, जिससे प्रचालन को कोर शीतलन की परिनियोजन के लिए पर्याप्त समय मिल सकता है।

## Accident Tolerant Fuel Cladding

1

### Development of Cr Coating on Zircaloy-4 as Accident Tolerant Fuel (ATF) Cladding under LOCA Conditions and Coating Thickness Dependent Impact on Reactivity of PHWRs

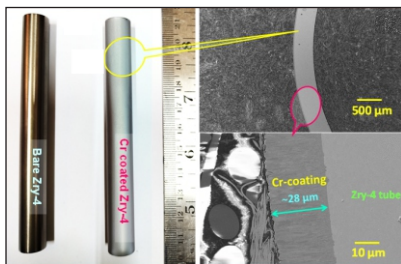
Subir Kumar Ghosh<sup>1\*</sup>, Satish C. Mishra<sup>1</sup>, V. S. V. Anantha Krishna<sup>2</sup>, Vishal Singh<sup>2</sup>, Supratik Roychoudhury<sup>2</sup>, Anmol Singh<sup>3</sup>, V. Harikrishnan<sup>3</sup>, Usha Pal<sup>3</sup>, R. Karthikeyan<sup>3</sup>, K. K. Yadav<sup>3</sup>, Alok Awasthi<sup>1</sup> and Raghvendra Tewari<sup>4</sup>

<sup>1</sup>Materials Processing & Corrosion Engineering Division, Bhabha Atomic Research Centre, Trombay, Mumbai - 400 085, INDIA

<sup>2</sup>Materials Science Division, Bhabha Atomic Research Centre, Trombay, Mumbai - 400 085, INDIA

<sup>3</sup>Reactor Physics Design Division, Bhabha Atomic Research Centre, Trombay, Mumbai - 400 085, INDIA

<sup>4</sup>Materials Group, Bhabha Atomic Research Centre, Trombay, Mumbai - 400 085, INDIA



Photographic images of bare and Cr-coated Zry-4 fuel tubes and X-section FESEM images of Cr coated fuel tube

### ABSTRACT

Fukushima accident has basically forced world-wide nuclear community to search for alternatives to long served well proven Zr-based claddings to mitigate design basis loss of coolant accident (DB LOCA) condition. Two different concepts- either complete replacement of Zr-based claddings or a suitably coated Zr-base claddings emerged as most promising solutions. In this connection, thick (20-30 μm), pore-free highly dense and adherent Cr coating was successfully developed on zircaloy-4 (Zry-4) substrates and fuel tubes by using DC magnetron sputtering. Post deposition, coatings were characterized in terms of composition, crystal structures, cross-section microstructure and adhesion with Zry-4 substrate in detail. Steam oxidation of full surface Cr coated Zry-4 coupons and bare Zry-4 in the temperature range 700-1200°C with different durations demonstrated excellent protection ability of Cr coating to the underneath Zry-4 substrate. A theoretical investigation was undertaken to analyze the impact of Cr coating thickness on nuclear reactivity in a 37 pin cluster of 700 MWe PHWR. For 15 μm thick Cr coating on Zry-4, it predicts burnup loss of 7.15%. This study highlights that a Cr coating thickness in the range 10-12 μm may be sufficient to protect the Zry-4 claddings under DB LOCA condition allowing sufficient coping time to the operator for restoration of core cooling.

KEYWORDS: Accident Tolerant Fuel (ATF) Cladding, Cr coating, Magnetron Sputtering, LOCA, Steam Oxidation

\*Author for Correspondence: Dr. Subir Kumar Ghosh  
E-mail: sgghosh@barc.gov.in

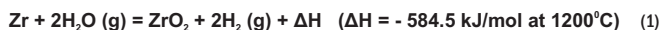
## Introduction

Since the installation of first pressurized reactor named Atomic Power Station-1 (APS-1) at Obninsk (USSR) in the year 1954, zirconium alloys have been selected as cladding and canister materials for UO<sub>2</sub> based fuels because of their very low thermal neutron absorption cross-section, good mechanical properties under neutron irradiation and fairly good oxidation resistance under normal operating conditions [1-3]. It is also well known that at temperatures higher than 450°C, Zr undergo severe oxidation following an exothermic reaction in water/steam environment [4-6]. Past six decades enormous efforts have been put forward to further improve the nuclear fuel performance under normal operating conditions in terms of enhanced fuel burn up for the minimization of waste [7], substantial reduction of fuel failure rates [8-9], increased power density for power upgradation, and extended operational service for economic competitiveness [10]. Despite narrow working temperature range and to meet ever increasing economic power demand without breaching the safety norms and reliability under normal operating conditions of nuclear power plant, several advanced Zr-based alloy claddings, such as Zircaloy-2 (Zry-2), Zircaloy-4 (Zry-4), ZIRLO™, M5, E110, E365, Zr-2.5 Nb, have been developed (Table 1) in a phased manner to mitigate several degradation phenomena such as corrosion (general corrosion, nodular corrosion, galvanic corrosion, shadow corrosion, crud induced localized corrosion), hydriding, debris fretting, cracking due to fission gas accumulation etc. [3,6,11] In fact, Indian PHWRs are also successfully operating safely last few decades utilizing Zry-4 as cladding materials.

## Limitations of Zr-based Fuel Claddings

Satisfactory performance, however, of these Zr-based fuel cladding materials are highly challenged once the operation condition breaches the design-basis accident (DBA, 1204°C) and beyond DBA (T>1204°C) scenarios. In the year 2011, accident in Fukushima Daiichi Nuclear Power Plant is one such example. A massive earthquake of magnitude 9.0 in Richter scale followed by 15 m tall tsunami severely damaged the reactor building and power supply was disabled leading to complete failure of emergency core cooling system (ECCS).

Due to lack of core cooling and spontaneous fission inside the reactor, the core temperature increased and the cooling water ultimately converted into superheated pressurized steam. As a result, Zr-based cladding suffered high-temperature steam oxidation reaction with release of large amount of hydrogen gas and heat:



Significant damage to the reactor building and the consequent release of radioactive fission products were caused by the accumulation of hydrogen gas, which was subsequently burned and exploded [12]. This is a kind of chemical accident rather than nuclear explosion. This is one kind of loss-of-coolant accident (LOCA) in nuclear industry due to fast and strong oxidation during the DBA and beyond DBA (BDBA). LOCA events can be caused by a breakup of the

Table 1: Composition of commercial Zr-based alloys used as claddings in water-cooled nuclear reactors.

Alloy	Nominal Alloy Composition (wt.%)						
	Zr	Sn	Nb	Fe	Cr	Ni	O
Zircaloy -2	Bal.	1.5	-	0.15	0.1	0.05	0.1
Zircaloy -4	Bal.	1.5	-	0.2	0.1	-	-
M 5®	Bal.	-	1.0	-	-	-	0.14
ZIRLO™	Bal.	1.0	-	0.1	-	-	0.1
E365	Bal.	1.2	1.0	0.35	-	-	-

primary cooling system that results in the loss of pressure in the nuclear core and vaporization of the coolant (water/heavy water). Under these conditions, the fuel temperature rises, thereby increasing the porosity of the fuel and resulting in its fragmentation. For example, ~125 kg of Zr metal in PWR reactor could produce 820 MJ of heat and >2.7 kg of H<sub>2</sub> after complete oxidation [4]. Therefore, depending upon a reactor design, several tons of Zr metal present in the reactor core, if fully oxidized, could produce excessive amount of heat and H<sub>2</sub> gas leading to extra burden on ECCS or may lead to explosion.

## Logic behind Accident Tolerant Fuel (ATF) Claddings

Post Fukushima Daiichi incident, primary focus was on to the reduction of burden on ECCS during severe accidental situation. This is a straightforward reason for switching away from Zr-based claddings to an accident tolerant fuel (ATF) cladding. This could be done only by adopting alternative claddings which ultimately decreases the rate of oxidation as well as amount of hydrogen generation due to total oxidation of cladding in the presence of superheated steam. In turn, it will decrease the rate of temperature rise during LOCA condition which ultimately would slower the core degradation process, allowing sufficient time to the operator for coping, and finally reducing the cooling threshold for accident mitigation [13-16]. Therefore, ATF cladding material should be such which can reduce the heating rate as well as total amount of heat generation as a consequence of steam oxidation.

Several investigations revealed that steam at very high temperatures is far more aggressive corrosive media than dry oxygen [17-18]. Fig.1 shows parabolic oxidation behavior of different cladding materials when they are exposed to high temperature steam and the resulting film formed [19-22]. It is evident that the parabolic oxidation rate of zirconia-forming materials has been two to three orders of magnitude higher than that of traditional materials that create protective layers of silica (SiO<sub>2</sub>), alumina (Al<sub>2</sub>O<sub>3</sub>) and chromia (Cr<sub>2</sub>O<sub>3</sub>). Reduction in oxidation rate of these claddings means decrease in the heating rate and consequently hydrogen generation under severe accidental condition. It is to bring in your notice that ZrO<sub>2</sub> exhibits excellent thermodynamic stability in steam environment retaining its strong adhesion with the base Zr even at T>1100°C [23]. However, it is a very good conductor of oxygen and lacks in protection ability to the underlying Zr metal. Therefore, in order to protect the cladding material from high temperature steam oxidation, the oxide film should be effective barrier for transport of oxidizing species by limiting the solid state diffusion of aggressive species such as H<sub>2</sub>O, OH<sup>-</sup>, O radical etc. retaining its other physical and chemical stability. Literature has shown that SiO<sub>2</sub>, Al<sub>2</sub>O<sub>3</sub> and Cr<sub>2</sub>O<sub>3</sub> exhibit excellent stability in steam along with effective barrier against diffusion of oxidizing species and other reaction products [24-25]. These oxide films maintain high-temperature oxidation resistance in the order Cr<sub>2</sub>O<sub>3</sub><Al<sub>2</sub>O<sub>3</sub><SiO<sub>2</sub> with approximately one order of magnitude higher in each.

Considering the thermochemical behavior, all these oxides including ZrO<sub>2</sub> are stable enough at high temperatures because of favorable Gibbs Free Energy [26]. Formation of ZrO<sub>2</sub> and Al<sub>2</sub>O<sub>3</sub> from Zr and Al respectively are most stable with very high negative enthalpy of oxidation (ΔH<sub>r</sub>) value, followed by SiO<sub>2</sub> and Cr<sub>2</sub>O<sub>3</sub> formation associated with significantly less exothermic oxidation of SiC and Cr [27]. It is also pertinent to mention here that volatility of oxides formed at high temperature steam environment is also a matter of concern to many investigators because it might affect the oxidation resistance of the claddings. However, it is now understood that oxide volatility at higher temperature is more relevant for long



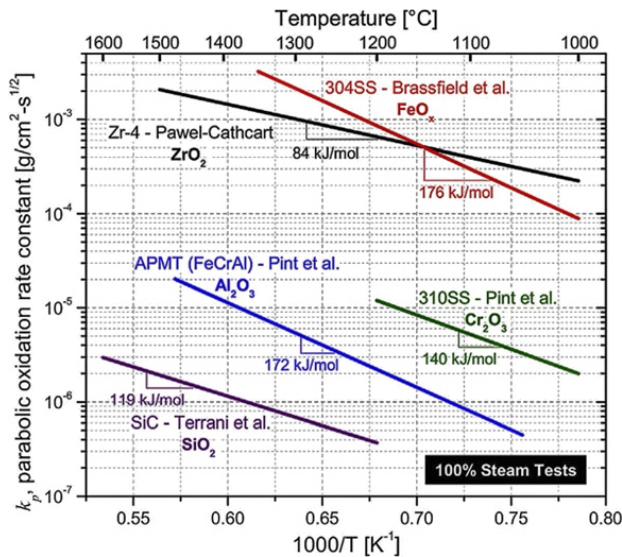


Fig.1: Parabolic oxidation rate of various materials and their corresponding oxides in steam as a function of temperature [19-22].

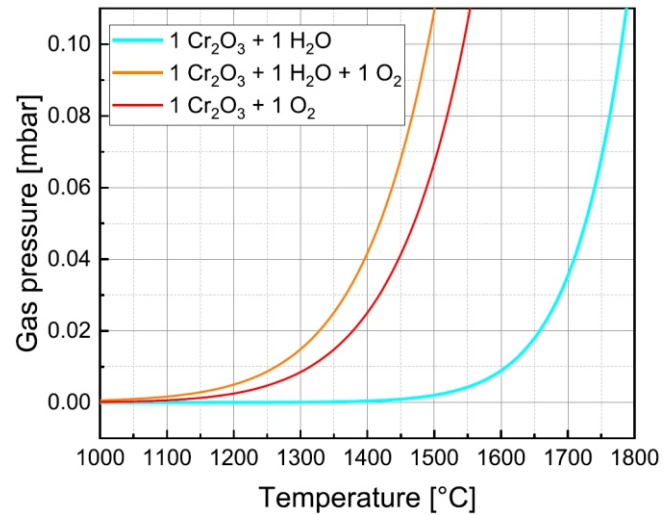


Fig.2: Total gas partial pressure of Cr-containing volatile species over Cr<sub>2</sub>O<sub>3</sub> in water, oxygen and mixed atmosphere [26].

exposure times e.g. in turbines, but for accident scenarios such as DB LOCA condition, volatility becomes trivial because of short duration event. Brachet et al [28] confirmed that volatilization of Cr<sub>2</sub>O<sub>3</sub> is negligible up to 1300°C in steam atmosphere and the parabolic oxidation rate of Cr in oxygen, air and steam differ significantly, as shown in Fig.2. It is also reported that in pure water vapor oxidation, partial pressure of gaseous Cr-species is 2-3 orders of magnitude lower than O<sub>2</sub> containing atmospheres. This confirms free oxygen is the primary reactant to initiate the oxidation reaction. It is also evident that rapid volatilization of Cr<sub>2</sub>O<sub>3</sub> starts in water vapor beyond 1400°C, (conditions similar to short durations LOCA) when other degradation mechanisms become active significantly enough to breach the protective behavior.

**Different Concepts of ATF Claddings**

Based on the design concept, two main ATF cladding strategies have been considered world-wide.

- One is revolutionary which is to replace the conventional zircaloy based claddings with newer SiC, / SiC composites [29-32], FeCrAl [4, 33-36], Mo alloys [36-40] etc. This approach is considered as long-term strategy considering involvement of total duration and expenditure for the development of a new type of cladding material.
- The second ATF approach is the development of protective coatings on Zr-based fuel claddings [12,41]. The major advantage of coatings on fuel claddings is to provide significant improvement of oxidation resistance of claddings during LOCA conditions with very little change in original fuel/components design, reactor structure and water chemistry. Therefore, readiness of a suitable coating technology and subsequent incorporation into nuclear fuel fabrication line has been considered as a near-term solution of enhanced ATF cladding.

However, the protective coatings should possess the following criteria:

- (i) It should form either Al<sub>2</sub>O<sub>3</sub>, Cr<sub>2</sub>O<sub>3</sub> or SiO<sub>2</sub> oxide layer due to oxidation so that it can provide high temperature oxidation resistance
- (ii) Good wear resistance
- (iii) Act as barrier for hydrogen absorption of Zr-based claddings

- (iv) Preferably low thermal neutron absorption cross-section
- (v) Retention of good adhesion with Zr-based cladding during thermal fluctuation
- (vi) It should possess good radiation resistance and good heat transfer characteristics
- (vii) It should have thermal expansion coefficient very close to Zr-based cladding materials.

Even though the coating technology is comparatively simpler approach, but to meet all these criteria for a given coating/Zr-based cladding under both normal and accident conditions requires enormous research investigations.

Till now, variety of coating materials have been developed to improve Zr-based cladding performance by deposition of pure metallic or alloys [42-53], non-metallic such as nitrides [54-57], carbides [58-59], MAX-phase coatings [12, 60-61]. However, studies have revealed cracking susceptibility of Ti-Al-C and Cr-Al-C MAX-phase coatings during high temperature steam oxidation, water corrosion and thermal cycling [62-63]. On the other hand, SiC coatings undergo corrosion and become unstable at 350°C/20MPa [64]. Also, SiC suffers severely micro-cracking due to its brittleness [10]. Similarly, metal nitride coatings such as CrN undergo decomposition into Cr<sub>2</sub>N and N<sub>2</sub> and cracking in the temperature range 500°C to 975°C [65-66]. Considering advantages and disadvantages of various coatings, it is now believed that simple metallic Cr coating might satisfy most of the criteria as a protective coating for Zr-based claddings:

- It provides excellent oxidation resistance to base claddings because of formation of Cr<sub>2</sub>O<sub>3</sub> during LOCA. There is wide difference in parabolic oxidation rate of Cr coating and Zircaloy-4 with values 0.05 mg.cm<sup>2</sup>.s<sup>1/2</sup> and 1.09 mg.cm<sup>2</sup>.s<sup>1/2</sup> respectively [23,67].
- Excellent retention of adhesion with Zr-based claddings during quenching of overheated fuel rods like accident condition, after deformation experiments such thermal expansion, ballooning and irradiation induced expansion of fuel tubes under normal operating conditions.
- Because of twice higher elastic modulus of Cr than Zr, the overall stiffness of the claddings gets improved [68].
- Thermal neutron absorption cross-section of Cr (2.9 barns)



Fig.3: Unbalance DC/RF magnetron sputtering system used for Cr coating.

is comparatively lower in comparison to other competitive coatings.

- Because of higher wettability of Cr than Zircaloy, the thermal-hydraulic performance of the claddings might get improved.
- The eutectic temperature of Cr-Zr (1332°C) is above the DBA temperature (1204°C). The former determines the upper limit of temperature for coatings protection ability during accidental situation [4].

However, in India, development towards ATF fuel claddings either by evolutionary or revolutionary strategies is very limited or absent. In view of these, in the present report, attempts have been made to develop Cr coating on Zry-4 by using magnetron sputtering for protection against superheated steam environment under LOCA condition.

## Experimental

### Development of Cr Coating on Zry-4

A four target unbalance magnetron sputtering system was used to deposit Cr coating on Zry-4 substrates by employing both DC power source. Prior to deposition the base vacuum achieved was  $8.5 \times 10^{-6}$  mbar and the deposition was conducted at  $5 \times 10^{-3}$  mbar using 99.999% Ar gas. At 250W power, a maximum deposition rate of Cr coating obtained was  $5.0 \pm 0.1 \mu\text{m} \cdot \text{h}^{-1}$ . As received Zry-4 samples were first cleaned in alkaline solution followed by acid dip in dil. HCl solution and washed in DI water. After cleaning, the coupons were air dried and placed inside the sputtering chamber. Once the base vacuum was achieved, the samples were first subjected to sputter cleaning by applying bias voltage of -400 V. Post sputter cleaning; Cr was deposited on the zircaloy substrate. Fig.3 shows a four target unbalanced magnetron sputtering system used for deposition of Cr coating. For high temperature steam oxidation, Zry-4 coupons of dimension 15 mm x 20 mm were coated with Cr all over the surfaces including edges by flipping the samples. After optimization of sputtering parameters for

Table 2: Average surface roughness, grain size and mechanical properties of the Cr coating.

Sample	Average Surface Roughness $S_a$ (nm)	Nanohardness (GPa)	Elastic Modulus (GPa)	Average Grain size (nm)
Cr coated Zry-4	$268.30 \pm 5.80$	$11.99 \pm 0.65$	$226.86 \pm 13.67$	$19.3 \pm 0.5$

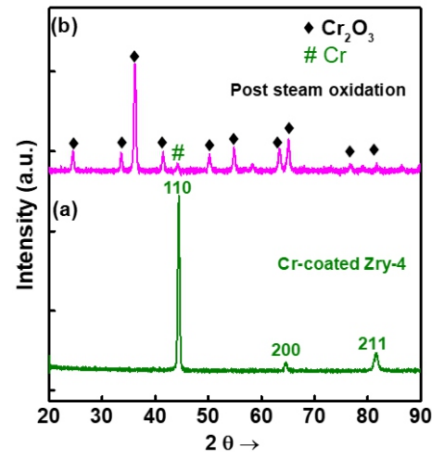


Fig.4: XRD pattern of (a) as deposited Cr coating on Zry-4 substrate and (b) post oxidation of Cr coating.

obtaining thick, dense highly adherent Cr coating, the process was demonstrated on OD surface of Zry-4 fuel tubes of length 100 mm with the help of a four target sputtering system.

## Results and Discussions

### Characterization of Cr Coating

Deposited coating was smooth, metallic appearance with matte finish and 3D-optical profilometer measurement showed average surface roughness of  $\sim 0.2 \mu\text{m}$ . The nanohardness and elastic modulus of the deposited Cr coating were  $11.99 \pm 0.65$  GPa and  $226.86 \pm 13.67$  GPa respectively as given in Table 2.

GIXRD pattern of DC sputtered Cr coated Zry-4 substrate is shown in Fig.4(a) which confirms deposition of crystalline bcc Cr with appearance of (110), (200) and (211) reflections. The XRD pattern was obtained using a  $\text{CuK}_{\alpha 1}$  X-ray source. Average grain size calculated from XRD peak broadening using Debye-Scherrer method was 19.3 nm after subtracting instrumental broadening.

Fig.5(a) represents as-deposited Cr coating top surface morphology consisting of mostly flat but with very small size nodules. Cross-section FESEM investigation confirms sharp Cr/Zry-4 interface without any of gap or voids (Fig.5(b)) indicating integrity of the coating with the substrate. The microstructure along the growth direction exhibits deposition of highly dense coating free from any kind of pores or voids with 20  $\mu\text{m}$  thickness. EDS line scan clearly shows deposition of Cr coating with very sharp composition profile at the interface.

Fig.6(a) displays photograph of bare and highly adherent Cr coated Zry-4 PHWR fuel tubes of 100 mm length and the corresponding X-section image (Fig.6(b)) shows deposition of uniform 28  $\mu\text{m}$  thick Cr coating all across the tubular surface. Fig.6(c) further demonstrates deposition of pore-free, highly adherent Cr coating with columnar grain structure. However, a careful observation shows fine grain equiaxed structures near the coating/substrate interface which gradually transformed



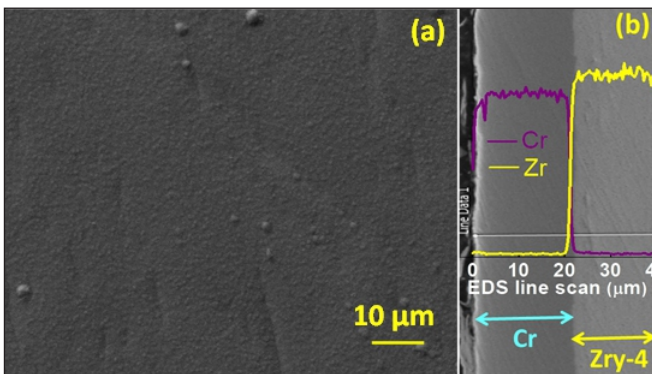


Fig.5: (a) FESEM surface topography of as deposited Cr coating on Zry-4 and (b) cross-section of the Cr/Zry-4 coupons showing uniformity and EDS composition line scan.

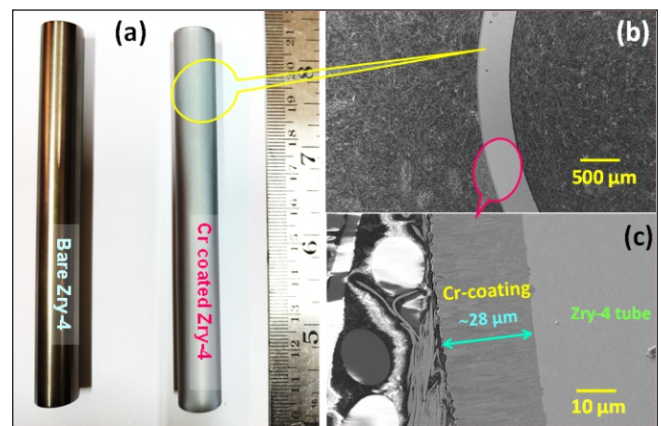


Fig.6: (a) Photographic images of bare and Cr-coated Zry-4 fuel tubes; (b) cross-section FESEM image of Cr-coated Zry-4 tube on OD surface at low magnification and (c) cross-section microstructure of the same at higher magnification.

into columnar grain structure along the growth axis at higher thickness. No flaking or peeling of the coating was observed throughout the surface.

Presence of residual stress especially tensile stress in high thickness sputter deposited coatings is inevitable and adhesion with substrate becomes a genuine issue. In order to confirm the quality of adhesion of Cr on Zry-4, micro-scratch adhesion test was performed on Cr-coated (20 μm) coupons using Rockwell diamond indenter having radius of 200 μm with loading rate of 30 N.min<sup>-1</sup>, maximum load of 40 N and a track length of 3 mm using M/s Rtec Instruments micro-scratch tester. The deposited Cr coating exhibited strong adhesion to the Zry-4 substrate, as confirmed by the scratch-adhesion test results. Fig.7(a) displays the scratch mark generated with initiation of arc tensile cracks (Lc1) at 15.8 N load, accompanied by simultaneous acoustic noise and changes in the coefficient of friction (not shown here). The Lc1 represents initiation of cohesive failure. As the normal load increased, the penetration depth increased accompanied by appearance of dense conformal cracks along the loading direction. However, there was no evidence of chipping or delamination of the coating observed up to a load of 40 N, indicating the absence of Lc2. This confirms excellent adhesion of Cr coating with Zry-4 substrate. The maximum scratch groove depth attained was 11.8 μm as confirmed by 2D-optical profilometer image (Fig.7(b)) which further indicates absence of delamination of coating. It was further confirmed by EDS composition line scan across the FESEM scratch groove as shown in Fig.7(c) with no evidence of Zr corroborating the optical profilometer image data.

### High Temperature Steam Oxidation

Steam oxidation tests were performed on bare as well as full surface Cr-coated Zry-4 coupons, for comparison, in the temperature range 700°C to 1200°C for different durations in a fabricated tubular furnace. A furnace with 100 mm hot zone was used for carrying out steam oxidation experiments. Oxidation rate was determined by measuring the difference in initial and post oxidation weights and initial surface area. Typical images of Cr-coated coupons before and after steam oxidation at different conditions are shown in Table 3. It is evident that bare Zry-4 suffered severe oxidation even at 700°C, 24 h with formation of non-adherent whitish oxide scale. With further rise in temperature, the severity increased and at 900°C, 16 h, the sample was mostly consumed and disintegrated because of extreme corrosion. Similar trend was continued till 1200°C. On the other hand, Cr-coated zircaloy coupons show highly adherent greenish colour chromium oxide scale formation at 700°C, 24 h which turned into

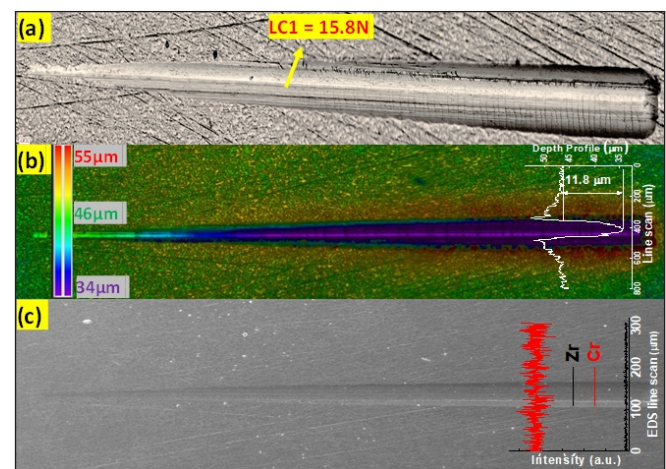


Fig.7: (a) Optical micrograph of the scratch groove generated along the length of the scratch mark; (b) corresponding 2D optical profilometer image showing depth of groove at maximum load of 40 N (11.8 μm) and (c) FESEM image of the scratch groove along with EDS line scan at maximum load 40 N confirming presence of Cr only and absence of adhesive failure.


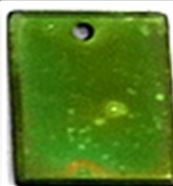

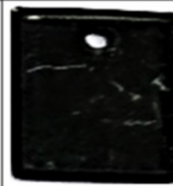





greenish black at 900°C, 16 h to black at 1200°C, 30 min. retaining the coupons shape. The nature of oxide layer formed on the Cr coating was further analyzed by GIXRD as shown in Fig.4(b). The observed peaks are matching well with Cr<sub>2</sub>O<sub>3</sub> oxide structure as confirmed from PCPDF Card No. 38:1479.

This kind of visual observation qualitatively indicates Cr coating indeed provides protection of underneath Zry-4 against steam oxidation till 1200°C for 30 min. In case of Cr-coated sample oxidized at 900°C, 16 h, a slight dimensional distortion could be visible due to edge effect. Sputtering being a line-of-sight process, the nature of coating and its thickness at the edges may not be identical to that on flat surfaces. As a result, the oxide layer touched the beneath zircaloy substrate at the edges and promoted Zry-4 oxidation via oxygen diffusion across the Cr<sub>2</sub>O<sub>3</sub> layer and hence the resulting dimensional distortion. However, one can easily address such thickness uniformity issues utilizing multiple gun sputtering system with modified sample holder.

For comparison, the weight gain for both oxidized bare and oxidized Cr coated Zry-4 coupons was compared as shown in Fig.8. At 700°C, 24 h, the weight gain was 59.55 mg.dm<sup>-2</sup> and 2003 mg.dm<sup>-2</sup> for Cr-coated Zry-4 and bare Zry-4 respectively. That means Cr-coated Zry-4 showed 33 times less oxidation



Table 3: Photographic images of bare and Cr-coated Zry-4 coupons before and after steam oxidation at different conditions.

Before Steam oxidation	Sample Description	After steam oxidation			
		700°C/24h	900°C/16h	1000°C/3h	1200°C/0.5h
	Cr coated Zry-4				
	Bare Zry-4		Completely disintegrated		

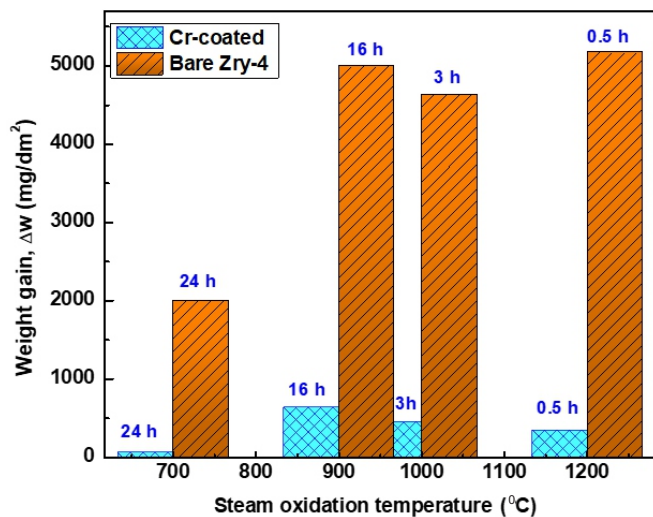


Fig.8: Weight gain vs. steam oxidation temperature histogram plot at different exposure durations.

than bare Zry-4. At 1200°C, 30 min., under DBA scenario, the Cr-coated Zry-4 with weight gain of 342.78 mg.dm<sup>-2</sup> exhibited 15 times less oxidation than bare Zry-4 with weight gain of 5174.15 mg.dm<sup>-2</sup>. These results corroborate the previous literature data on steam oxidation [12, 69-71]. We note that while transferring the bare oxidized zircaloy-4 samples there was loss of ZrO<sub>2</sub> powdery scale depending upon the extent of oxidation and hence the measured weight gain could be lower than the reported data. Careful analysis of the weight gain histogram reveals that upto 900°C, the oxidation rate is rather slow which converts into very high rate of oxidation from 1000°C onwards for both Cr as well as bare Zry-4. These weight gain results clearly show significant improvement in high temperature oxidation behavior of Cr-coated Zry-4 compared to bare sample.

Cross-section FESEM investigation of the oxidized Cr coated Zry-4 samples at two different temperatures 1000°C and 1200°C are shown in Fig.9(a-b). At 1000°C, 3h, the oxide layer thickness is found to be ~3-4 μm but intact with the underneath Cr layer. EDS composition line scan shows oxygen diffusion is very limited within the Cr layer and the Cr/Zr

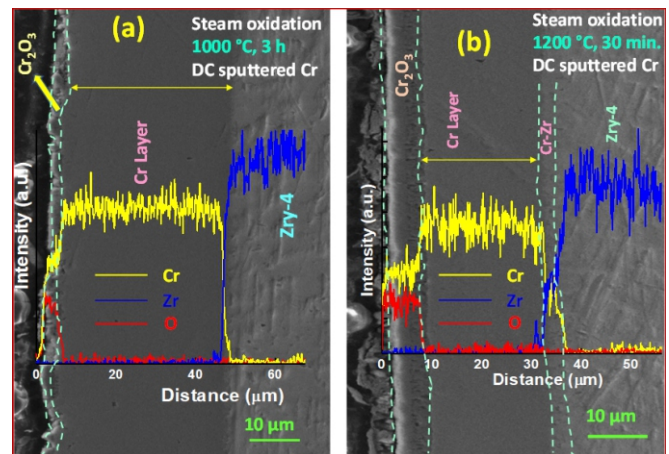


Fig.9: Cross-section FESEM micrographs of steam oxidized Cr coated Zry-4 samples (a) at 1000°C, 3 h; and (b) 1200°C, 30 min. with corresponding EDS composition line scan showing oxide layer as well as unreacted Cr layer thickness, coatings integrity with substrate and Cr diffusion into Zry-4 layer.

interface is very sharp indicating absence of Cr interdiffusion within the Zry-4 layer. There is no crack or peel off sign within the oxide layer. Due to enhanced severity of oxidation at 1200°C, the Cr<sub>2</sub>O<sub>3</sub> oxide layer thickness was grown to 7-8 μm even at 30 minutes of exposure to steam environment. Very careful observation revealed a bilayer structure into Cr<sub>2</sub>O<sub>3</sub> oxide film; one porous oxide layer attached to Cr layer with a non-porous oxide cap at the top but no cracks could be seen throughout the cross-section. But the Cr<sub>2</sub>O<sub>3</sub> layer is highly adherent to the Cr layer. EDS composition line scan also supports the visual X-section morphology consisting of 4 layer structure Cr<sub>2</sub>O<sub>3</sub>/Cr/Cr-Zr/Zry-4 corroborating the results of most the previous investigation [10,12,23]. At the Cr/Zr interface, a small fraction of Cr diffusion into Zry-4 layer could be seen at 1200°C (Fig.9(b)) unlike 1000°C (Fig.9(a)). Insertion of a suitable metallic interlayer such as Mo could stop such Cr interdiffusion into Zry-4 layer. This investigation highlights that even ~10 μm Cr coating may be sufficient to protect the Zry-4 claddings from oxidation during DB LOCA scenario. However, it may be necessary to arrest the Cr diffusion into Zry-4 so that formation of Cr-Zr low melting eutectic (1332°C) can be avoided. This can be a problem for future investigation.

Table 4: Steady state analysis of reactivity load of PHWR 37 pin fuel assembly at zero burnup.

No.	Cr thickness (μm)	$k_{\infty}$ (v-TRAC)	$\rho$ (mk) (v-TRAC)	$\rho$ (mk) (OpenMC)	$\rho$ (mk) (DRAGON)
1	Uncoated (Ref.)	1.12460	0.0	0.0	0.00
2	10	1.11905	-4.41	-4.19	-4.3
3	15	1.11630	-6.62	-6.56	
4	20	1.11355	-8.83	-8.71	-8.5
5	25	1.11082	-11.03	-10.92	
6	30	1.10810	-13.24	-13.13	-12.8
7	35	1.10540	-15.45	-15.10	
8	40	1.10271	-17.66	-17.30	-17.1

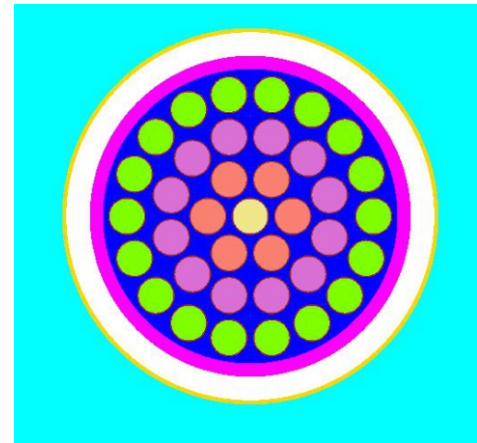


Fig.10: Cross section view of PHWR fuel assembly.

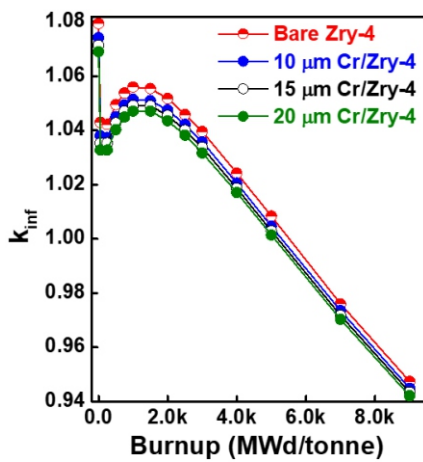


Fig.11: Variation of  $k_{inf}$  with burnup for PHWR fuel assembly for different coating thickness.

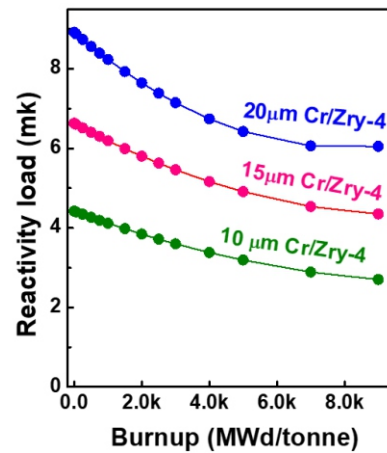


Fig.12: Reactivity load with burnup for 700 MWe PHWR fuel assembly for different thickness of Cr on clad.oxidation temperature histogram plot at different exposure durations.

Therefore, this study demonstrates successful deposition of thick (20-30 μm), pore-free and highly adherent Cr coating on Zry-4 coupons as well as Zry-4 PHWR’s fuel claddings by DC magnetron sputtering. High temperature steam oxidation of the Cr coated Zry-4 in the temperature range 700°C to 1200°C showed very good protection of underneath Zry-4 claddings even under DB LOCA scenario. This study also envisages that minimum 10-12 μm thick Cr coating may be sufficient to protect Zry-4 claddings from severe steam oxidation by providing enough coping time to the operators during DB LOCA condition.

**Theoretical Investigation**

**Effect of Cr Coating on Nuclear Reactivity in PHWR**

Since the thermal neutron absorption cross-section of Cr (2.9 b) is significantly greater than that of Zry-4 (0.22 b), it follows that cladding coated with Cr is likely to adversely affect neutron flux and subsequently core reactivity. An assessment of reactivity effect of Cr coating on the clad outer surface in the context of development of ATF was performed. In this study, the 37 fuel pin PHWR fuel assembly (FA) was analyzed with Cr coating. Calculations were performed using codes v-TRAC, DRAGON, and OpenMC for different coating thicknesses. Assessment of burnup reactivity load was carried out using DRAGON and OpenMC. Excellent behavior as well as significant advantage of neutron economy has resulted in the use of Zr

alloy as the cladding material for most of the thermal reactors operating in the world. However, extensive metal-water reaction in the event of severe accidents and subsequent hydrogen generation is a big disadvantage for Zr alloy. This disadvantage has also resulted in grave consequences both during Chernobyl and Fukushima accidents. Many attempts have been initiated worldwide to find accident tolerant cladding material. One way is to coat the fuel pin clad outer surface with Cr that ensures the safety of fuel in accident scenario by preventing high temperature Zr-water reaction. This study analyzes the reactivity load incurred due to Cr coating of varying thickness on the clad of a 37 fuel pin cluster in a typical PHWR.

**Methods and Codes**

The results obtained from multiple codes are presented for comparison and benchmarking purposes. Among these, the indigenous lattice transport code v-TRAC, based on the Method of Characteristics (MOC), is designed for the neutronic analysis of complex heterogeneous lattice cells using ENDF format multigroup cross section data. v-TRAC has a modular structure, where each module serves a distinct function. The process begins by reading input data and ends with presenting and visualizing lattice results. Further details on the computational methodology are provided in references [72-73]. Additionally, the open source Monte Carlo code OpenMC is also used to compare the results between two codes at zero

burnup. It is based on Monte Carlo method to solve the neutron transport equation. The code analyzes the 3-D fuel assembly geometry using Constructive Solid Geometry (CSG). The inbuilt burnup routine of OpenMC is used to simulate fuel depletion in FA. The FA is simulated as rings of similar burnup, with the power corresponding to 700 MWe PHWR. OpenMC has an inbuilt burnup routine. It is used for burnup analysis in the present study. Thermal scattering is modeled using free gas and thermal scattering law  $S(\alpha, \beta)$  models [74]. Both OpenMC and v-TRAC utilize the ENDF/B-VII.1 based nuclear data library, in ACE and multigroup format respectively. Further, DRAGON code is also used for calculation using JEFF3.1 library and results are compared in Table 4.

### Analysis of Theoretical Results

In this study, a 37 pin cluster of 700 MWe PHWR was analyzed with Cr coating (Fig.10) to assess its impact on the infinite neutron multiplication factor  $k_{\infty}$  and reactivity load ( $\rho$ ). Table 4 highlights a consistent decrease in  $k_{\infty}$  and corresponding reactivity load with increasing Cr coating thickness. For the uncoated reference,  $k_{\infty}$  was 1.12460 (v-TRAC). At 10  $\mu\text{m}$  Cr coating, reactivity load was 4.41 mk (v-TRAC), 4.19 mk (OpenMC), and 4.3 mk (DRAGON), while at 40  $\mu\text{m}$ , it reached 17.66 mk (v-TRAC), 17.30 mk (OpenMC), and 17.1 mk (DRAGON). As expected, there is an increase in reactivity load with thickness of Cr coating.

Fig.11 illustrates the variation in  $k_{\text{inf}}$  as a function of burnup for the bare Zry-4 and coated cases with 10, 15 and 20  $\mu\text{m}$  thickness, showing a clear reactivity load from Cr coating throughout the burnup cycle. It is seen from Fig. 12 that the reactivity load due to Cr coating shows a tendency of reduction with burnup. Reactivity load increases with coating thickness, demonstrating a trade-off between reduced neutron multiplication and enhanced accident tolerance. In case of 700 MWe PHWRs, considering a Cr coating thickness of 10  $\mu\text{m}$  on Zry-4 claddings, the reactivity loss is nearly 3 mk as can be seen Fig.12 which is equivalent to typically a burnup loss of  $\sim 300$  MWd/tonne i.e. 4.28%. With increased thickness of 15  $\mu\text{m}$ , the reactivity loss can be limited to within 5 mk which typically translates as a burnup loss of  $\sim 500$  MWd/tonne and in terms of percentage  $\sim 7.15\%$ . At 20  $\mu\text{m}$  thickness, the percentage loss of burnup turns out to be  $\sim 8.92\%$ . That means upto 20  $\mu\text{m}$  Cr coating thickness, the burnup loss can be limited to  $<10\%$ . These results underline the importance of optimizing Cr coating thickness to achieve a balance between safety and reactivity performance. This kind burnup loss can be negligible in the case of the PHWRs using reprocessed U or fuel with slightly higher content of  $\text{U}^{235}$ .

### Conclusion

A thick (20-30  $\mu\text{m}$ ), pore-free highly adherent Cr coating was successfully developed for flat specimen as well as for 100 mm length tubular shape Zry-4 substrates (OD surface) by DC magnetron sputtering. GIXRD and EDS composition analyses confirmed deposition of pure bcc-Cr coatings with a sharp Cr/Zry-4 interface as revealed by cross-section FESEM examination. Micro-scratch tests confirmed excellent adhesion of the Cr coating with Zry-4 substrate. The steam oxidation of Cr coated Zry-4 in the temperature range 700-1200°C showed formation of highly adherent protective  $\text{Cr}_2\text{O}_3$  layer on Cr. Upon steam exposure to 700°C, 24 h, the oxidation rate of Cr coated Zry-4 samples was  $\sim 33$  times less than bare Zry-4, whereas, at 1200°C, 30 min (DB LOCA condition) the oxidation of Cr/Zry-4 was 15 times less in comparison to bare Zry-4. These experiments have shown that an adherent and compact  $\text{Cr}_2\text{O}_3$  layer on the Cr acted as an effective barrier for

the ingress of oxidizing species. At steam exposure condition of 1200°C, 30 min (DB LOCA scenario), a four layer structure consisting of  $\text{Cr}_2\text{O}_3/\text{Cr}/\text{CrZr}/\text{Zry-4}$  was formed with 7-8  $\mu\text{m}$  thick protective  $\text{Cr}_2\text{O}_3$  layer.

The neutron multiplication factor was assessed under cold and hot conditions, both with and without Cr coating. Results for  $k_{\infty}$  from v-TRAC, OpenMC and DRAGON agree closely at zero burnup. Additionally, the impact of burnup on  $k_{\infty}$  for hot conditions was analyzed for different coating thicknesses. These results highlight the impact of Cr coatings on reducing the multiplication factor of the fuel cluster. Optimal thickness of Cr coating depends on both reactivity load as well as material properties through a comprehensive analysis to achieve a balance between safety and fuel utilization. Considering a thickness of  $\sim 15$   $\mu\text{m}$ , the reactivity loss can be limited to within 5 mk which typically translates as a burnup loss of 500 MWd/tonne in PHWRs (700 MWe). This study highlights that Cr coating thickness in the range 10-12  $\mu\text{m}$  may be sufficient to protect the Zry-4 claddings under DB LOCA condition with minimum effect on nuclear reactivity in turn burnup loss in 700 MWe PHWRs.

### Acknowledgement

Technical support from NAL Bengaluru is highly appreciated.

### References

- [1] T. R. Allen, R. J. M. Konings, A. T. Motta, Corrosion of Zirconium Alloys, In: R. J. M. Konings, Editor. Comprehensive Nuclear Materials. Oxford, UK, Elsevier, 2012, 49-68.
- [2] K. A. Terrani, S. J. Zinkle, L. L. Snead, Advanced oxidation-resistant iron-based alloys for LWR fuel cladding, J. Nucl. Mater., 2014, 448, 420-435.
- [3] A. T. Motta, A. Couet, R. J. Comstock, Corrosion of zirconium alloys used for nuclear fuel cladding, Annu. Rev. Mater. Res., 2015, 45, 311-343.
- [4] K. A. Terrani, Accident tolerant fuel cladding development: Promise, status, and challenges. J. Nucl. Mater., 2018, 501, 13-30.
- [5] C. L. Whitmarsh, Review of Zircaloy-2 and Zircaloy-4 Properties Relevant to N.S. Savannah Reactor Design; ORNL-3281; Oak Ridge National Laboratory: Oak Ridge, TN, USA, 1962.
- [6] R. B. Rebak, Accident Tolerant Materials for Light Water Reactor Fuels, Elsevier Book. 2020.
- [7] G. Ledergerber, S. Valizadeh, J. Wright, M. Limback, L. Hallstadius, D. Gavillet, et al., Fuel performance beyond design e exploring the limits, in: Top Fuel, 2010, 513-524.
- [8] IAEA, Fuel Failure in Normal Operation of Water Reactors: Experience, Mechanisms and Management, IAEA TECDOC 709, IAEA, Vienna, 1993.
- [9] Review of Fuel Failures in Water Cooled Reactors, IAEA, Vienna, 2010.
- [10] J. Yang, M. Steinbruck, C. Tang, M. Grobe, J. Liu, J. Zhang, S. Yun, S. Wang, Review on chromium coated zirconium alloy accident tolerant fuel cladding, J. Alloy. Compds. 2023, 895, 162450.
- [11] Z. Karoutas, J. Brown, A. Atwood, L. Hallstadius, E. Lahoda, S. Ray, J. Bradfute, The maturing of nuclear fuel: Past to Accident Tolerant Fuel. Prog. Nucl. Energy, 2018, 102, 68-78.
- [12] C. Tang, M. Stueber, H. J. Seifert, M. Steinbrueck, Protective coatings on zirconium-based alloys as accident-tolerant fuel (ATF) claddings. Corros. Rev., 2017, 35, 141-165.



- [13] L. J. Ott, K. R. Robb, D. Wang, Preliminary assessment of accident-tolerant fuels on LWR performance during normal operation and under DB and BDB accident conditions, *J. Nucl. Materials*, 2018, 448, 520-533.
- [14] K. R. Robb, Analysis of the FeCrAl accident tolerant fuel concept benefits during BWR station blackout accidents, *Proc. 16th Int. Top. Meet. Nucl. React. Therm. Hydraulics*, 2015, 1183-1195.
- [15] M. T. Farmer, L. Leibowitz, K. A. Terrani, K. R. Robb, Scoping assessments of ATF impact on late-stage accident progression including molten core-concrete interaction, *J. Nucl. Materials*, 2014, 448, 534-540.
- [16] B. J. Merrill, S. M. Bragg-Sitton, P. W. Humrickhouse, Modification of MELCOR for severe accident analysis of candidate accident tolerant cladding materials, *Nucl. Eng. Design*, 2017, 315, 170-178.
- [17] T. Cheng, J. R. Keiser, M. P. Brady, K.A. Terrani, B. A. Pint, Oxidation of fuel cladding candidate materials in steam environments at high temperature and pressure, *J. Nucl. Materials*, 2012, 427, 396-400.
- [18] B. A. Pint, K. A. Terrani, M. P. Brady, T. Cheng, J. R. Keiser, High temperature oxidation of fuel cladding candidate materials in steam-hydrogen environments, *J. Nucl. Materials*, 2013, 440, 420-427.
- [19] B. A. Pint, K. A. Terrani, Y. Yamamoto, L. L. Snead, Material Selection for accident tolerant fuel cladding, *Metall. Mater. Trans. E*, 2015, 2 (3), 190-196.
- [20] H. C. Brassfield, J. F. White, L. Sjobahl, J. T. Bittel, Recommended Property and Reaction Kinetics Data for Use in Evaluating a Light-water-cooled Reactor Loss of Coolant Incident Involving Zircaloy-4 or 304SS Clad UO<sub>2</sub>, GEMP-482, General Electric Co., 1968.
- [21] J. V. Cathcart, R. E. Pawel, R. A. McKee, R. E. Druschel, G. J. Yurek, J. J. Campbell, et al., Zirconium Metal water Oxidation Kinetics, IV: Reaction Rate Studies, ORNL/NUREG-17, Oak Ridge National Laboratory, 1977.
- [22] K. A. Terrani, B. A. Pint, C. M. Parish, C. M. Silva, L.L. Snead, Y. Katoh, Silicon carbide oxidation in steam up to 2 MPa, *J. Am. Ceram. Society*, 2014, 97, 2331-2352.
- [23] M. Steinbrück, N. Ver, M. Große, Oxidation of advanced zirconium cladding alloys in steam at temperatures in the range of 600-1200 °C, *Oxid. Met.*, 2011, 76, 215-232.
- [24] D. J. Young, *High Temperature Oxidation and Corrosion of Metals*, (Elsevier Ltd., Amsterdam, 2016).
- [25] N. Birks, G. Meier, and F. Pettit, *Introduction to the High Temperature Oxidation of Metals*, 2nd ed (Cambridge University Press, Cambridge, 2006).
- [26] Outotec, *HSC Chemistry 10*, (PPORI, 1974–2023).
- [27] M. Steinbrueck, M. Grosse, C. Tang, J. Stuckert, H. J. Seifert, An Overview of Mechanisms of the Degradation of Promising ATF Cladding Materials During Oxidation at High Temperatures, *High Temp. Corr. Mater.*, 2024, 101, 621-647.
- [28] J. C. Brachet, E. Rouesne, J. Ribis, T. Guilbert, S. Urvoy, G. Nony, C. Toffolon-Masclat, M. Le Saux, N. Chaabane, H. Palancher, A. David, J. Bischoff, J. Augereau, E. Pouillier, High temperature steam oxidation of chromium-coated zirconium-based alloys: Kinetics and process, *Corr. Sci.*, 2020, 167, 108537-15.
- [29] D. Kim, H. G. Lee, J. Y. Park, W. J. Kim, Fabrication and measurement of hoop strength of SiC triplex tube for nuclear fuel cladding applications. *J. Nucl. Mater.*, 2015, 458, 29–36.
- [30] Y. Katoh, L. L. Snead, C. H. Jr Henager, T. Nozawa, T. Hinoki, A. Iveković, S. Novak, S. G. De Vicente, Current status and recent research achievements in SiC/SiC composites. *J. Nucl. Mater.*, 2014, 455, 387–397.
- [31] X. Zhou, H. Wang, S. Zhao, Progress of SiC<sub>y</sub>/SiC composites for nuclear application. *Adv. Ceram.*, 2016, 37, 151–167.
- [32] B. Qiu, J. Wang, Y. Deng, M. Wang, Y. Wu, S. Qiu, A review on thermohydraulic and mechanical-physical properties of SiC, FeCrAl and Ti<sub>3</sub>SiC<sub>2</sub> for ATF cladding. *Nucl. Eng. Technol.*, 2020, 52, 1–13.
- [33] J. Liu, X. Zhang, D. Yun, A complete review and a prospect on the candidate materials for accident-tolerant fuel claddings. *Mater. Rev.*, 2018, 32, 1757–1778.
- [34] S. M. Bragg-Sitton, M. Todosow, R. Montgomery, C. R. Stanek, W. J. Carmack, Metrics for the technical performance evaluation of light water reactor accident-tolerant fuel. *Nucl. Technol.*, 2016, 195, 111–123.
- [35] H. Chen, X. Wang, R. Zhang, Application and development progress of Cr-based surface coatings in nuclear fuel element: I. Selection, preparation, and characteristics of coating materials. *Coatings*, 2020, 10, 808.
- [36] H. Chen, X. Wang, R. Zhang, Application and Development Progress of Cr-Based Surface Coating in Nuclear Fuel Elements: II. Current Status and Shortcomings of Performance Studies. *Coatings*, 2020, 10, 835.
- [37] B. Cheng, Fuel behavior in severe accidents and Mo-alloy based cladding designs to improve accident tolerance. *Atw. Int. Z. Fuer Kernenerg.*, 2013, 59, 158–160.
- [38] A. Nelson, E. Sooby, Y. -J Kim, B. Cheng, S. Maloy, High temperature oxidation of molybdenum in water vapor environments. *J. Nucl. Mater.* 2014, 448, 441–447.
- [39] B. Cheng, P. Chou, Y. -J. Kim, Evaluations of Mo-alloy for light water reactor fuel cladding to enhance accident tolerance. *EPJ Nucl. Sci. Technol.*, 2016, 2, 5.
- [40] B. Cheng, P. Chou, Y. -J. Kim, Development of Mo-Based Accident Tolerant LWR Fuel Cladding; International Atomic Energy Agency: Vienna, Austria, 2016.
- [41] B. Maier, H. Yeom, G. Johnson, T. Dabney, J. Walters, J. Romero, H. Shah, P. Xu, K. Sridharan, Development of cold spray coatings for accident-tolerant fuel cladding in light water reactors. *JOM* 2018, 70, 198–202.
- [42] J. C. Brachet, T. Guilbert, M. Le Saux, J. Rousselot, G. Nony, C. Toffolon-Masclat, A. Michau, F. Schuster, H. Palancher, J. Bischoff, Behavior of Cr-coated M5 claddings during and after high temperature steam oxidation from 800 °C up to 1500 °C (Loss-of-Coolant Accident & Design Extension Conditions), in: *Proceedings of the Topfuel 2018*, Prague, Czech Republic, 2018.
- [43] X. Han, J. Xue, S. Peng, H. Zhang, An interesting oxidation phenomenon of Cr coatings on Zry-4 substrates in high temperature steam environment, *Corros. Sci.*, 2019, 156, 117–124.
- [44] H. -G. Kim, I. -H. Kim, Y. -I. Jung, D. -J. Park, J. -Y. Park, Y. -H. Koo, High-temperature oxidation behavior of Cr-coated zirconium alloy, in: *Proceedings of the LWR Fuel Performance Meeting/Topfuel*, Charlotte, USA, 2013, 842–846.
- [45] Y. Wang, W. Zhou, Q. Wen, X. Ruan, F. Luo, G. Bai, Y. Qing, D. Zhu, Z. Huang, Y. Zhang, T. Liu, R. Li, Behavior of plasma sprayed Cr coatings and FeCrAl coatings on Zr fuel cladding under loss-of-coolant accident conditions, *Surf. Coat. Technol.*, 2018, 344, 141–148.

- [46] T. Wei, R. Zhang, H. Yang, H. Liu, S. Qiu, Y. Wang, P. Du, K. He, X. Hu, C. Dong, Microstructure, corrosion resistance and oxidation behavior of Cr-coatings on Zircaloy-4 prepared by vacuum arc plasma deposition, *Corros. Sci.*, 2019, 158, 108077.
- [47] Z. Yang, Y. Niu, J. Xue, T. Liu, C. Chang, X. Zheng, Steam oxidation resistance of plasma sprayed chromium-containing coatings at 1200 °C, *Mater. Corros.*, 2019, 70, 37–47.
- [48] M. Lenling, H. Yeom, B. Maier, G. Johnson, T. Dabney, J. Graham, P. Hosemann, D. Hoelzer, S. Maloy, K. Sridharan, Manufacturing oxide dispersion-strengthened (ODS) steel fuel cladding tubes using the cold spray process, *JOM*, 2019, 71, 2868–2873.
- [49] J. -M. Kim, T. -H. Ha, I. -H. Kim, H. -G. Kim, Microstructure and oxidation behavior of CrAl laser-coated Zircaloy-4 alloy, *Metals*, 2017, 7, 59.
- [50] J. -M. Kim, T. -H. Ha, J. -S. Park, H. -G. Kim, Effect of laser surface treatment on the corrosion behavior of FeCrAl-coated TZM alloy, *Metals*, 2016, 6, 29.
- [51] C. P. Massey, K. A. Terrani, S. N. Dryepontd, B. A. Pint, Cladding burst behavior of Fe-based alloys under LOCA, *J. Nucl. Mater.*, 2016, 470, 128–138.
- [52] X. Li, C. Meng, X. Xu, X. He, C. Wang, Effect of Al content on high-temperature oxidation behavior and failure mechanism of CrAl-coated Zircaloy, *Corros. Sci.*, 2021 192, 109856.
- [53] N. Sekido, K. Soeta, K. Yoshimi, Liquidus projection and solidification paths in the Zr-Si-Al ternary system, *J. Alloy. Compd.*, 2021, 885, 160911.
- [54] W. Xiao, H. Deng, S. Zou, Y. Ren, D. Tang, M. Lei, C. Xiao, X. Zhou, Y. Chen, Effect of roughness of substrate and sputtering power on the properties of TiN coatings deposited by magnetron sputtering for ATF, *J. Nucl. Mater.*, 2018, 509, 542–549.
- [55] M. A. Tunes, F.C. da Silva, O. Camara, C. G. Schön, J. C. Sagás, L. C. Fontana, S. E. Donnelly, G. Greaves, P. D. Edmondson, Energetic particle irradiation study of TiN coatings: are these films appropriate for accident tolerant fuels? *J. Nucl. Mater.*, 2018, 512, 239–245.
- [56] E. Alat, A. T. Motta, R.J. Comstock, J. M. Partezana, D. E. Wolfe, Multilayer (TiN, TiAlN) ceramic coatings for nuclear fuel cladding, *J. Nucl. Mater.*, 2016, 478, 236–244.
- [57] O. V. Maksakova, R. F. Webster, R. D. Tilley, V. I. Ivashchenko, B. O. Postolnyi, O.V. Bondar, Y. Takeda, V. M. Rogoz, R. E. Sakenova, P. V. Zukowski, M. Opielak, V. M. Beresnev, A. D. Pogrebnyak, Nanoscale architecture of (CrN/ZrN)/(Cr/Zr) nanocomposite coatings: Microstructure, composition, mechanical properties and first-principles calculations, *J. Alloy. Compd.*, 2020, 831, 154808.
- [58] A. Michau, F. Maury, F. Schuster, I. Nuta, Y. Gazal, R. Boichot, M. Pons, Chromium carbide growth by direct liquid injection chemical vapor deposition in long and narrow tubes, experiments, modeling and simulation, *Coatings*, 2018, 8, 220.
- [59] J. G. Gigax, M. Kennas, H. Kim, T. Wang, B.R. Maier, H. Yeom, G.O. Johnson, K. Sridharan, L. Shao, Radiation response of Ti<sub>2</sub>AlC MAX phase coated Zircaloy-4 for accident tolerant fuel cladding, *J. Nucl. Mater.*, 2019, 523, 26–32.
- [60] C. Tang, M. Steinbrück, M. Große, T. Bergfeldt, H. J. Seifert, Oxidation behavior of Ti<sub>2</sub>AlC in the temperature range of 1400 °C–1600 °C in steam, *J. Nucl. Mater.*, 2017, 490, 130–142.
- [61] C. Tang, M. Große, S. Ulrich, M. Klimenkov, U. Jäntschi, H. J. Seifert, M. Stüber, M. Steinbrück, High-temperature oxidation and hydrothermal corrosion of textured Cr<sub>2</sub>AlC-based coatings on zirconium alloy fuel cladding, *Surf. Coat. Technol.*, 2021, 419, 127263.
- [62] P. Richardson, D. Cuskelly, M. Brandt, E. Kisi, Microstructural analysis of in-situ reacted Ti<sub>2</sub>AlC MAX phase composite coating by laser cladding, *Surf. Coat. Technol.*, 2020, 385, 125360-8.
- [63] Y. Lei, L. Chen, J. Zhang, F. Xue, G. Bai, Y. Zhang, T. Liu, R. Li, S. Li, J. Wang, Influence of Al concentration on mechanical property and oxidation behavior of Zr-Al-C coatings, *Surf. Coat. Technol.*, 2019, 372, 65–71.
- [64] Y. Al-Olayyan, G. E. Fuchs, R. Baney, J. Tulenko, The effect of Zircaloy-4 substrate surface condition on the adhesion strength and corrosion of SiC coatings, *J. Nucl. Mater.*, 2005, 346, 109–119.
- [65] C. Meng, L. Yang, Y. Wu, J. Tan, W. Dang, X. He, X. Ma, Study of the oxidation behavior of CrN coating on Zr alloy in air, *J. Nucl. Mater.*, 2015, 515, 354–369.
- [66] J. Krejčí, J. Kabátová, F. Manoch, J. Kočí, L. Cvrček, J. Málek, S. Krum, P. Šutta, P. Bublíková, P. Halodová, H.K. Namburi, M. Ševeček, Development and testing of multicomponent fuel cladding with enhanced accidental performance, *Nucl. Eng. Technol.*, 2020, 52, 597–609.
- [67] J. C. Brachet, I. Idarraga-Trujillo, M. Le Flem, M. Le Saux, V. Vandenberghe, S. Urvoy, E. Rouesne, T. Guilbert, C. Toffolon-Masclat, M. Tupin, C. Phalippou, F. Lomello, F. Schuster, A. Billard, G. Velisa, C. Ducros, F. Sanchette, Early studies on Cr-Coated Zircaloy-4 as enhanced accident tolerant nuclear fuel claddings for light water reactors, *J. Nucl. Mater.*, 2019, 517, 268–285.
- [68] F. Qi, Z. Liu, Q. Li, H. Yu, P. Chen, Y. Li, Y. Zhou, C. Ma, C. Tang, Y. Huang, B. Zhao, H. Lu, Pellet-cladding mechanical interaction analysis of Cr-coated Zircaloy cladding, *Nucl. Eng. Des.*, 2020, 367, 110792.
- [69] J. C. Brachet, M. Saux, M. Le Flem, S. Urvoy, E. Rouesne, T. Guilbert, C. Cobac, F. Lahogue, J. Rousselot, M. Tupin, P. Billaud, C. Hossepied, F. Schuster, F. Lomello, A. Billard, G. Velisa, E. Monsifrot, J. Bischoff, J. A. Ambar, On-going studies at CEA on chromium coated zirconium based nuclear fuel claddings for enhanced accident tolerant LWRs fuel. In: *Proceedings of 2015 LWR Fuel Performance/TopFuel*, Zurich, Switzerland, September, 2015, 13–19, 31–38.
- [70] H. G. Kim, I. H. Kim, Y. I. Jung, D. J. Park, J. Y. Park, Y. H. Koo, Adhesion property and high-temperature oxidation behavior of Cr-coated Zircaloy-4 cladding tube prepared by 3D laser coating, *J. Nucl. Mater.*, 2016, 465, 531–539.
- [71] D. J. Park, H. G. Kim, Y. Jung, J. H. Park, J. H. Yang, Y. H. Koo, Behavior of an improved Zr fuel cladding with oxidation resistant coating under loss-of-coolant accident conditions, *J. Nucl. Mater.*, 2016, 482, 75–82.
- [72] A. Singh, U. Pal, R. Karthikeyan, Evaluation of integral parameters of BAPL and AERE benchmarks using v-TRAC code and ENDF/B VIII.0 library, *Nuclear and Particle Physics Proceedings*, 2023, 339–340, 78–87.
- [73] A. Singh, U. Pal, R. Karthikeyan, V. Harikrishnan, Study of MOX-fueled VVER-1000 pin cell using v-TRAC with ENDF/B-VIII.0 library, *Physics Open* 2024, 19, 100212.
- [74] P. K. Romano, B. Forget, The OpenMC Monte Carlo particle transport code, *Ann Nucl Energy*, 2013, 51, 274–281.

# आण्विक उत्सर्जन को अनुकूलित करना

2

## शोर से ज्ञान तक : लेज़र-प्रेरित प्लाज़्मा में बोरॉन आण्विक उत्सर्जन स्पेक्ट्रा का उपयोग

आनंदु मोहन<sup>1</sup>, अनन्या बैनर्जी<sup>2</sup>, राजेश वी. पै<sup>1,2</sup>, एवं अर्नब सरकार<sup>1,2\*</sup>

<sup>1</sup>होमी भाभा राष्ट्रीय संस्थान, अणुशक्तिनगर, ट्रांबे, मुंबई-400 094, भारत

<sup>2</sup>ईंधन रसायन प्रभाग, भाभा परमाणु अनुसंधान केंद्र, ट्रांबे, मुंबई-400 085, भारत



अव्यवस्थित शोर जैसे पैटर्न को क्रमबद्ध करना और कार्यात्मक आण्विक संकेतों में परिवर्तित करना।

### सारांश

यह अध्ययन लेज़र प्रेरित प्लाज़्मा (एलआईपी) में बोरॉन आण्विक उत्सर्जन स्पेक्ट्रा की खोज करता है और अंशांकन-मुक्त लेज़र अब्लेटेड मॉलिक्यूलर आइसोटोपिक स्पेक्ट्रोमेट्री (सीएफ-एलएएमआईएस) का उपयोग करके आइसोटोपिक विश्लेषण के लिए इसकी क्षमता पर प्रकाश डालता है। BO और BO<sub>2</sub> जैसी क्षणिक प्रजातियों का विश्लेषण करके, शोध वर्णक्रमीय व्यतिकरण में चुनौतियों और आण्विक उत्सर्जन को अनुकूलित करने हेतु प्लाज़्मा तापमान की भूमिका को उजागर करता है। समस्थानिक संरचना में ~2% सटीकता प्राप्त करते हुए, निष्कर्ष गुणात्मक और मात्रात्मक दोनों अनुप्रयोगों के लिए आण्विक उत्सर्जन की व्यावहारिक और विश्लेषणात्मक प्रासंगिकता को रेखांकित करता है।

## Optimizing Molecular Emissions

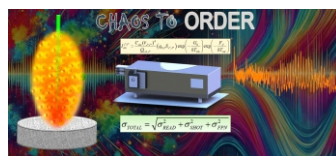
2

## From Noise to Knowledge: Harnessing Boron Molecular Emission Spectra in Laser-Induced Plasma

Anandhu Mohan<sup>1</sup>, Anannya Banerjee<sup>2</sup>, Rajesh V. Pai<sup>1,2</sup> and Arnab Sarkar<sup>1,2\*</sup>

<sup>1</sup>Homi Bhabha National Institute, Anushakti Nagar, Trombay, Mumbai-400 094, INDIA

<sup>2</sup>Fuel Chemistry Division, Bhabha Atomic Research Centre, Trombay, Mumbai-400 085, INDIA



Conversion of chaotic noise-like patterns into ordered and functional molecular signals.

### ABSTRACT

This study explores boron molecular emission spectra in Laser Induced Plasma (LIP) and highlights their potential for isotopic analysis using Calibration-Free Laser Ablated Molecular Isotopic Spectrometry (CF-LAMIS). By analyzing transient species such as BO and BO<sub>2</sub>, the research identifies challenges in spectral interferences and the role of plasma temperature in optimizing molecular emissions. Achieving ~2% accuracy in isotopic composition, the findings underscore the practical and analytical relevance of molecular emissions for both qualitative and quantitative applications.

**KEYWORDS:** Laser induced plasma, Molecular isotopic spectrometry, Plasma temperature, Isotopic composition

\*Author for Correspondence: Arnab Sarkar  
E-mail: arnab@barc.gov.in



## Introduction

Laser-induced plasma (LIP) is a powerful analytical tool that generates transient plasma through the interaction of high-intensity laser pulses with matter. This plasma contains a complex mixture of ions, atoms, and molecules, emitting signals that can be ionic, atomic, or molecular depending on acquisition delay times. These molecular emission signatures are uniquely characterized by molecular band structures, enabling experiments under ambient conditions. Such emissions have significant applications, including isotopic and actinide detection [1].

Early studies by Hornkohl et al. investigated CN molecular spectra in LIP, followed by work from Harilal et al., who explored vibrational temperature and population distribution of CN bands [2,3]. Russo et al. later introduced isotopic analysis using diatomic molecular emissions, while Sarkar et al. refined isotopic ratio predictions for boron using chemometrics techniques [4,5].

Building on this foundation, our research delves deeper into the potential of boron molecular emissions, focusing on diatomic (BO) and polyatomic (BO<sub>2</sub>) species. Through high-resolution optical setups, we aim to advance the understanding of molecular emission signatures and optimize their analytical applications.

### Experimental setup

The experimental setup mirrors the LIBS configuration, utilizing a Q-switched Nd:YAG laser (1064 nm) to ablate the sample surface and create micro-plasma. Second and fourth

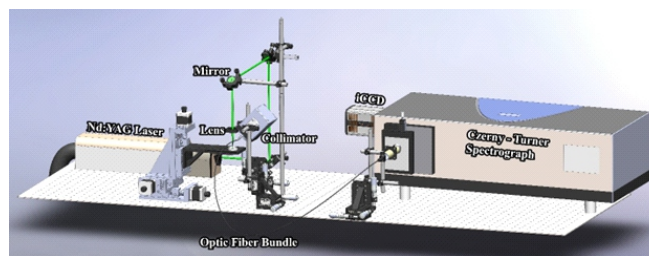


Fig.1: Instrumentation setup.

harmonic attachments enable additional laser wavelengths of 532 nm and 266 nm. Emissions are collected at a 45° angle using a collimator and delivered to a Czerny-Turner spectrograph via an optical fiber bundle. The spectrograph employs three gratings, offering resolutions of  $\Delta\lambda = 55$  pm, 35 pm, and 25 pm, depending on the grating used.

The plasma's emission spectrum is recorded by accumulating an optimized number of single laser shots on fresh sample surfaces. Ambient air conditions are maintained, and LabView software is employed for algorithm development and data analysis. This setup ensures precise spectral recording for subsequent analysis.

## Results and Discussion

### Molecular emission spectra of transient boron species

In an oxygen rich LIP, boron can form mainly two transient species BO and BO<sub>2</sub> by various reactions. Some of these reactions are  $B + O \rightarrow BO$ ,  $B + O_2 \rightarrow BO_2$ ,  $BO + O \rightarrow BO_2$ ,  $BO + O_2 \rightarrow$

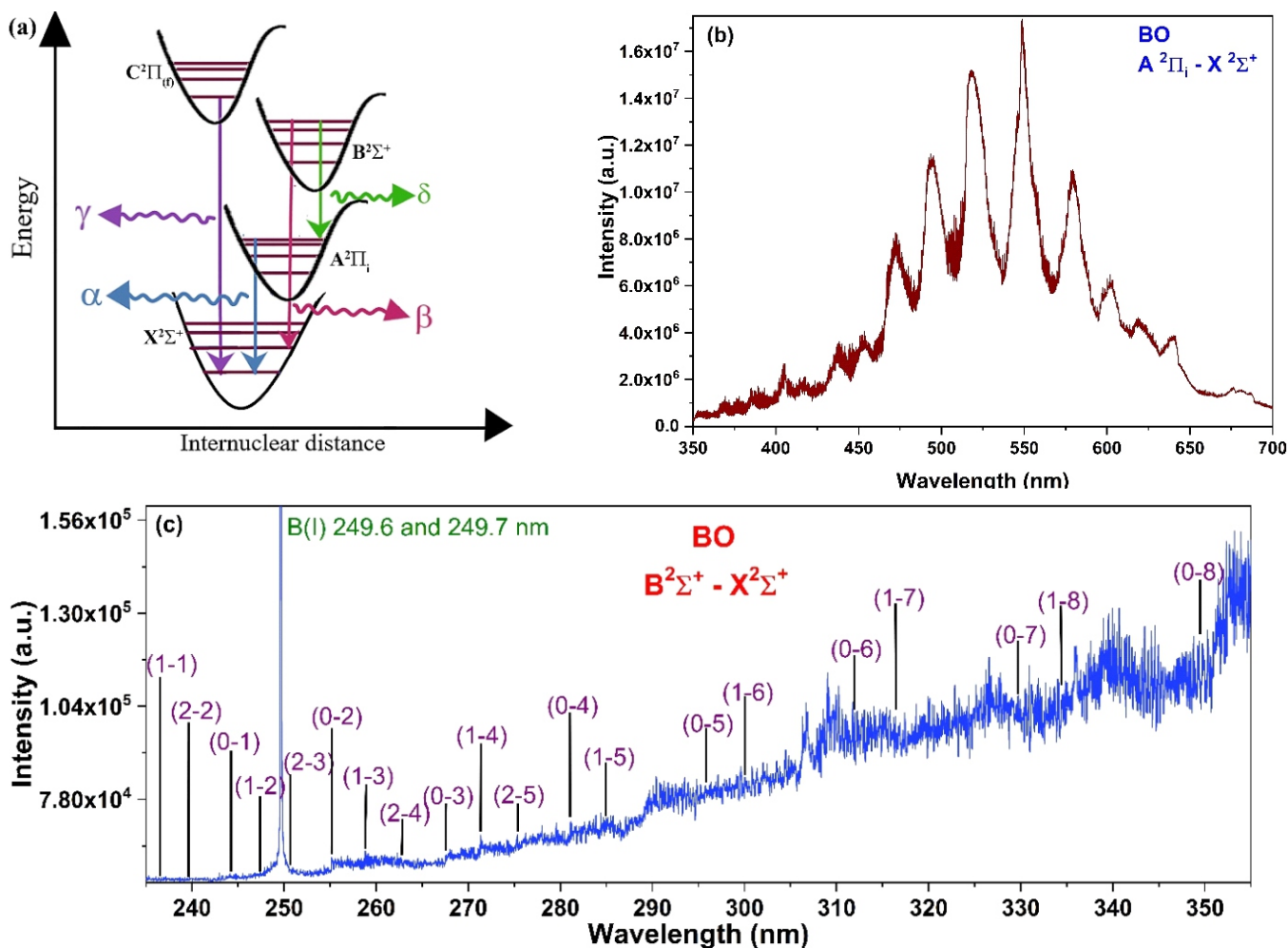


Fig.2: (a) Plausible electronic transitions of boron monoxide. Experimentally recorded spectra of (b) BO:A-X and (c) BO:B-X transitions.

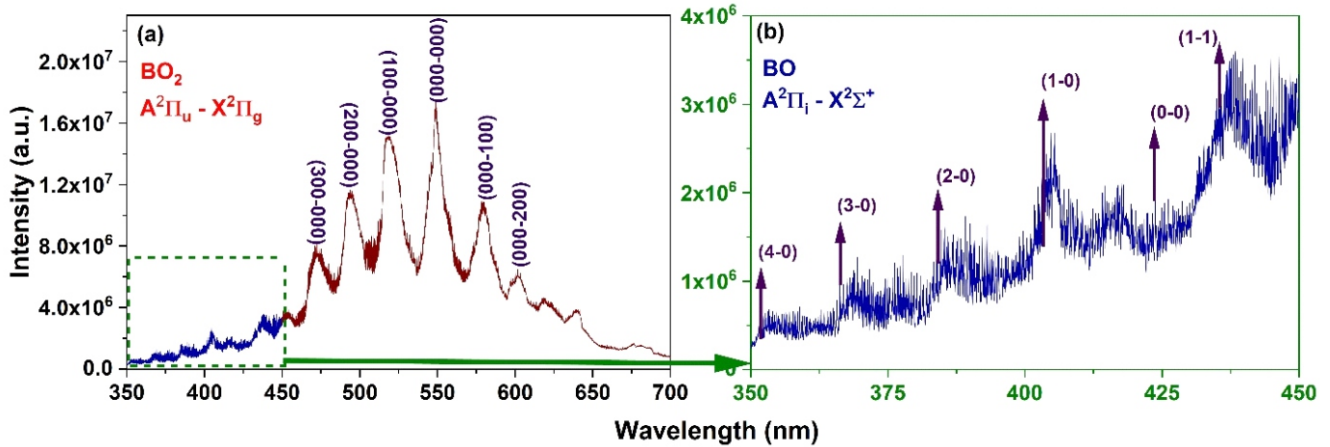


Fig.3: Revised emission spectra of (a)  $BO_2$ :A-X and (b)  $BO$ :A-X transition.

$BO_2 + O$  [6]. These transient molecules show various emission signals according to the electronic transition taking place.

$BO$  exhibits transitions across four electronic states:  $C^2\Pi_{(g)}$ ,  $B^2\Sigma^+$ ,  $A^2\Pi_i$  and  $X^2\Sigma^+$ . The transition between these states result in various electronic transitions such as A-X or  $\alpha$ -band (350–650 nm), B-X or  $\beta$ -band (230–330 nm), C-X or  $\gamma$ -band (181–230 nm), and B-A or  $\delta$ -band (458–595 nm) (Fig.2(a)). The occurrence of the  $\gamma$ -band in the deep UV region makes it difficult to record with the available detector setup. The  $\delta$ -band is difficult to record spectroscopically due to its low intensity and overlap with the  $\alpha$ -band. This leaves the  $\alpha$ -band and  $\beta$ -band as the most straightforward for studying the ro-vibrational band (RVB) structure [7]. Fig.2(b) shows the experimentally recorded spectra of the  $BO$ :A-X transition and Fig.2(c) shows the recorded spectra of various RVBs in the  $BO$ :B-X transition.

For transient  $BO_2$  species, the highly intense transition was identified to be the  $BO_2$ :A-X transition, which coexists with the  $BO$ :A-X molecular bands. Since the possibility of polyatomic transient molecule formation in LIP was not recognized until recent times [8], researchers initially assumed that the recorded spectral region belonged to the  $BO$ :A-X transition, and various analyses were performed. The  $BO_2$ :A-X transition is observed to be an electronic transition with higher emission intensity compared to the electronic transitions of  $BO$  molecules [7]. The revised RVB emission bands of polyatomic  $BO_2$  species and  $BO$ :A-X molecular bands are shown in Fig.3.

**Molecular emission signatures and spectral interferences**

To understand the amount of useful information in molecular emission spectra, an analytical figure of merit, the signal-to-envelope ratio (SER), was introduced [7,9]. Intensity decay studies of  $BO$ :B-X,  $BO$ :A-X, and  $BO_2$ :A-X RVBs showed that all RVBs of similar electronic transitions exhibit the same intensity decay pattern unless the RVB is spectrally interfered with. This study also helps identify atomic and molecular spectral interferences in various molecular emission bands of transient boron molecular species. Since the  $BO$ :A-X transition occurs between the  $BO$ :B-X and  $BO_2$ :A-X transitions, the  $BO$ :A-X bands consistently experience interferences from other molecular transitions. The RVBs of the  $BO_2$ :A-X transition are always observed to be spectrally pure due to their high intensity compared to  $BO$  transitions [7].

**Importance of plasma temperature**

The study observed a linear relationship between plasma temperature decay and emission intensity decay for  $BO$ :B-X and  $BO_2$ :A-X transitions, with optimal temperatures of 10,000–11,000 K for  $BO$  and 8,000–9,000 K for  $BO_2$  (Fig.4). Deviation from linearity in  $BO$ :A-X transitions was attributed to spectral interferences, underscoring the necessity of maintaining optimal plasma conditions for reliable data acquisition [10].

**Analytical applications of molecular emissions**

Despite the potential of LAMIS method, the scarcity of enriched isotopic standards necessitates a calibration-free approach where no standard is required for isotopic composition determination. Our group developed a CF-LAMIS methodology for the isotopic composition determination of

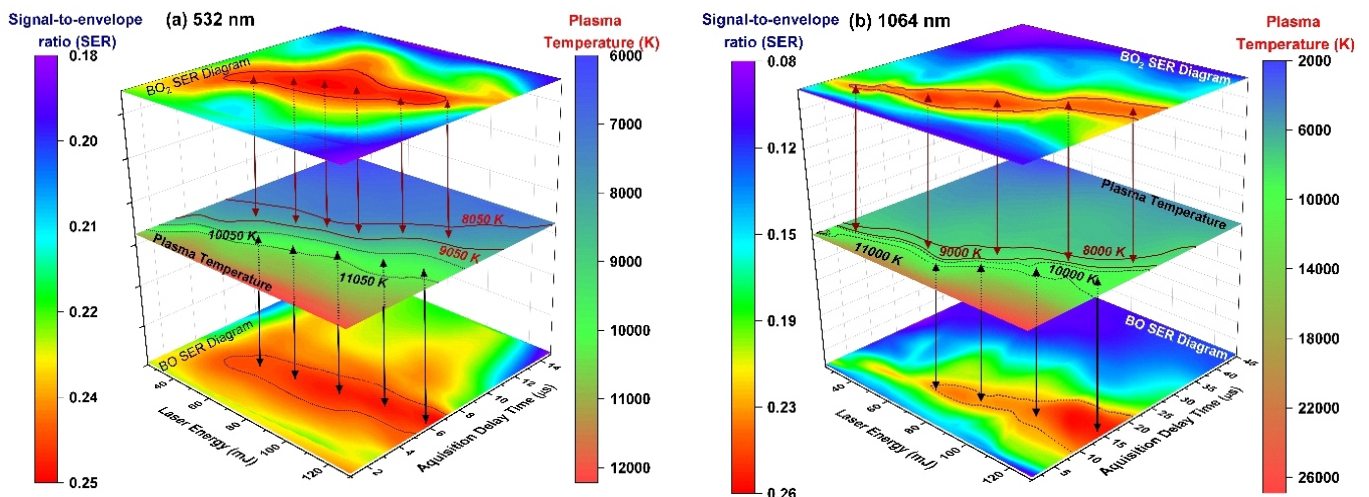


Fig.4: Relationship between the plasma temperature and molecular information (a) 532 nm and (b) 1064 nm.

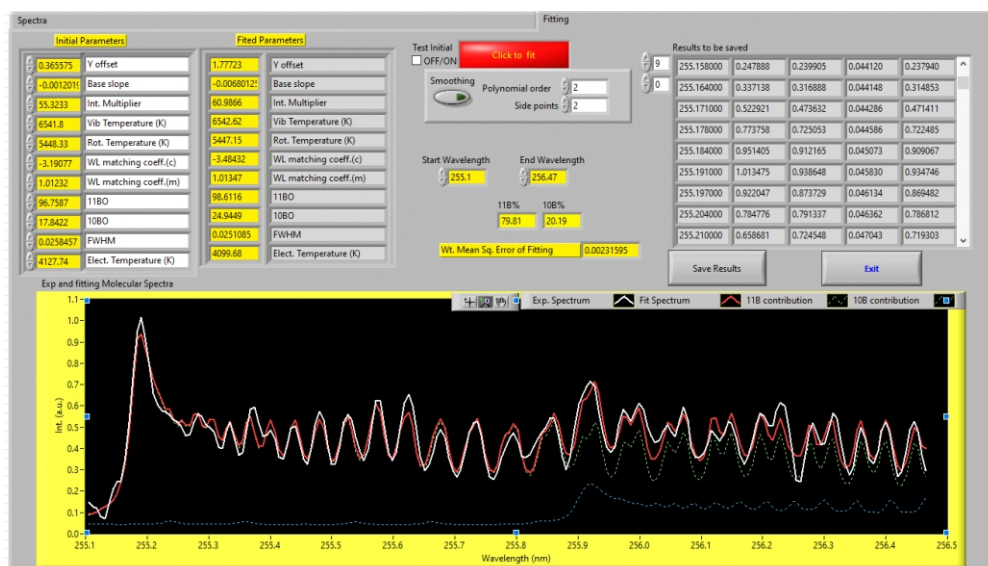


Fig.5: Graphical user interphase of the MAHADEV algorithm.

boron samples using the MAHADEV algorithm. The algorithm is based on the Born-Oppenheimer approximation, Boltzmann equilibrium, and Lorentzian intensity, named **Molecular spectra simulator under Born-Oppenheimer Approximation and Boltzmann Equilibrium environment (MAHADEV)** and isotopic compositions of boron samples were determined with ~2% accuracy. The algorithm's GUI, shown in Fig.5, enables efficient simulation and experimental data correlation, providing a robust framework for non-linear curve fitting [9].

### Conclusion

This study underscores the transition of molecular emission signatures from perceived noise to valuable analytical signals. By addressing challenges like spectral interferences and optimizing plasma conditions, significant advancements were achieved in isotopic composition analysis using boron molecular emissions. The CF-LAMIS methodology offers a novel, accurate, and efficient approach, cementing the role of laser-induced plasma in cutting-edge spectroscopic applications. Future work aims to expand this methodology to other molecular systems, broadening its applicability across diverse fields.

### References

[1] R. E. Russo, Laser ablation research and development: 60 years strong, *Applied Physics A* 129(3) (2023) 168.  
 [2] J. O. Hornkohl, C. Parigger, J. W. L. Lewis, Temperature measurements from CN spectra in a laser-induced plasma, *Journal of Quantitative Spectroscopy and Radiative Transfer* 46(5) (1991) 405-411.  
 [3] S. S. Harilal, R. C. Issac, C. V. Bindhu, G. K. Varier, V. P. N. Nampoori, C.P.G. Vallabhan, Spatial and time resolved analysis of CN bands in the laser induced plasma from graphite, *Pramana*

46(2)(1996) 145-151.

[4] R. E. Russo, A. A. Bol'shakov, X. Mao, C. P. McKay, D. L. Perry, O. Sorkhabi, *Laser Ablation Molecular Isotopic Spectrometry*, *Spectrochimica Acta Part B: Atomic Spectroscopy* 66(2) (2011) 99-104.  
 [5] A. Sarkar, X. Mao, R. E. Russo, Advancing the analytical capabilities of laser ablation molecular isotopic spectrometry for boron isotopic analysis, *Spectrochimica Acta Part B: Atomic Spectroscopy* 92 (2014) 42-50.  
 [6] T. R. Burkholder, L. Andrews, Reactions of boron atoms with molecular oxygen. Infrared spectra of BO, BO<sub>2</sub>, B<sub>2</sub>O<sub>2</sub>, B<sub>2</sub>O<sub>3</sub>, and BO-2 in solid argon, *The Journal of Chemical Physics* 95(12) (1991) 8697-8709.  
 [7] A. Mohan, A. Banerjee, A. Sarkar, Unveiling the temporal evolution of boron oxide exciplex species in laser-induced plasma: A detailed analysis of ro-vibrational spectra, *Spectrochimica Acta Part B: Atomic Spectroscopy* 211 (2024) 106838.  
 [8] M. Gaft, L. Nagli, N. Eliezer, Y. Groisman, Boron- and iron-bearing molecules in laser-induced plasma, *Spectrochimica Acta Part B: Atomic Spectroscopy* 110 (2015) 56-62.  
 [9] A. Mohan, A. Banerjee, A. Sarkar, Calibration free laser ablation molecular isotopic spectrometry (CF-LAMIS) for boron isotopic composition determination, *Journal of Analytical Atomic Spectrometry* 38(8) (2023) 1579-1591.  
 [10] A. Mohan, A. Banerjee, A. Sarkar, Exploring the influence of plasma temperature on the evolution of boron molecular species in laser-induced plasma, *Journal of Physics B: Atomic, Molecular and Optical Physics* 57(21) (2024) 215701.



## दंत संक्रमण नियंत्रण

3

### दंत सतहों पर संक्रमण नियंत्रण के लिए एक नए शीत वायुमंडलीय प्लाज्मा उपकरण (सीएपी) की रोगाणुरोधी प्रभावकारिता/क्षमता

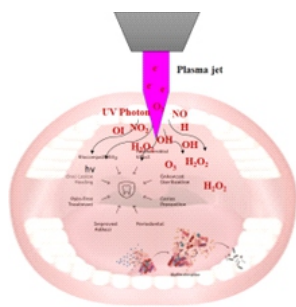
विशाखा भेंडे<sup>1,2</sup>, वंदन नागर<sup>1,3</sup>, वी. सापले<sup>4</sup>, एम. दोशी<sup>4</sup>, सी. वर्मा<sup>4</sup>, आर.एल. भारद्वाज<sup>2</sup>, राजीव कार<sup>1,2,\*</sup>

<sup>1</sup>होमी भाभा राष्ट्रीय संस्थान, अणुशक्तिनगर, ट्रांबे, मुंबई-400 094, भारत

<sup>2</sup>लेजर एवं प्लाज्मा प्रौद्योगिकी प्रभाग, भाभा परमाणु अनुसंधान केंद्र, ट्रांबे, मुंबई-400 085, भारत

<sup>3</sup>खाद्य प्रौद्योगिकी प्रभाग, भाभा परमाणु अनुसंधान केंद्र, ट्रांबे, मुंबई-400 085, भारत

<sup>4</sup>आयुर्विज्ञान प्रभाग, भाभा परमाणु अनुसंधान केंद्र, ट्रांबे, मुंबई-400 085, भारत



ठंडे प्लाज्मा उपकरण का व्यवस्था चित्र

#### सारांश

शीत वायुमंडलीय प्लाज्मा (सीएपी) सतह निर्जर्मीकरण, सामग्री संशोधन और जैव चिकित्सा उपचार सहित विभिन्न अनुप्रयोगों के साथ एक गैर-तापीय, लागत प्रभावी उपकरण के रूप में उभरा है। हमारी प्रयोगशाला में, हमने एक नए 10 MHz आरएफ टेस्ला कुंडली-आधारित सीएपी उपकरण विकसित किया, जो पहले ग्राम-धनात्मक स्टैफिलोकोकस ऑरियस (एस. ऑरियस) और ग्राम-ऋणात्मक एस्चेरिचिया कोलाई (ई. कोलाई) को प्रभावी ढंग से निष्क्रिय करने हेतु दर्शाया गया। इसके आधार पर, हमने ताजा निकाले गए मानव दांतों पर इसकी रोगाणुरोधी निष्क्रियता प्रभावकारिता की जांच की। 5 मिनट के लिए 32 V और 0.5 A पर आर्गन प्लाज्मा का उपयोग करते हुए, ऑप्टिकल एमिशन स्पेक्ट्रोस्कोपी (ओएस) ने प्रमुख जीवाणुनाशक प्रजातियों, जैसे OH (~309 nm), N<sub>2</sub> एसपीएस (~337 nm), और OI (~777.4 nm) की उपस्थिति की पुष्टि की। नियंत्रण और दो उपचार समूहों में विभाजित 99 दांतों पर दो उपचार प्रोटोकॉल (टीपी-1 और टीपी-2) का परीक्षण किया गया। उपचारित नमूनों ने 88.7% की औसत माइक्रोबियल हानि की दक्षता दर्शायी जबकि कुछ मामलों में यह 99% तक थी। ये निष्कर्ष दंत सतहों पर प्रभावी सूक्ष्मजीव भार में कमी के लिए सीएपी की क्षमता को प्रदर्शित करते हैं, जो नैदानिक सेटिंग्स में संक्रमण नियंत्रण के लिए एक आशाजनक, अघातक दृष्टिकोण प्रदान करते हैं। आगे के शोध का उद्देश्य कम से कम 2-लॉग पैमाने (99%) द्वारा लगातार माइक्रोबियल हानि हेतु मानकीकृत प्रोटोकॉल विकसित करना है।

## Dental Infection Control

3

### Antimicrobial Efficacy of a Novel Cold Atmospheric Plasma Device (CAP) for Infection Control on Dental Surfaces

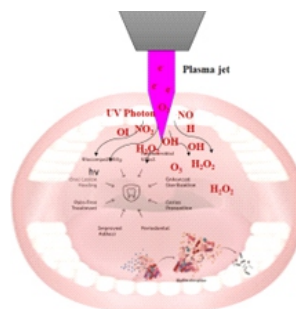
Vishakha Bende<sup>1,2</sup>, Vandan Nagar<sup>1,3</sup>, V. Saple<sup>4</sup>, M. Doshi<sup>4</sup>, C. Verma<sup>4</sup>, R.L. Bhardwaj<sup>2</sup>, Rajib Kar<sup>1,2,\*</sup>

<sup>1</sup>Homi Bhabha National Institute, Anushakti Nagar, Trombay, Mumbai-400 094, INDIA

<sup>2</sup>Laser & Plasma Technology Division, Bhabha Atomic Research Centre, Trombay, Mumbai-400 085, INDIA

<sup>3</sup>Food Technology Division, Bhabha Atomic Research Centre, Trombay, Mumbai-400 085, INDIA

<sup>4</sup>Medical Division, Bhabha Atomic Research Centre, Trombay, Mumbai-400 085, INDIA



Schematic of cold plasma device

#### ABSTRACT

Cold Atmospheric Plasma (CAP) has emerged as a non-thermal, cost-effective tool with diverse applications, including surface sterilization, material modification, and biomedical treatments. In our lab, we developed a novel 10 MHz RF Tesla coil-based CAP device, previously shown to effectively inactivate Gram-positive *Staphylococcus aureus* (*S. aureus*) and Gram-negative *Escherichia coli* (*E. coli*). Building on this, we investigated its antimicrobial inactivation efficacy on freshly extracted human teeth. Using argon plasma at 32 V and 0.5 A for 5 minutes, Optical Emission Spectroscopy (OES) confirmed the presence of key bactericidal species, such as OH (~309 nm), N<sub>2</sub> SPS (~337 nm), and OI (~777.4 nm). Two treatment protocols (TP-1 and TP-2) were tested on 11 teeth divided into control and two treated groups. Treated samples showed an average microbial reduction efficiency of 88.7%, with some cases achieving up to 99%. These findings demonstrate the potential of CAP for effective microbial load reduction on dental surfaces, offering a promising, non-invasive approach to infection control in clinical settings. Further research aims to develop standardized protocols for consistent microbial reduction by at least 2-log scales (99%).

KEYWORDS: Cold atmospheric plasma, Optical emission spectroscopy, Gram-positive, Gram-negative

\*Author for Correspondence: Rajib Kar  
E-mail: rajibkar@barc.gov.in

## Introduction

Cold atmospheric plasma (CAP) stands at the forefront of innovation across various domains, presenting a non-thermal, cost-effective solution for cutting-edge research in surface sterilization, material modification, and biological applications [1-3]. In our lab, we have indigenously developed a novel 10 MHz RF Tesla coil-based CAP device, specifically for research into biomedical applications. This device has been previously characterized using electrical and optical diagnostics, demonstrating its ability to decimate both Gram-positive *S. aureus* and Gram-negative *E. coli* bacteria [4]. Motivated by these findings, we advanced our study to explore the antimicrobial inactivation efficacy of the device on dental surfaces. CAP has shown promise as a non-invasive alternative to conventional dental treatments, particularly advantageous for patients unsuitable for traditional interventions or those with contraindications to specific treatments. Particularly for patients unsuitable for traditional methods [5,6]. However, advancing CAP towards clinical applications requires further preclinical and clinical studies to understand its mechanisms, optimize parameters, and ensure its safety for oral tissues. Current research endeavours prioritize elucidating the ideal parameters and protocols for CAP-based therapies, ensuring their safety profile and exploring their antimicrobial efficacy. In collaboration with the Dental Section of BARC Hospital, we conducted ex-vivo treatments on extracted human teeth to evaluate the antimicrobial efficacy of our device.

## Materials and Methods

The Dental Section of the Medical Division at BARC Hospital supplied 11 freshly extracted infectious human teeth obtained from informed patients. Immediately following extraction, all teeth were submerged in saline solution and transported for cold atmospheric plasma (CAP) treatment. These teeth were then divided into two distinct groups to undergo two different Cold Plasma Treatment Protocols (TP). Eight teeth were assigned to TP 1, while the remaining three were designated for TP 2. It's important to note that each tooth harbours its own unique micro biome, comprising various bacteria. When placed together in saline, these bacteria have the opportunity to freely mingle and facilitate the formation of a complex microbial film over the tooth surfaces. This formation poses a challenge during CAP treatment, as it necessitates addressing a complex microbial environment.

### Treatment Protocol 1

Fig.2 depicts the experimental procedure employed TP 1. Initially, four randomly selected teeth were individually placed in Falcon tubes, with each tube containing 3 ml of saline

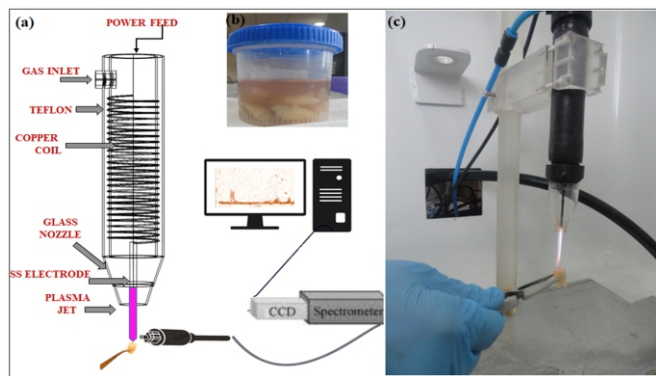


Fig.1: (a) Schematic of cold plasma device, (b) depicts a photograph of the extracted teeth stored in saline within a jar, (c) a typical image captures the CAP treatment procedure being performed on one of the teeth

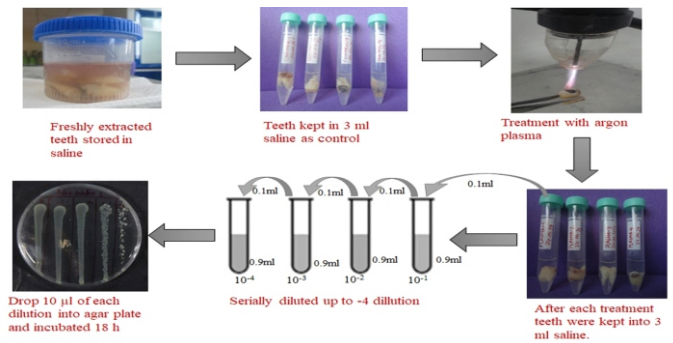


Fig.2: Procedural schematic of Treatment Protocol 1.

solution, serving as the control group. Concurrently, another set of four randomly chosen teeth underwent individual treatment with argon cold atmospheric plasma (CAP), facilitated by tweezers. Each extracted tooth was meticulously subjected to cold CAP treatment, held under the CAP source with tweezers, and rotated continuously for a duration of 5 minutes. This rigorous approach ensured that every surface and corner of the tooth received uniform exposure to the CAP treatment, as illustrated. Subsequently, following each treatment session, the treated tooth was transferred into a Falcon tube containing 3 ml of saline solution for further analysis.

### Treatment Protocol 2

In this case, the remaining three teeth were individually placed in 3 ml of saline as controls. These control samples were serially diluted and enumerated on plate count agar by incubating at 37°C for 18 h. Colony forming unit per ml (CFU/ml) were counted for each control sample next day. Same 3 teeth along with the saline in which they were kept, treated with cold plasma under the same conditions as Treatment 1. After treatment, each tooth was individually kept into falcon tube containing 3 ml of saline.

After treatment all control as well as treated sample were serially diluted up to -4 dilution and ten microliters of each dilution were dispersed in agar plate and incubated for 18 hrs. CFU/ml were counted for each sample next day after 18 h of incubation.

## Result

Optical emission spectroscopy (OES) was performed to detect reactive species in the Ar plasma with gas flow rate of 8 litres per minute (LPM) used for plasma generation during treatment. We specifically used a flow rate of 8 LPM in our experiments to ensure stable plasma generation, proper jet length (25mm), and a gas temperature of less than 42°C. Fig.4 depict the OES spectrum (200–950 nm) is dominated by

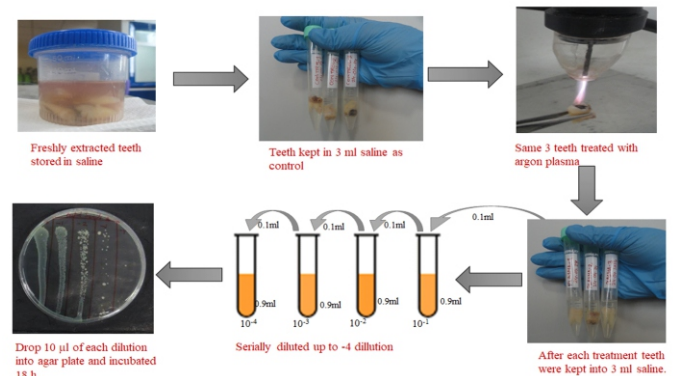


Fig.3: Procedural schematic of Treatment Protocol 2.

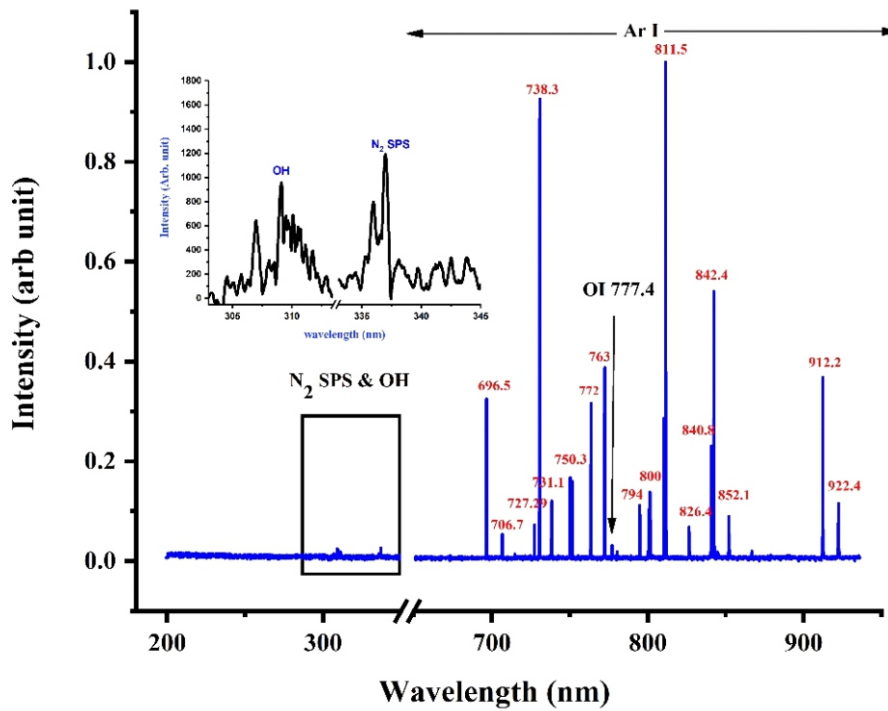


Fig.4: OES spectrum of the plasma used for bacterial inactivation. Inset photograph shows the zoomed spectrum of OH and N2 SPS.

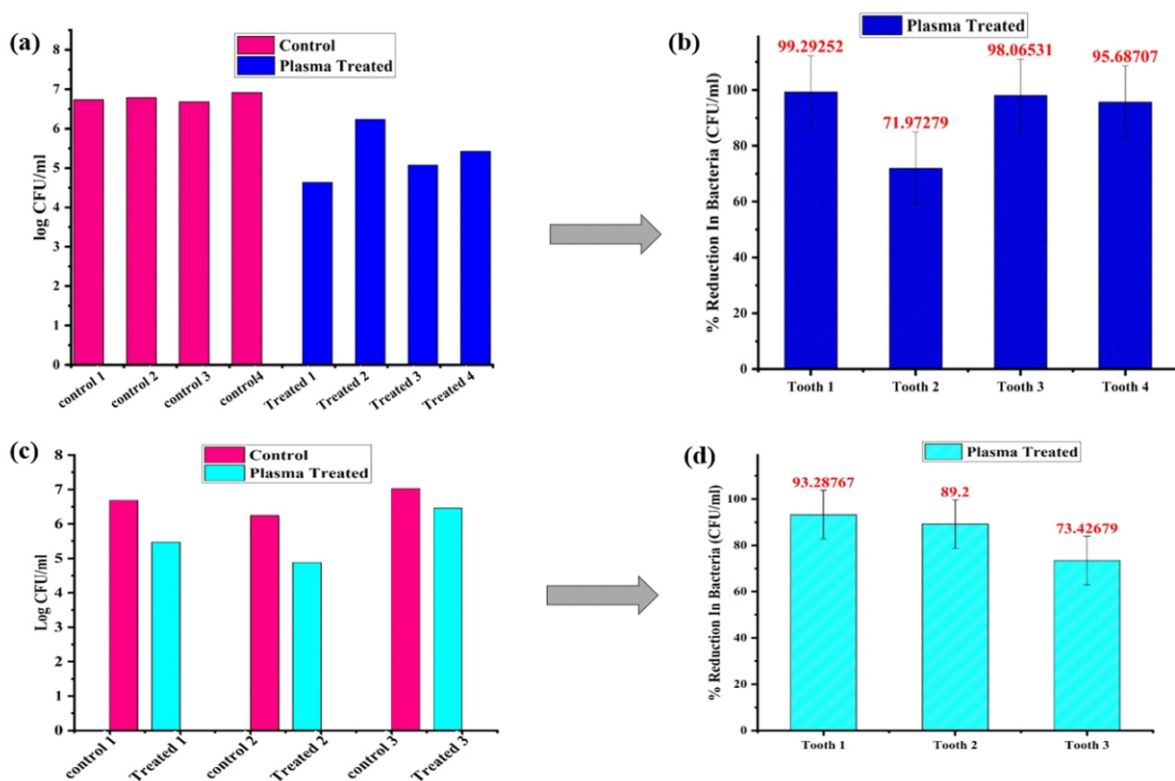


Fig.5: Reduction in bacterial counts post CAP treatment (a) TP1 (b) Percentage reduction in treated of TP 1 (c) TP 2 (d) Percentage reduction in treated of TP 2.

intense peaks of excited Ar atoms (4p–4s transitions) in the 696.5–922 nm range. UVA bands (335–340 nm) from N<sub>2</sub> second positive system via penning ionization, and a strong atomic oxygen (OI) peak (777.4 nm) from O<sub>2</sub> ionization was observed. An OH band (~309 nm) from air moisture was also seen. These OH and atomic oxygen (O) play crucial roles in bacterial inactivation by damaging lipids, proteins, and DNA [7,8]. OH radicals disrupt membrane lipids, induce DNA damage through oxidative stress, and break C–O, C–N, and

C–C bonds in peptidoglycan, as shown by MD simulations [9,10]. Additionally, UV photon could contribute to UV-induced DNA damage, such as pyrimidine dimer formation, contributes to inactivation by disrupting bacterial replication and transcription [11]. In the OES spectrum (Fig.3), OH emission was observed in the UVB band at ~309 nm, and the N<sub>2</sub> SPS band appeared in the UVA region. The generation of such biologically active species highlighting the capability of the developed CAP device to effectively inactivate bacteria.



In Fig.5, the percentage reduction in microbial count following CAP treatment for TP 1 and TP 2 is illustrated. The findings indicate that a 5-minute CAP treatment administered by the developed device effectively eradicates approximately 72% of pathogens, with some instances achieving a remarkable destruction efficiency exceeding 99%.

On average, the CAP treatment demonstrates a substantial pathogenic destruction efficiency of approximately 88.7%, encompassing both TP 1 and TP 2 protocols. These results underscore the potency and efficacy of the CAP treatment delivered by the developed device in significantly reducing microbial load on dental surfaces, thereby highlighting its potential utility in clinical settings for infection control and sterilization purposes.

### Conclusion

The developed cold atmospheric pressure plasma (CAP) device demonstrated significant efficacy in reducing microbial load on dental surfaces. Optical emission spectroscopy confirmed the presence of reactive species, such as excited Ar atoms, atomic oxygen, and OH radicals, which play a crucial role in bacterial inactivation. Experimental results revealed that a 5-minute CAP treatment achieved an average microbial reduction efficiency of 88.7% across both treatment protocols, with some cases exceeding 99% pathogen destruction. These findings highlight the potential of CAP as a promising, non-invasive tool for infection control and sterilization in dental applications, paving the way for its integration into clinical settings.

### References

- [1] R. Kar, N. Chand, A. Bute, N. Maiti, A. N. Rao, V. Nagar, R. Shashidhar, D. Patil, S. Ghosh, and A. Sharma, Cold plasma: Clean technology to destroy pathogenic micro-organisms, *Transactions of the Indian National Academy of Engineering*, vol. 5, pp. 327-331, 2020.
- [2] V. Viswanadh, R. P. Gaikwad, R. Kar, V. Nagar, C. D. Dhalkari, A. Banodkar, and N. Maiti, Cold atmospheric plasma: Its time-dependent effects on the elimination of bacterial colony on periodontal manual scalers, *Journal of Indian Society of Periodontology*, vol. 27, no. 5, pp. 503-507, 2023.
- [3] M. Laroussi, S. Bekeschus, M. Keidar, A. Bogaerts, A. Fridman, X. Lu, K. Ostrikov, M. Hori, K. Stapelmann, and V. Miller, Low-temperature plasma for biology, hygiene, and medicine: Perspective and roadmap, *IEEE Transactions on Radiation and Plasma Medical Sciences*, vol. 6, no. 2, pp. 127-157, 2021.
- [4] V. Bende, V. Nagar, V. Sekar, N. Maiti, and R. Kar, Design and Development of a Novel Tesla Coil-Based Cold Plasma Device for Plasma Medicine: Decoupling the Effect of Plasma-Generated Species, *IEEE Transactions on Plasma Science*, 52, 2024, 2144-2156.
- [5] S. Lata, S. Chakravorty, T. Mitra, P. K. Pradhan, S. Mohanty, P. Patel, E. Jha, P. K. Panda, S. K. Verma, and M. Suar, Aurora Borealis in dentistry: The applications of cold plasma in biomedicine, *Materials Today Bio*, vol. 13, pp. 100200, 2022.
- [6] N. Silva, J. Marques, M. B. da Cruz, H. Luís, S. Sérgio, and A. Mata, The applications of cold atmospheric plasma in dentistry, *Plasma Processes and Polymers*, vol. 20, no. 12, pp. e2300067, 2023.
- [7] F. Tampieri, M.-P. Ginebra, and C. Canal, Quantification of plasma-produced hydroxyl radicals in solution and their dependence on the pH, *Analytical chemistry*, vol. 93, no. 8, pp. 3666-3670, 2021.
- [8] P. Attri, Y. H. Kim, D. H. Park, J. H. Park, Y. J. Hong, H. S. Uhm, K.-N. Kim, A. Fridman, and E. H. Choi, Generation mechanism of hydroxyl radical species and its lifetime prediction during the plasma-initiated ultraviolet (UV) photolysis, *Scientific reports*, vol. 5, no. 1, pp. 1-8, 2015.
- [9] M. Laroussi, Mechanisms of interaction of cold plasma with bacteria. pp. 87-90.
- [10] M. Yusupov, Atomic scale simulations for a better insight in plasma medicine, *Universiteit Antwerpen*, 2014.
- [11] N. Bono, F. Ponti, C. Punta, and G. Candiani, Effect of UV irradiation and TiO<sub>2</sub>-photocatalysis on airborne bacteria and viruses: an overview, *Materials*, vol. 14, no. 5, pp. 1075, 2021.

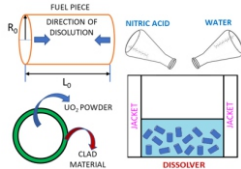
# भुक्तशेष ईंधन का विघटन

4

## भारतीय पीएचडब्ल्यूआर के लिए यूएनएफ के विघटन की दर का मूल्यांकन

आर्या दास\*, के. जयनारायणन

प्रक्रम अभिकल्पन प्रभाग, नाभिकीय पुनर्चक्रण बोर्ड, भाभा परमाणु अनुसंधान केंद्र, ट्रांबे, मुंबई-400 085, भारत



यूएनएफ के विशिष्ट कटे हुए ईंधन के टुकड़े और विलायक का योजनाबद्ध प्रदर्शन जहां कटे हुए टुकड़ों को पानी में गिराया जाता है और फिर कटे हुए ईंधन के विघटन के लिए सांद्रित नाइट्रिक अम्ल मिलाया जाता है।

### सारांश

ईंधन पुनर्चक्रण का एक महत्वपूर्ण चरण प्रयुक्त नाभिकीय ईंधन (यूएनएफ) का विघटन है तथा अभिक्रिया की दर अभिकारक की सांद्रता एवं अभिक्रिया तापमान पर निर्भर करती है। भारतीय पीएचडब्ल्यूआर भुक्तशेष ईंधन हेतु अभिक्रिया दर की गणना करने के लिए सिकुड़ते कोर मॉडल (एससीएस) का उपयोग किया गया। इसके अलावा, विकिरणित पीएचडब्ल्यूआर ईंधन के अभिक्रिया दर की गणना हेतु वैज्ञानिक साहित्यों में बताए गए विभिन्न तरीकों का भी उपयोग किया गया। दरार की उपस्थिति में दर में काफी वृद्धि हुई है। वर्तमान विधि का उपयोग, तापीय एवं तीव्र रिएक्टर के किसी भी भुक्त ईंधन के विघटन की दर का मूल्यांकन करने के लिए किया जा सकता है।

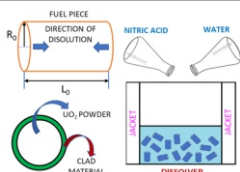
## Spent Fuel Dissolution

4

## Evaluation of Rate of Dissolution of UNF for Indian PHWR

Arya Das\*, K. Jayanarayanan

Process Design Division, Nuclear Recycle Board, Bhabha Atomic Research Centre, Trombay, Mumbai-400 085, INDIA



Schematic representation of typical chopped fuel piece of UNF and the dissolver where the chopped pieces are dropped into water and then concentrated nitric acid has been added for dissolution of chopped fuel.

### ABSTRACT

The dissolution of used nuclear fuel (UNF) is a key step for fuel reprocessing and the rate of reaction depends on the reactant concentration and reaction temperature. Shrinking core model (SCM) is used to calculate the rate of reaction for Indian PHWR spent fuel. Further, the different methods reported in the literature are also applied to compute the rate of reaction for irradiated PHWR fuel. The rate is increased significantly in the presence of cracking. The present method can be used to evaluate the rate of dissolution for any spent fuel of thermal and fast reactor.

KEYWORDS: Dissolution, UNF, PHWR, SCM, Fuel reprocessing

\*Author for Correspondence: Arya Das  
E-mail: aryadas@barc.gov.in

## Introduction

India adopted close fuel cycle to utilize the resources efficiently and also to meet the increasing energy demand [1-2]. The spent fuel reprocessing [3-4] is bridging between 1<sup>st</sup> and 2<sup>nd</sup> stages of Indian Nuclear Power Program [5]. In this context, the reprocessing of used nuclear fuel (UNF) has immense importance to satisfy the close fuel cycle and also to reduce the high-active solid waste. So, the reprocessing of UNF from fast reactor also needs to place. Hence, the journey for UNF reprocessing from thermal to fast reactor, the major step is the efficient dissolution of UNF. In dissolution process, the chopped fuel is dissolved into concentrated nitric acid to obtain (Uranium and Plutonium) metal nitrate is formed. The rate of dissolution primarily depends on temperature and acid concentration. It has been found that the rate of dissolution is reduced with increasing plutonium content during the dissolution of mixed oxide (MOX) fuel [6-7]. Moreover, it is practically not possible to dissolve the MOX fuel in HNO<sub>3</sub> alone when PuO<sub>2</sub> increases beyond 35% by weight [8]. One has to introduce strong oxidizing agent to increase the dissolution rate [9-11]. So, the type of oxidizing agent has an important role in the rate of dissolution reaction. India has only commercialized the nuclear power production through thermal reactors. So, the reprocessing of UNF from thermal reactor is only concerned in the present scenario to operate the fast reactor with MOX fuel which is a more attractive and wiser option for self-sustained power production.

The understanding of dissolution reaction is essential to design an efficient process. Several studies have been carried out in recent past to understand the mechanism of dissolution of various fuel compositions like UO<sub>2</sub>, PuO<sub>2</sub> or MOX. Researchers carried out extensive studies to find out the role of various parameters like surface area, fuel content, HNO<sub>3</sub> concentration, temperature, mixing rate, size of pellet. Mineo et. al. proposed a simple rate equation for LWR spent fuel accounting the cracks formed during irradiation cycles and suggested that the initial effective dissolution area may increase in presence of cracks [12]. The HNO<sub>3</sub> penetration into the cracks was not considered. Further, Desigan et. al. investigated the effect of mixing rate and the rate of dissolution beyond 600 rpm shows negligible changes [13]. They also reported that the reaction is expected to be both diffusion and reaction controlled based on the estimated value of activation energy (E<sub>a</sub>) as 26 kJ/mol. In general, if the E<sub>a</sub> > 40 kJ/mol, then the rate is guided by chemical reaction & when E<sub>a</sub> < 20 kJ/mol, it is diffusion controlled. Whereas E<sub>a</sub> lies between 20 and 40 kJ/mol, signifies a mixed controlled regime [14]. A few studies also reported that the reaction mechanism may belong to both the transport and the surface controlled [15-16]. Additionally, Desigan et. al. observed that the rate is chemical controlled and the rate of reaction is increased with increasing initial HNO<sub>3</sub> concentration [17]. So, the evaluation of rate of dissolution for PHWR fuel has not been attended. Hence, the present studies have been carried out to calculate the rate of dissolution reaction of UNF for Indian PHWR.

## Model and Methodology

The UNF containing 19 pins fuel bundles are chopped into pieces using gang chopper and the typical chopped pieces along with the dissolver are shown in Fig.1. The L<sub>0</sub> and R<sub>0</sub> define the initial length and initial radius of fuel piece. Here, the dissolution is considered as a semi-batch process where the HNO<sub>3</sub> is limiting reactant. The exothermic reaction for UO<sub>2</sub> fuel dissolution is as:

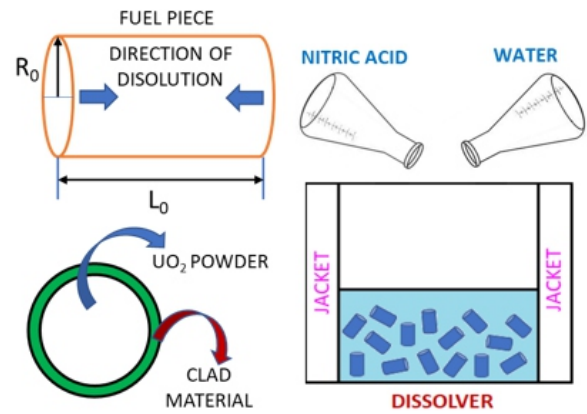
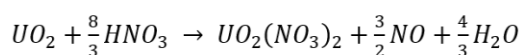


Fig.1: Schematic representation of typical chopped fuel piece of UNF and the dissolver where the chopped pieces are dropped into water and then concentrated nitric acid has been added for dissolution of chopped fuel.

The dissolution of UNF belongs to the domain of heterogeneous reaction where liquid and solid are reacted to produce liquid, solid and solid-liquid products. The behavior of solid-liquid interactions can be modelled using the shrinking core model (SCM) because the reaction takes place at the surface of the solid and the reaction zone moves into the solid core leaving behind the converted material. So, the SCM has been chosen to study the dissolution kinetics in HNO<sub>3</sub>. The dissolution reaction can be expressed as



The heterogeneous reaction has been carried out through five steps (Levenspiel, 1972) [18]. **Step 1:** Diffusion of reactant A through liquid film surrounding the solid surface, **Step 2:** Diffusion of reactant A to the surface of unreacted core, **Step 3:** Reaction of liquid reactant A with the solid reactant B at the reaction surface, **Step 4:** Diffusion of the product P formed during reaction through to reach solid surface and **Step 5:** Diffusion of product through liquid film to reach bulk phase. The above reaction is either diffusion controlled or reaction controlled. If it is diffusion controlled then Steps 1, 2, 4 and 5 will be the rate determining steps whereas Step 3 will be the controlling step when it is reaction controlled. A schematic representation of the heterogeneous reaction is provided in Fig.2.

Further, the rate of reaction is directly proportional to the effective dissolution area and the rate equation can be expressed according to the stoichiometry of the reaction as

$$\frac{1}{s} \frac{dN_B}{dt} = \frac{1}{n} k C_A = k_L (C_{A0} - C_{AS}) \quad (1)$$

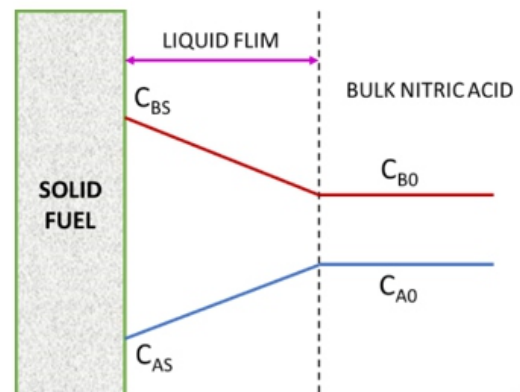


Fig.2: The schematic representation of the solid-liquid heterogeneous reaction with respective concentrations at solid surface at liquid film and at bulk liquid.



Where S denotes the dissolution area,  $N_B$  is the moles of solid B reacting at time t, n is the stoichiometric coefficient of liquid reactant A and k denotes rate constant.  $C_{A0}$  and  $C_{AS}$  are the concentration of liquid in the bulk and at the solid surface respectively. Here, the liquid–solid interaction is only possible through cross sectional area of the chopped fuel piece because the fuel has clad material (see Fig.1) and liquid is unable to access from axial side. Also, the acid attack through the pellet-clad gap has been neglected due to very narrow passage. So, the dissolution through axial direction is not considered here. Further, some assumptions have been made to solve the rate equation as: 1) The diffusion resistance of  $HNO_3$  cannot be considered because no ash is formed on the surface of unreacted core. 2) The bulk resistance of reactant A is neglected under air sparging condition and 3) The diffusion resistance of product (metal nitrate) is also neglected under air sparging condition. Hence, the rate of reaction is only controlled by reaction and the reaction is pseudo-first order with respect to  $HNO_3$ . Design et al also suggested that the dissolution reaction is controlled by reaction in the temperature range of 233 – 363 K based on activation energy calculation [13]. Therefore, the rate equation (eqn. 1) can be solved by considering reaction controlled.

Now, the rate equation provided by Levenspiel is for spherical geometry [18]. So, the equations are modified according to the cylindrical geometry.

The eqn. (1) can be arranged based on  $C_{A0}$  is nearly equal to  $C_{AS}$ .

$$\frac{1}{(2\pi r^2)} \frac{dN_B}{dt} = \frac{1}{n} k C_A \quad (2)$$

As per the assumption of SCM, it can be written that

$$N_B = \rho_B V \text{ and } \frac{L_0}{R_0} = \frac{l}{r} = \delta \quad (3)$$

Where,  $\rho_B$  is the molar density of B in solid and V denotes its volume. The l and r are the length and radius of the shrinking particle at any given time and  $\delta$  is the aspect ratio of the fuel piece at any instant.  $N_B$  can be rewritten in terms of r as

$$-dN_B = -3\pi\rho_B\delta r^2 dr \quad (4)$$

The rate of the reaction in terms of shrinking radius of the unreacted core can be expressed as

$$\frac{r}{R} = (1 - X_B)^{\frac{1}{3}} = 1 - \frac{2}{3} \frac{kC_B}{n\delta\rho_B R} t \quad (5)$$

The eqn. (5) denotes the rate equation for dissolution of fuel pieces with clad.  $X_B$  is the fraction of moles of reactant B that has reacted at time t. In another way,  $(1-X_B)$  is the unreacted fraction of reactant B present at time t. The above equation can be arranged for the dissolution of UNF in nitric acid as.

$$\left(1 - \frac{[U]_t}{[U]_f}\right)^{\frac{1}{3}} = 1 - \frac{2}{3} \frac{kC_B}{n\delta\rho_B R} t \quad (6)$$

$[U]_t$  and  $[U]_f$  are molar concentration of uranium at any time t and at the end of the dissolution reaction respectively. The rate constant of the dissolution reaction can be calculated from the slope of eqn. (6).

Further, the rate of dissolution reaction occurred at the fuel surface can be expressed as [12]:

$$\frac{dW}{dt} = W_0 \frac{d\beta}{dt} = a \cdot IDR \quad (7)$$

Where, W signifies the dissolved weight of spent fuel,  $W_0$  is the initial weight of U in the spent fuel.  $\beta$  denotes the fraction of dissolved fuel at time t and a is the effective dissolution area. IDR signifies the dissolution per unit area [12]. The effective dissolution area can be expressed as:

$$a = a_0 F(\beta) \quad (8)$$

Where,  $a_0$  denotes the initial effective dissolution area and  $F(\beta)$  is the ratio of effective dissolution area at a fraction of  $\beta$  to the initial effective dissolution area. It is worthy to find out the difference in effective dissolution area for unirradiated and irradiated fuels. It alters significantly from unirradiated fuel because the irradiated fuels have cracks which may affect the dissolution area. It is expected that  $a_0$  can be increased in presence of cracks which finally influences the rate of reaction. The cracks may be present in radial and axial directions. The number of cracks and the angle between two cracks are the function of the rod power experienced in the reactor [12]. It has been assumed that the dissolution may occur in the axial and radial directions as indicated by arrows in the Fig.1. Now, the equation developed by Mineo et al. can be expressed as [12].

$$(1 - \beta)^{(1-p)} = 1 - (1 - p) \frac{a_0}{W_0} k (C_H)^n t \quad (9)$$

So, the profile obtained by plotting a graph between  $(1-\beta)^{(1-p)}$  and t is a straight line with an intercept 1.0. The rate constant of irradiated fuel can be evaluated from the slope of eqn. (9).

### Experimental

In the present dissolution experiments, typical UNF from Indian PHWR (220 MWe) have been used. The physical characteristics of the fuel piece are given in Table 1.

The dissolution has been carried out in recirculation type SS dissolver for 100 fuel bundles and the experiment has been monitored through PLC/SCADA system. The air sparger in the

Table 1: Physical properties of chopped fuel piece.

Parameters	Value
Diameter of fuel pin (D), mm	14.47
Length of fuel piece (L), mm	40
Stoichiometric coefficient (n)	2.67
Molar density of B ( $\rho_B$ ), gm/cc	10.5
Aspect Ratio ( $\delta = L/R$ )	5.53

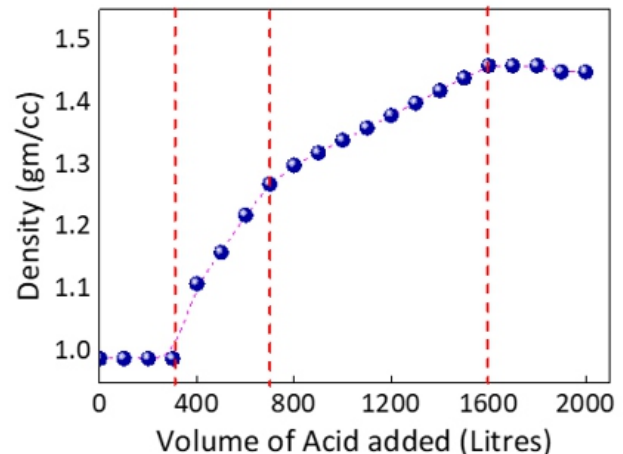


Fig.3: Density profile of spent fuel dissolution as a function of volume of 12M nitric acid.

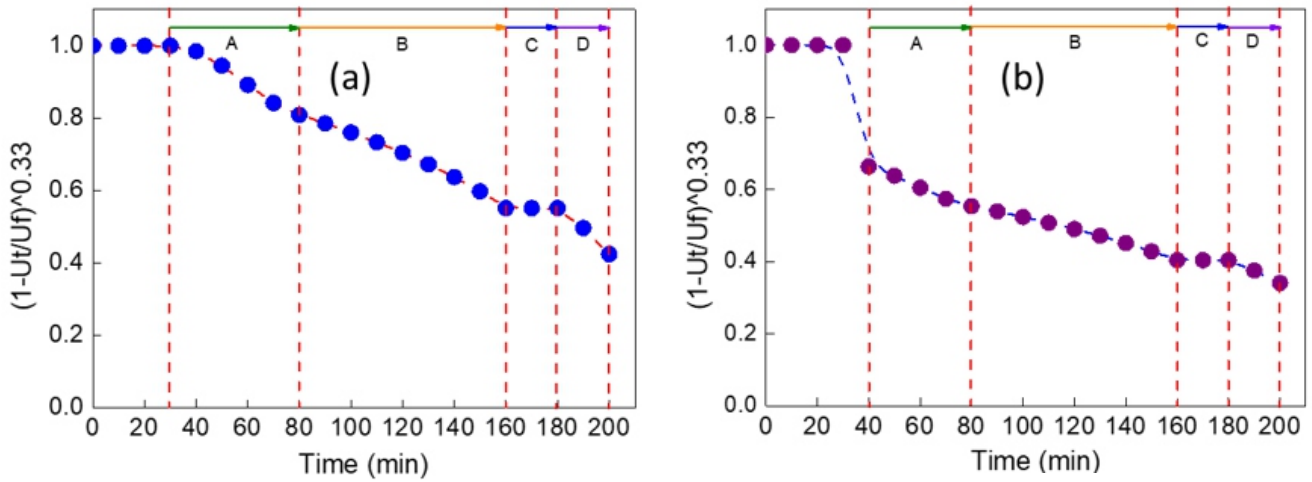


Fig.4: The Profile of  $[1 - ([U]t/[U]f)]^{1/3}$  as a function of time (t) illustrating a decreasing trend (a) calculation based on uranium density in solution and (b) based on the solution density of uranyl nitrate.

dissolver has been kept on during the experiment for proper mixing of the dissolver content. The off-gas generated during the dissolver has been taken care in the off-gas treatment system. Initially the dissolver holds some volume of strip acid to reduce the impact of chopped fuel pieces. Then, the volume of 12M HNO<sub>3</sub> added in the dissolver is 2000 liters at a rate of 10 liter/min. The exothermic reaction has been started and continued till the temperature rises. No external heating or boiling has been carried out in the present experiment. The data has been collected from the SCADA system until the exothermic reaction is going on.

**Results & Discussions**

The dissolution reaction has been initiated after achieving a certain solution acidity. The density of U dissolved in nitric acid solution has been plotted against the volume of acid addition and an increasing trend is appeared (see Fig.3). It is obvious because the rate of reaction is proportional to the acidity of the solution. Further, it has been observed that the reaction is initiated after around 300 liters of acid addition and the overall acidity of the solution at that moment is approximately 2M. So, it is the minimum acid molarity required to start the exothermic reaction. Again, the slope is higher at initial stage because the rate of reaction is very high due to the high solid concentration. Then, the slope is comparatively lower because the increasing HNO<sub>3</sub> concentration and the decreasing solid concentration counter each other. Finally, the slope becomes flat which indicates the completion of exothermic reaction. The different zones based on variable slopes has been marked with vertical red dashed line. It has been noticed that the dissolution is achieved nearly 93%, not 100%. Because the rate of reaction is very slow due to low solid inventory and low overall acidity. The rate can only be increased by applying the external energy like heating or boiling which increases the temperature and also increases the rate constant. But in the present study, we are only interested to calculate the rate constant of exothermic reaction in absence of any external energy input.

So, the rate of reaction is varied with the time length of dissolution. According to the eqn. (6), the  $[1 - ([U]t/[U]f)]^{1/3}$  has been computed from the experimental data and plotted against the time. The profile is displayed in Fig.4(a) and the rate of reaction can be evaluated from the slope of curve. The profile shows a decreasing trend with variable slopes and the various zones are marked with vertical red dashed line starting from Zone-A to Zone-D in Fig.4. The rate constant is obtained as  $3.48 \times 10^{-3}$  m/s using time average method. Further, the slopes have been calculated at different zones & it is ranging from

-0.00269 to -0.00635. Then, the rate is appeared as  $5.27 \times 10^{-3}$  m/s using zone average method. So, the rate of dissolution obtained from time average method underestimates the rate obtained from zone average method. Next, the rate has been computed using the solution density of uranyl nitrate [see Fig.4(b)]. It has been found that the density is reflected after 30 minutes and a sudden fall in profile has been observed which is absent when the calculation has been carried out using uranium density. Here, the calculated rate is  $2.67 \times 10^{-3}$  m/s which underestimates the value obtained from uranium density. The rate obtained from zone average is  $5.7 \times 10^{-3}$  m/s which is in good agreement with the calculation using uranium density. The reported dissolution rate for UO<sub>2</sub> pellet at 70°C is  $3.08 \times 10^{-3}$  m/s with initial nitric acid concentration of 10.28M [13]. It is obvious because higher concentration of HNO<sub>3</sub> (12M) has been used in the present study for dissolution. Hence, the zone average method is quite accurate for rate calculation.

In addition to that, the rate of reaction for irradiated UNF containing cracks has also been evaluated to find out the effect of cracks on the rate constant. The rate can be computed using eqn. (9) where the crack is considered in the radial direction. The inputs are provided in Table 2.

According to the eqn. (9), a profile has been generated when  $(1-\beta)^{(1-p)}$  plotted as y-axis and t as x-axis using our experimental data for both the angles of 90° and 180° and it is displayed in Fig.5(a) and Fig.5(b) respectively. The trends are similar for both the angles. The rate of reaction has been calculated from the slope of the curve using zone average method and they are  $4.1 \times 10^{-2}$  m/s for 90° and  $3.1 \times 10^{-2}$  m/s for 180°. The rate of dissolution is quite high in the presence of cracks and it is around 10 times higher compared to that of the non-cracking condition. But there is no significant change in

Table 2: Inputs for irradiated fuel.

Parameters	Value
a <sub>0</sub> (m <sup>2</sup> )	22.73 x 10 <sup>6</sup>
W <sub>0</sub> (gm)	64
p	0.4896 (θ = 90°) 0.3352 (θ = 180°)
Temperature (T), K	333
Conc. of HNO <sub>3</sub> (C <sub>H</sub> ), M	6.5
n	2.67

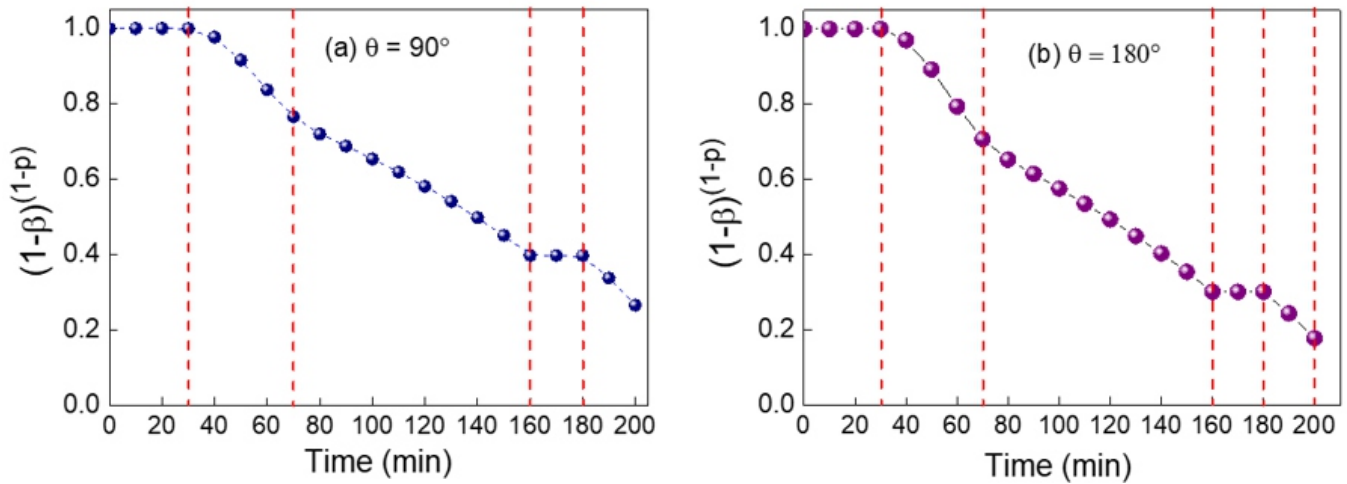


Fig.5: The Profile of  $[1 - ([U]t/[U]f)]^{1/3}$  as a function of time (t) illustrating a decreasing trend (a) calculation based on  $\theta = 90^\circ$  and (b) based on  $\theta = 180^\circ$ .

Table 3: Rate of dissolution calculated using three models in presence of cracking and rate of dissolution evaluated in present study.

Rate of Dissolution (m/s)	Method	Ohsaki Model	Fukasawa Model	Nemoto Model	Present Study
$(\theta = 90)$	Time average	0.062	0.014	0.101	0.018
	Zone average	0.124	0.033	0.190	0.041
$(\theta = 180)$	Time average	0.073	0.016	0.119	0.021
	Zone average	0.095	0.025	0.146	0.031

the rate of reaction for  $90^\circ$  and  $180^\circ$ . So, it can be stated that the rate of dissolution has negligible dependency on the angle between cracks. It can be noted that the rate calculation using zone average method is more accurate.

Further, Mineo et al reported various prescription to calculate the rate of dissolution reaction based on temperature and nitric acid concentrations [12]. So, the rate has been computed using all the models proposed by Ohsaki et al [19], Fukasawa et al [20] and Nemoto et al [21] and displayed in Table 3. The rate of dissolution predicted by Ohsaki and Nemoto is overestimating the rate calculated from the experiment whereas Fukasawa model is in good agreement with the present study. Because the stoichiometry of the reaction considered by Fukasawa et al converges to our experimental studies. The stoichiometric ratio for other models is comparatively low which leads to a high rate of dissolution reaction.

**Conclusions**

The rate of dissolution reaction has been computed for UNF of Indian PHWR using shrinking core model (SCM) and found the rate of reaction is in the range of  $5.27 \times 10^{-3}$  to  $5.70 \times 10^{-3}$  m/s using zone average method. The calculated rate of reaction obtained from experiment is in well agreement with the reported value. The zone average method is quite promising for calculation of rate of reaction. Further, the rate of reaction for irradiated fuel has been improved in presence of cracks and the rate is obtained in the range of  $3.1 \times 10^{-2}$  to  $4.1 \times 10^{-2}$  m/s. Hence, the present methodology can be applied to calculate the rate of reaction for the dissolution of fast reactor used nuclear fuel during reprocessing.

**Acknowledgement**

The authors are thankful to Smt. B. M. Biswas, AGM (Reprocessing Design), NRB, Shri H. R. Pimparkar, ED (Design), NRB and Shri U. Dani, Chief Executive, NRB for

encouragement. We are also especially thankful to Shri P. K. Singh, Operation Superintendent, PREFRE-II, Tarapur and Shri S. Gulati, AGM, R&WM, Tarapur and all the operation staffs of PREFRE-II for their tremendous support to carry out the experiments.

**References**

- Banerjee, S., Gupta, H. P., 2017a. Prog. Nucl. Ener. 101 (Part A), 4–18.
- Vijayan, P. K., Shivakumar V., Basu, S., Sinha, R. K., 2017. Progress in Nuclear Energy 1-10.
- Simpson, M. F., Law, J. D., 2010. Nuclear Fuel Reprocessing, Idaho National Laboratory.
- Zabunoglu, O. H., 1988. "Reprocessing of long-cooled nuclear fuel: Process description and plant design" Retrospective Theses and Dissertations.
- Maitra, R., 2009. "Indian Nuclear Program at a Crossroads" Executive Intelligence Review, archived from the original on 2013, retrieved 2012.
- Ryan, J. L., Bray, L. A., 1980. ACS (Am. Chem. Soc.) Symp. Ser. 117, 449.
- Ikeuchi, H., Shibata, A., Sano, Y., Koizumi, T., 2012. Procedia Chem. 7, 77–83.
- Uriarte, A. L., Rainey, R. H., 1965. Oak Ridge National Laboratory report ORNL-3695.
- Harmon, H. D., 1975a. Savannah River Laboratory Report DP-1371. Harmon, H. D., 1975b. Savannah River Laboratory Report DP-1383.
- Bray, L. A., Ryan, J. L., 1982. In: Navratil, J. D., Schulz, W. W. (Eds.), vol. 6. Harwood Academic Publishers, London, p. 129.
- Bray, L. A., Ryan, J. L., Wheelwright, E.J., 1986. Pacific Northwest Laboratory report PNL-6027.



12. Mineo, H., Isogai, H., Morita, Y., Uchiyama, G., 2004. *Journal of Nuclear Science and Technology*, 41(2), 126-134.
13. Desigan, N., Augustine, E., Murali, R., Pandey, N. K., Mudali, U. K., Natarajan, R., Joshi, J. B., 2015. *Progress in Nuclear Energy* 83, 52-58.
14. Yu, J. F., Ji, C., 1992. *Chem. J. Chin. Univ.* 13, 224-226.
15. Berner, R. A., 1978. *Am. J. Sci.* 278, 1235-1252.
16. Jordan, G., Rammensee, W., 1996. *Geochim. Cosmochim. Ac.* 60, 5055-5062.
17. Desigan, N., Maji, D., Ananthasivan, K., Pandey, N. K., Mudali, U. K., Joshi, J. B., 2019. *Progress in Nuclear Energy* 116, 1-9.
18. Octave Levenspiel, *Chemical Reaction Engineering*, Ind. Eng. Chem. Res. 1999, 38, 11, 4140-4143.
19. Ohsaki, H., Private communication.
20. Fukasawa, T., Ozawa, Y., 1986. *J. Radioanal. Nucl. Chem., Lett.*, 106[6], 345.
21. Nemoto, S., Shibata, A., Shioura, T., Okamoto, F., Tanaka, Y., 1995. *Donen-Gihou*, 95, 43.

# अपशिष्ट उपचार विधि

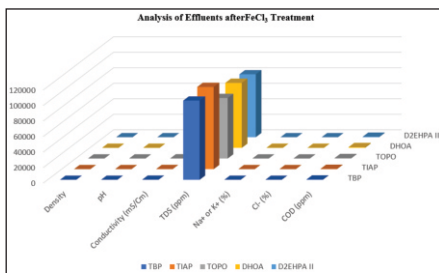
5

## विलायक उत्पादन संयंत्र अपशिष्ट की भौतिक रासायनिक विशेषताएँ और इसकी अपशिष्ट उपचार विधि

ए.एस.जे. हैमिल्टन<sup>1\*</sup>, एम. श्रीनिवास<sup>1</sup>, एस. सुकुमार<sup>2</sup> एवं जी. वेंकटेशु<sup>2\*</sup>

<sup>1</sup>बिट्स पिलानी, हैदराबाद, भारत

<sup>2</sup>भारी पानी संयंत्र, तुतीकोरिन, भारत



FeCl<sub>3</sub> उपचार के बाद एक अपशिष्ट की भौतिक रासायनिक विशेषताएँ।

### सारांश

भारी जल संयंत्र (एचडब्ल्यूपी) के अंदर काम करने वाला विलायक उत्पादन संयंत्र (एसपीपी), संवृत नाभिकीय ईंधन चक्र प्रक्रमों के अग्र भाग और पश्च भाग जैसी विभिन्न नाभिकीय ऊर्जा गतिविधियों के लिए विलायक के संश्लेषण में महत्वपूर्ण भूमिका निभाता है। विलायकों के उत्पादन से सोडियम क्लोराइड के साथ जलीय घोल के रूप में कार्बनिक अवशेष के साथ पोटेशियम क्लोराइड लवण अपशिष्ट उत्पन्न हुआ है। उपचार से पहले अपशिष्टों से रासायनिक ऑक्सीजन मांग (सीओडी) 2000 से 14000 ppm की बहुत उच्च सीमा प्रदर्शित करती है, लेकिन फेरिक क्लोराइड (FeCl<sub>3</sub>) उपचार के बाद एक बार के FeCl<sub>3</sub> अवक्षेपण में 350 ppm से 900 ppm की सीमा में स्तर को क्रमिक रूप से कम हुआ है और साथ ही 2100 वर्ग मीटर सतह क्षेत्र के साथ सौर तालाब में छोड़े गए उपचारित अपशिष्ट विसर्जन किया गया और उत्पन्न लवणों का उपयोग कई फ्रेन्चाइजी गतिविधियों में किया जाएगा। FeCl<sub>3</sub> का उपयोग कर रासायनिक उपचार सीओडी को कम करने में सफल सिद्ध हुआ और pH के स्तर को 6 से 7 की सीमा में नीचे लाया है लेकिन किसी भी तरह से टीएनपीसीबी (तमिलनाडु प्रदूषण नियंत्रण बोर्ड) की निर्धारित सीओडी सीमा के साथ सुरक्षित नहीं है जो कि 250 ppm से कम है। यह अध्ययन अपशिष्ट की भौतिक रासायनिक विशेषताएँ सटीक प्रदूषक सांद्रता स्तर और मौजूदा अपशिष्ट उपचार को निर्धारित करती हैं जो प्रदूषक सांद्रता को सफलतापूर्वक कम करने में व्यवहार्य है और इस अध्ययन में प्राप्त परिणाम भविष्य में एक उन्नत अपशिष्ट उपचार प्रणाली विकसित करने हेतु एक डेटाबेस के रूप में काम करेगा।

## Effluent Treatment Method

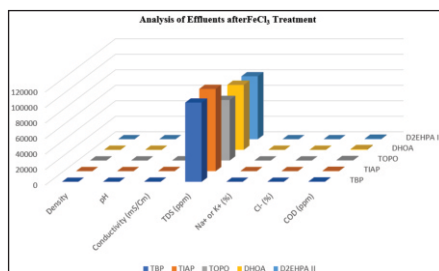
5

## Physicochemical Characteristics of Solvent Production Plant Effluent & its Effluent Treatment Method

A.S.J. Hamilton<sup>1\*</sup>, M. Srinivas<sup>1</sup>, S. Sukumar<sup>2</sup> and G. Venketesu<sup>2\*</sup>

<sup>1</sup>BITS Pilani, Hyderabad, INDIA

<sup>2</sup>Heavy Water Plant, Tuticorin, INDIA



Physicochemical characteristics of an effluent after FeCl<sub>3</sub> treatment.

### ABSTRACT

The Solvent Production Plant (SPP) functioning inside the Heavy Water Plant (HWP), plays a crucial role in synthesizing solvent for various Atomic Energy activities like front end and back end of closed nuclear fuel cycle processes. The effluent generated from the production of solvents is in the form of aqueous solution with sodium chloride, potassium chloride salts with organic traces. The Chemical Oxygen Demand (COD) exhibits a very high range of 2000 to 14000 ppm from the effluents before treatment but after the Ferric Chloride (FeCl<sub>3</sub>) treatment the level has been successively reduced in the range of 350 ppm to 900 ppm in one time FeCl<sub>3</sub> precipitation as well as the treated wastewater discharged to the solar pond with 2100 m<sup>2</sup> surface area and generated salts will be scrapped and used the same in several franchise activities. The Chemical Treatment of using FeCl<sub>3</sub> was successfully proved in reduction of COD and brings down the level of pH in the range of 6-7 but anyhow not aligned with the prescribed COD limit of TNPCB (Tamil Nadu Pollution Control board) which is less than 250 ppm. The physicochemical characteristics of effluent in this study determines the precise pollutant concentration level and the existing effluent treatment viable in reducing the pollutant concentration successfully and the results obtained in this study would serve as a database for developing for future scope of developing an advanced effluent treatment system.

KEYWORDS: SPP, HWP Tuticorin, Effluents, FeCl<sub>3</sub> precipitation, COD

\*Authors for Correspondence: A.S.J. Hamilton & G. Venketesu

E-mail: p20220429@hyderabad.bits-pilani.ac.in & gm@tut.hwb.gov.in

## Introduction

The Solvent Production Plant (SPP) in Heavy Water Plant (HWP) was mainly established intended in production of solvents like Tributyl Phosphate (TBP), Tri Iso Amy Phosphate (TIAP), Tri Octyl Phosphine Oxide (TOPO), DI Hexyl Octanamide (DHOA), Mono ester of Di-2-Ethyl Hexyl Phosphonic Acid (D<sub>2</sub>EHPA-II) for important applications in DAE (Department of Atomic Energy) activities in front end and back end of nuclear fuel cycles specifically for the recovery of special nuclear materials.

## Role of Heavy Water Plant in Solvent Production and the Effluents Generation

In the production of solvents, the effluents generation are inevitable in the form of hyper saline NaCl, KCl with organic traces due to hydrolysis, alkali and water washing in order to obtain a pure product. The Chemical Oxygen Demand (COD) of the effluents ranges from 2000 to 14000 ppm which is multi-fold times higher than the prescribed limit 250 ppm of Tamil Nadu Pollution Control Board (TNPCB). The current R&D studies were undertaken to treat the effluents by Chemical treatment through Ferric chloride precipitation method. This Ferric chloride (FeCl<sub>3</sub>) precipitation process is in successful reduction of COD level but not aligned with the limit of TNPCB in a single step precipitation. The sludge generated out in the FeCl<sub>3</sub> precipitation treatment from the SPP is calculated as around 400 MT per annum.

In the purview of R& D studies carried out with the effluents of SPP, it is clearly noticed that the areas mandate to focus are the concept of green chemistry, sustainability, eco-friendly and economically feasible to determine an alternate effluent treatment system suitable to the prescribed limit of TNPCB (Tamil Nadu Pollution Control Board) and Central Pollution Control Board (CPCB).

## Methods and Materials

The methodology followed in studying physicochemical characteristics of an effluent elucidates to ensure the right quality and quantity of effluents and studying thoroughly with all the aspects into consideration [1]. The various factors which are to be considered for the discharge of effluents for any purpose are:

- The quantity of effluents discharged per day [2].
- Seasonal variation in quantity as well as quality [3].
- Analysis of important parameters suitable to the prescribed limit of Pollution Control Agencies [4].
- Influence of Industrial wastewater in environmental impacts and ecological imbalance [5].
- Cost involved in continuous supply of discharge in post treatment and cost effectiveness in sludge disposal [6].

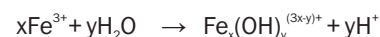
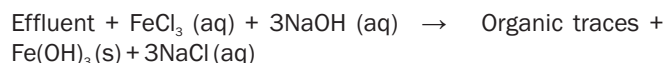
The primary data related to n-butanol effluents were taken from the lab study of PC & AL of SPP unit (mostly from the n-butanol traces discharged in solvent production shown in table 1) for the purpose of calibration assessment and the

secondary data concerned with the quantification of parameters like density (Mettler Toledo Weighing Machine), pH (pH meter LABINDIA), Conductivity (Conductivity meter LABINDIA), TDS - Total Dissolved Solids (Standard Glass fibre filtration and evaporation method), Sodium ion Na<sup>+</sup> (Flame Photometer ELICO), Chloride ion Cl<sup>-</sup> (Argentometric Titration Method), COD (standard titration method using reagents of Potassium Dichromate K<sub>2</sub>Cr<sub>2</sub>O<sub>7</sub>, mixture of silver sulphate AgSO<sub>4</sub> and sulphuric acid H<sub>2</sub>SO<sub>4</sub>, Ferroin indicator [Fe(C<sub>12</sub>H<sub>8</sub>N<sub>2</sub>)<sub>3</sub>SO<sub>4</sub>]). These parameters were estimated in simulated samples of effluent from production of TBP, TIAP, TOPO, DHOA, D<sub>2</sub>EHPA-II.

## Ferric Chloride Precipitation (FeCl<sub>3</sub>) Precipitation Method of Treating Effluents from SPP

The mechanism of removal of organic contaminants in saline solutions were done by using Ferric Chloride (FeCl<sub>3</sub>) precipitation method [7,8]. In the lab study addition of FeCl<sub>3</sub> in the aqueous medium of effluent and further adjusting pH to neutral value, the trivalent metal cations hydrolysed to form positively charged monomeric and polymeric species that have a very large surface area and they tend to adsorb negatively charged organic matter and form insoluble precipitates which eventually settle down as sludge.

In our present study for simple understanding of sludge generation, the following equation may suffice the context of FeCl<sub>3</sub> role in chemical precipitation.



The chemical precipitation of butanol derivatives most predominant effluent from Tri Butyl Phosphate (TBP) effluent is through the adsorption of butanol ions by metal ions to form metal butanolates.



The pH influences the type of metal hydroxide formed when the metal salt is dissolved in water. The earlier studies influence the pH on chemical coagulation [8]. The organic effluent precipitation rate increases with increase in pH at very high pH values. This may be due to increased ionization of butanol ions into butanolate ions under higher alkaline conditions. The higher availability of butanolic ions at higher pH conditions increases the conversion of metal ions to metal butanolates. The chemical precipitation is highly dependent on the dose of FeCl<sub>3</sub>. The use of high doses of metal salt improves the rate of precipitation by two mechanisms such as: a) increasing concentration of metal hydroxide and aggregation rate, and b) by enmeshing the organic ligands into large aggregates by sweep floc coagulation [8]. The lab investigation of Ferric Chloride (FeCl<sub>3</sub>) precipitation procedure is followed by the flowchart below in Fig.1.

Table 1: Preliminary study from Butanol effluents (before and after treatment).

Parameters	Density (g/cc)	pH	Conductivity (ppm)	TDS (ppm)	Na <sup>+</sup> (%)	Cl <sup>-</sup> (%)	COD (ppm)
Before FeCl <sub>3</sub> treatment	1.045	7.3	88	58,667	2.0	2.0	8000
After FeCl <sub>3</sub> treatment	1.058	6.9	142.9	95,473	5.6	3.2	556



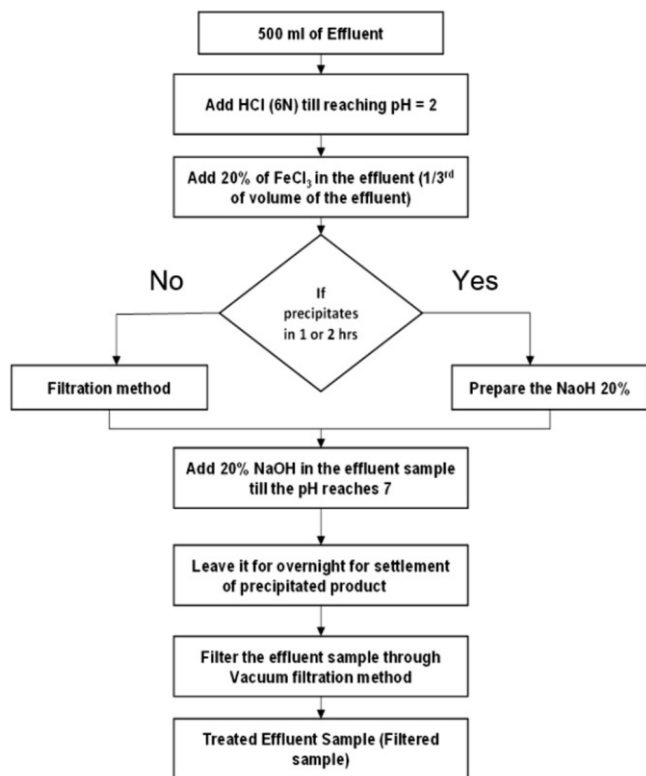


Fig.1: FeCl<sub>3</sub> procedure in Lab scale method for investigation of the effluent treatment.

**Results and Discussion**

The effluents from the Solvent Production Plant (SPP) of a Heavy Water Plant (HWP) Tuticorin were analyzed in Process Control and Analytical (PC & AL) Laboratory and results were estimated in both pre and post FeCl<sub>3</sub> precipitation method according to the pollutant concentration of each solvent effluent category and solid waste generated from the FeCl<sub>3</sub> precipitation of the effluent discharged at the disposal site.

The effluent management system of ETP (Effluent Treatment Plant) in a SPP unit envisaged to control and monitor effluents from the well-planned laboratory studies of physicochemical characteristics before and after FeCl<sub>3</sub> treatment (Table 2).

**Effluent Generation and Analysis of parameters of an effluent before FeCl<sub>3</sub> treatment**

The effluents generated from the solvent production due to the process of esterification, distillation, substitution reaction (adding sodium as well as medium like Tetra hydra Furan, Triethyl amine, hexane), alkylation, water washing, recovery through batch distillation, alkali hydrolysis, acid hydrolysis, final water washing, purification of a crude product and cooling & drawl of product.

The predominant nature of the effluents mainly composed of Sodium salts (NaCl) and organic traces of nuclear solvents left out in the chain of synthesis in process operation and production of solvents. The sample analyzed from the effluents of SPP in the PC & AL laboratory of Heavy Water Plant (Tuticorin) clearly pointed the pollutant concentration (Table 2) and the high range of COD and TDS (Fig.2) indispensably shows organic traces mainly discharged with the effluents of sodium salt (NaCl) as well as other chemicals used for synthesis operation and reaction processes.

**Analysis of Parameters of an effluent after FeCl<sub>3</sub> Treatment**

The chemical precipitation was brought about by mixing a predetermined quantity of Ferric Chloride (FeCl<sub>3</sub>) to 500 ml effluent solution at a particular pH as per the method studied in the section 3. The addition of FeCl<sub>3</sub> initially produced dark brown floc which eventually forms larger aggregates and settles down as sludge.

The precipitate can be separated from the solution by filtration (vacuum filtration method). The supernatant obtained from the centrifugation was clear and lighter in colour. The characteristics of effluents from the five solvent types have been investigated in laboratory methods of FeCl<sub>3</sub> chemical treatment method (Table 4). It was observed that the addition of FeCl<sub>3</sub> reduced the pH and COD to a reasonable level (Fig. 3). It is predicted that the solid waste generated from the precipitation ranges from 370 to 565 kg for the 7m<sup>3</sup>/day of effluent discharged after treatment (table 3) to the solar pond of surface area 2100 m<sup>2</sup> in real time effluent treatment. It is of most important concern that the COD of sludge ranges from 850 to 900 pm but there is no concern for the environmental effects from the sludge since the sludge is being scrapped and sold to other chemical or cement industries for further extraction of useful source for reuse in further operations. The

Table 2: Pollutant concentration analysis before and after FeCl<sub>3</sub> Treatment.

Name of the solvent preparation	EFFLUENT PARAMETERS													
	Density (g/cc)		pH		Conductivity (mS/cm)		TDS (ppm)		Na <sup>+</sup> (%)		Cl <sup>-</sup> (%)		COD (ppm)	
	BT*	AT*	BT	AT	BT	AT	BT	AT	BT	AT	BT	AT	BT	AT
TBP	1.078	1.092	10.5	7.01	100.7	153.5	67,133.33	102,133.4	4.1	3.72	0.01	6.4	4339	352
TIAP	1.062	1.085	10.4	7.0	102	158.2	68,340	1,05,994	4.5	5.8	0.011	3.5	4482	370
TOPO	1.0108	1.0364	10.9	6.6	32.9	117	21,993.4	78,000	1.4	2.5	0.0085	4.16	14,144	520
DHOA	1.008	1.034	3.15	4.17	68.04	125	45586.8	83750	1.58	2.87	2.4	4.5	13,200	900
D2EHPA-II	1.024	1.0306	8.01	7.6	108	121.1	72000	81137	2.56	2.6	3.0	5.6	2600	600

\*BT-Before Treatment

\*AT-After Treatment

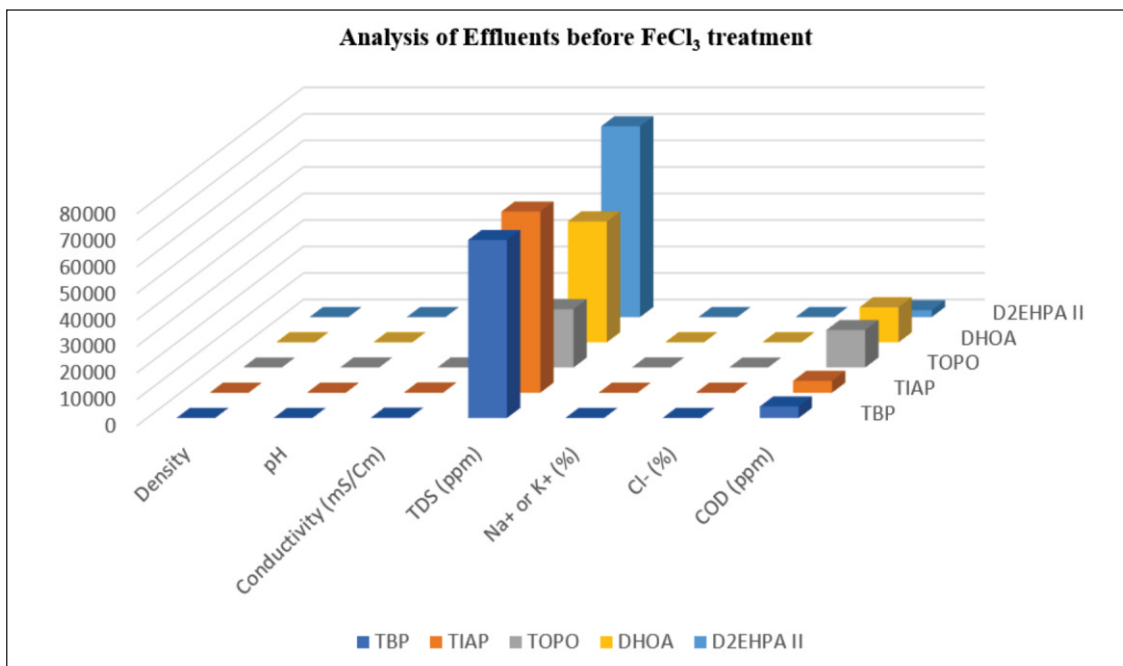


Fig.2: Physicochemical characteristics of an effluent before FeCl<sub>3</sub> treatment.

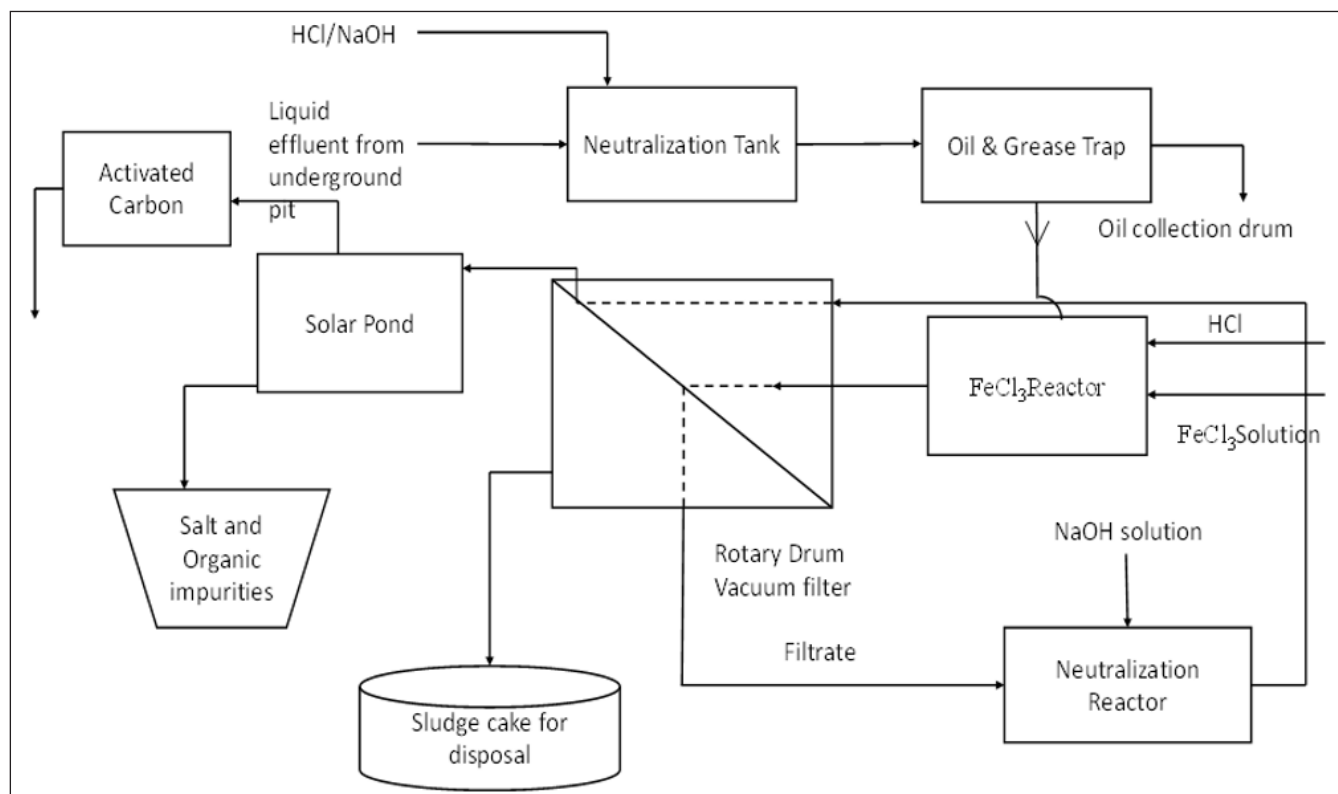


Fig.3: Schematic diagram of Ferrichloride (FeCl<sub>3</sub>) based Effluent Treatment Plant in SPP.

schematic of Ferrichloride (FeCl<sub>3</sub>) precipitation method used in the Effluent Treatment Plant (ETP) of Solvent Production Plant (SPP) is shown in the Fig. 2.

**Comparative analysis of an effluent before and after FeCl<sub>3</sub> treatment**

The SPP effluents before and after treatment comparative analysis gives a clear picture about the successful Ferric chloride (FeCl<sub>3</sub>) precipitation method in reduction pH and COD but there is a noticeable increase in other parameters especially TDS due to the reagents used in the FeCl<sub>3</sub> process of

Table 3: Approximate Sludge Generation (ferric oxides) from FeCl<sub>3</sub> chemical treatment method.

S. No	Effluent from the Solvent	Solid waste (sludge) generated in kg from the effluent treatment
1	TBP	560
2	TIAP	562
3	TOPO	327.6
4	DHOA	378
5	D2EHPA-II	372.96
6	TBP	560

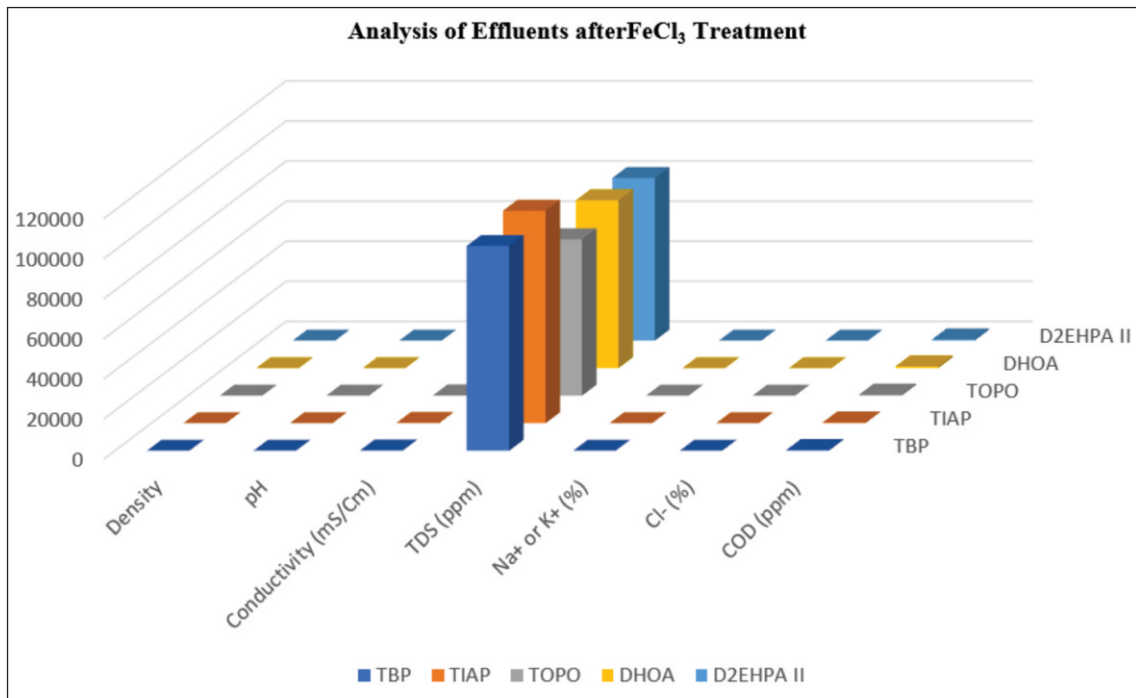


Fig.3: Physicochemical characteristics of an effluent before FeCl<sub>3</sub> treatment.

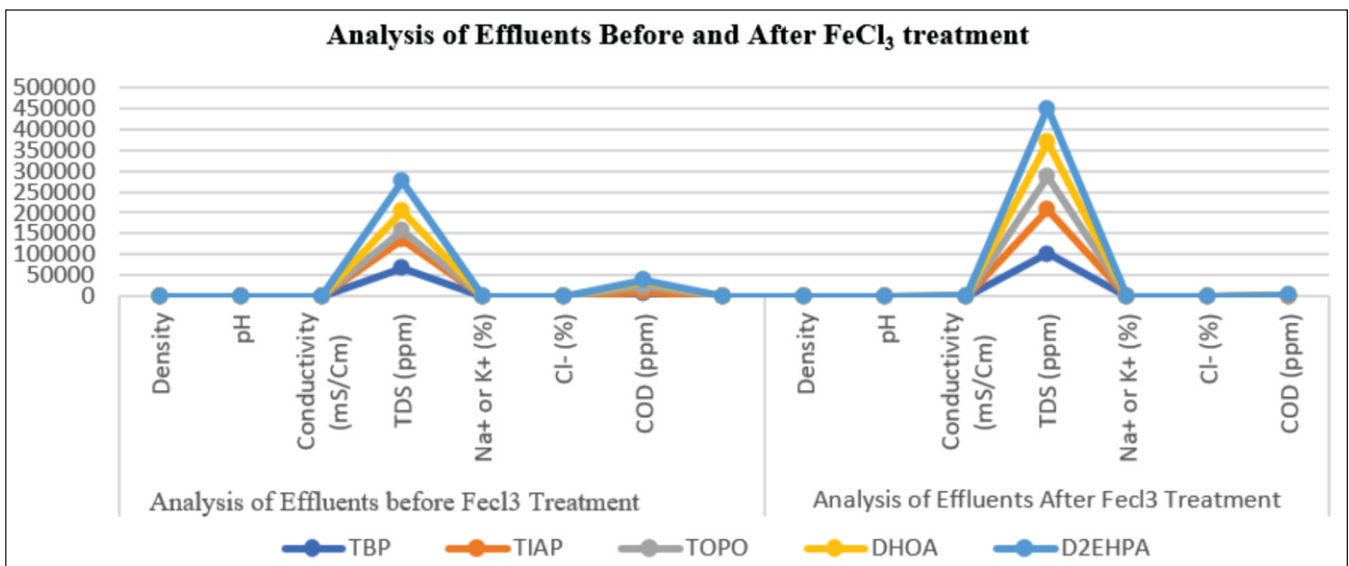


Fig.4: Comparison of SPPEffluents before and after FeCl<sub>3</sub> Treatment.

chemical treatment.

The remarkable changes in COD reduction level and pH neutrality (Fig.4) in the discharge of effluents after FeCl<sub>3</sub> treatment determines the chemical treatment method in SPP is somewhat successful in reducing the organics at the time of discharge but the parameters the Conductivity, TDS, Na<sup>+</sup>, K<sup>+</sup>, Cl<sup>-</sup> foresighted the possibilities of enormous amount of salts and sludge caused by the FeCl<sub>3</sub> precipitation method.

**Conclusion**

The studies of the proposed research gives a significant view of different types of solvent production processes associated with the effluent generation in SPP unit of HWP Tuticorin. From the physicochemical characteristics of SPP effluents before and after treatment indicated that the localized polluted water mainly composed of organic traces and hyper saline in nature. The acidic hydrolysis, alkali wash

from Na<sub>2</sub>CO<sub>3</sub> (Sodium Carbonate) and NaOH (Sodium Hydroxide) in solvent production processes leads to the generation of effluents and the current effluent treatment method of FeCl<sub>3</sub> (Ferric chloride) precipitation method was successful in reducing the main parameter of COD (Chemical Oxygen Demand) ranges of 320 – 900 ppm from higher level of 14000 ppm but not fulfilled the standard of meeting the statutory limits of Tamil Nadu Pollution Control Board (TNPCB) COD level of 250 ppm. It is widely believed and anticipated that the multiple treatments of FeCl<sub>3</sub> method requirement would suffice the soaring level of COD to the acceptable limit of State Pollution Control Board (SPCB – TNPCB) as well as Central Pollution Control Board (CPCB). Furthermore, the FeCl<sub>3</sub> precipitation chemical treatment induces coagulation of dissolved solids and flocculates it to settle down as sediment at the end of the treatment processes. The associated solid waste generated for the 7m<sup>3</sup> of effluent per day from the ETP of SPP unit ranges from 327 to 562 kg per batch of solvent production



process and the quantity may differ depends upon the requirement of solvent production in levels. The treated effluent discharged to the solar pond of surface area 2100 m<sup>2</sup> formed as solid waste left after evaporation of discharged wastewater; the solid waste is composed of hyper saline particles contaminated with traces of organic waste would be scrapped to either reuse in extraction of organic materials in chemical or cement industries in the nearby vicinity of Tuticorin. The Environmental indicators analyzed in this study would serve as a data base of future comparative analysis with other developed effluent treatment systems with a main aim of reducing the COD level to the TNPCB limit while eliminating the sludge or residual waste in post treatment of effluent.

### References

- [1] Gray N., Water Technology. 3<sup>rd</sup> edition. London: CRC Press; 2017.
- [2] APHA. Standard Methods for the Examination of water and waste water. 21<sup>st</sup> edu. Washington, DC. American Public health Association; 2005.
- [3] American society for Testing of Materials. 1969. Manual on water (3<sup>rd</sup> edu.) ASTM, Philadelphia, U.S.A.
- [4] Journal of Toxicology and Environmental Health (Hemisphere Publishing Corporation, 1025, Verment Avenue, N.W., Washington D.C., 20005, U.S.A.
- [5] Ihsan Hamawand, 'Energy Consumption in Water/Wastewater Treatment Industry - Optimisation Potentials', Energies Journal 2023 MDPI, Basel, Switzerland vol. 16: 24-33.
- [6] Sachchida Nand Singh, Gaurav Srivastav and Arun Bhatt, Physicochemical Determination of Pollutants in Wastewater in Dheradun, Journal: Current World Environment, vol. 7 (1),133-138 (2012).
- [7] Roohollah Noori, Ronny Berndtsson, Majid Hosseinzadeh, Jan Franklin Adamowski, 'A Critical Review on the Application of the National Sanitation Foundation Water Quality Index', Journal: Environmental Pollution, Elsevier Publication, Vol. 244, 575-587(2019).
- [8] Water Quality Analysis of PC and AL Laboratory of SPP, HWP Unit, 2023.
- [9] N. Kumara Swamy, Pratibha Singh and Indira P. Sarethy, 'Precipitation of Phenols from Paper Industry Wastewater using Ferric Chloride'. Journal of Chemistry: vol. 4, No.2(2011), 452-456.
- [10] Kavindra Kumari Kesari, Ramendra Soni, Pooja Tripathy, 'Wastewater Treatment and Reuse: A Review of its applications and health implications'. Water Air Soil pollution (2021) 232: 208.

# Tracing the Footprints of Contaminants In Water through Stable Isotope Techniques

## Isotope Technology for Societal Benefits

K. Tirumalesh

Isotope Radiation and Application Division, Bhabha Atomic Research Centre, Trombay-400085, INDIA

\*E-mail for Correspondence: tirumal@barc.gov.in

The contamination of freshwater resources is a significant challenge in achieving the Sustainable Development Goals (SDGs) proposed for the future well being of the world. The current state of water health worldwide is concerning. According to the World Health Organization (WHO), over 2 billion people reside in water-stressed countries, and nearly 1.7 billion people consume contaminated water. Climate change and anthropogenic factors have severely impacted both the quantity and quality of accessible water resources. To unravel the primary causes of pollution and find effective remediation techniques, a thorough and in-depth study is imperative. Among number of available techniques, Isotope techniques offer a significant advantage in identifying pollution origins, clarifying breakdown pathways, and evaluating the dynamics of both widespread and emerging pollutants such as microplastics, pesticides, fugitive gases, greenhouse emissions, and persistent organic compounds.

Environmental isotopes have been used as potential tools in geochemical & hydrogeological investigations, land-biosphere-atmosphere interfaces, nutrient cycling, degradation behavior of contaminants and identification of origin of contaminants. Environmental radioisotopes, on the other hand, provide a measure of groundwater residence time and its renewability. A bibliographic analysis of SCOPUS data from 2012 to 2018 indicates the potential of isotope applications in biodegradation, water treatment, water pollution, water quality and monitoring etc (Fig.1).

The isotope studies in the early stages were mainly concentrated on the water isotopes, i.e., stable water isotopes ( $^2\text{H}$  and  $^{18}\text{O}$ ). The outcome from these studies were helpful in examining the processes occurring at rock-water interface, recharge and transport mechanism, geochemical evolution and interconnection among water sources (Fig.2(left)). In later stages,  $^{13}\text{C}$  became an isotope of interest, especially for distinguishing natural and anthropogenic sources in various groundwater systems. This differentiation is based on the distinct isotopic signatures between biogenic (derived from living organisms) and thermogenic (from ancient, buried organic matter) hydrocarbon. It was subsequently realized that dual isotopic signatures provide better demarcation among contaminant sources with similar nature. Dual isotope systematic of  $\text{NO}_3^-$  ( $^{15}\text{N}$  and  $^{18}\text{O}$ ) can be used to identify the nitrogen source and understand the transformation process in surface and groundwater systems (Fig.2(right)). The  $\delta^{34}\text{S}$  signature was also used to identify the climate-driven redox change. It can also provide information on shift in bottom-water and/or sediment oxygenation from glacial oxic to interglacial anoxic/euxinic conditions that are primarily driven by climate-induced changes in biogenic productivity. Metal isotopes are also very helpful in representing different sources and processes in water systems. Noble gas isotopes serve as valuable tracers, revealing Earth's environmental history and providing insights into hydrological processes and climate changes. Aspects like groundwater migration, age dating, palaeoclimate assessment through measurement of the recharge temperatures, geochemical processes in the shallow waters can be studied using noble gases and their isotopic ratios.

As contamination of water varies between regions, tailored approaches become necessary for remediation, which must account for the diverse climate, geology, hydrogeology, geomorphology, and other factors. Creating big database of isotopes and integrating it with advanced techniques (geo-statistical, geo-informatics, remote sensing); and modeling tools (including machine learning) can lead to solving problems on a regional scale with predictive modeling capabilities. Finally, efforts should be made towards

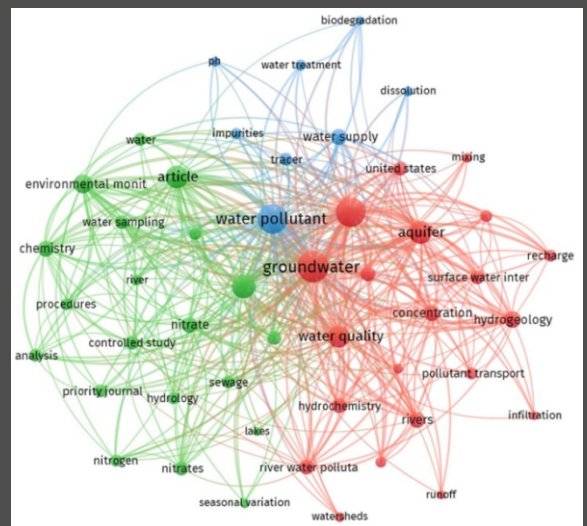


Fig.1: Network visualization of water contamination studies and their temporal association.

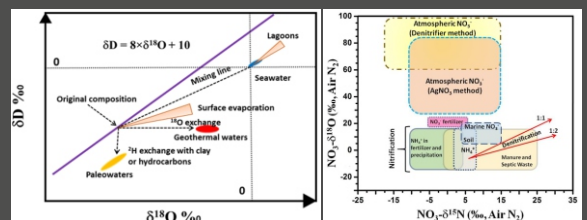


Fig.2: Isotope systematics of water isotopes indicating various end-members (left), Dual isotope plot of  $^{15}\text{N}$  and  $^{18}\text{O}$  isotopes demonstration various sources and processes (right).

interdisciplinary collaborations looping in water authorities, public health units, pollution control and sanitation departments for safeguarding the water resources against contamination threats, and pave the path for achieving the SDGs. The complete article can be found at Current Opinion in Environmental Science & Health, 2024, 40:100559.



Dr. Tirumalesh Keesari is a Scientific Officer-H & Head, Isotope Hydrology Section of Isotope and Radiation Application Division (BARC) and also Associate Professor in Chemical Sciences (HBNI).

His research interests include isotope hydrology, water contamination, geochemical modelling, groundwater recharge and application of AI/ML tools. He has over 100 international journal publications to his credit and also a recipient of National Geoscience Award, IANCAS Tarun Datta Memorial Award, DAE Science and Technology Award, DAE Group Achievement Award and Indo-US Science and Technology Award.



## Accelerating India's Defence Innovation Ecosystem to 2047

In a recent address to the Trombay Colloquium audience (on January 15, 2025) on the topic 'R&D in Defence Sector', the Secretary, DDR&D and Chairman, DRDO, Dr. Samir V. Kamat, articulated several key advancements and strategic initiatives undertaken by India in the defence sector and allied domains. Some of the key talk snapshots are presented here.

### Global Context and Technology Evolution...

India is emerging as an important pole in the transitioning multi-polar world. Technology obsolescence has accelerated dramatically, shortening from 15+ years to just 3 years. Warfare has expanded beyond traditional domains of land, air, and sea to include space, cyber, information, and psychological warfare. This shift presents unique challenges for India, which studies indicate is among the most targeted countries in the cyber domain.

### Current Status of Defence Self-Reliance...

India has achieved self-reliance in missile systems and platforms through DRDO's efforts. The country is largely self-sufficient in radar systems and has made significant progress in SONAR technologies. However, domestic semiconductor manufacturing remains limited to 180 nm chips, with advanced chips still sourced from overseas. Defence exports reached Rs. 20,000 crore last fiscal year, with a target of Rs. 50,000 crore set for the year 2028.

### Defence R&D Ecosystem...

India's defence innovation operates through a three-tier system: basic research by academia, applied R&D by DRDO, and production by industry partners. DRDO technologies have reached a Technology Readiness Level (TRL) of 8, indicating systems tested and validated in relevant environments. Better organizational synergies are needed to avoid duplication of efforts and maximize the impact of R&D resources.

### Civil-Military Fusion...

The civilian sector currently leads in AI and communication technologies adoption. DRDO is working to adapt these civilian innovations for military applications. Promoting defence exports is considered essential for building a viable domestic defence ecosystem. This civil-military fusion approach is identified as a key factor for India's future defence technological competitiveness.

### Skill Development Initiatives...

Educational initiatives include defence-focused academic courses such as M. Tech in Defence Technology and internship opportunities for students in DRDO laboratories. There's recognition that the education system needs revision to foster R&D aptitude from school level. These skill development efforts are crucial for creating the human capital necessary to drive innovation in India's defence sector.

### Future Defence Technology Priorities...

Priority areas include Underwater Domain Awareness, Space Situational Awareness, Cyber Defence, Quantum Communication,

**Dr. Samir V. Kamat**

Advanced Medium Combat Aircraft development, hypersonic missiles, indigenous aero engines, advanced sensors, and Electromagnetic Aircraft Launch Systems. Critical enabling technologies include AI/ML, stealth technology, semiconductor materials, and advanced manufacturing. R&D spending currently stands at less than 5% of the defence budget, significantly below the 10-20% spent by China and the US. Increasing this investment is essential for achieving complete self-reliance in the defence sector by 2047.





NSD 2025 Inaugural Day (From left to right): Dr. R.N. Singh, Chairman, NSD-2025 in BARC, Dr. Raghvendra Tewari, Director, Materials Group, Shri Vivek Bhasin, Director, BARC, Shri S.A. Bhardwaj, Former Chairman of AERB and Program Chief Guest, Dr. Ajit Kumar Mohanty, Chairman AEC & Secretary, DAE and Dr. Sanjib Majumdar, Convener of NSD-2025 in BARC unveil the Souvenir on the theme Transition to Clean, Green Viksit Bharat: Advanced Materials & Nuclear Technology.

## Catalyzing Curiosity: BARC's National Science Day and the Path to Viksit Bharat

The Bhabha Atomic Research Centre (BARC) hosted a three-day National Science Day celebration from February 28 to March 2, 2025, with the theme "Transition to Clean, Green Viksit Bharat: Advanced Materials & Nuclear Technology." The event drew approximately 300 students and their teachers each day from schools across Mumbai and Maharashtra, offering them a unique opportunity to explore India's nuclear science landscape and understand the role of advanced materials and nuclear energy in building a developed India (Viksit Bharat).

### Inaugural Session

The opening day set the tone for the celebration with distinguished speakers highlighting the importance of nuclear science and technology in India's sustainable development journey.

Shri S. A. Bhardwaj, Chief Guest and Former Chairman, AERB, emphasized the 'Reduce, Recycle, and Reuse' philosophy central to India's nuclear energy ecosystem. Dr. Ajit Kumar Mohanty, Chairman, AEC & Secretary, DAE, discussed the exploration of light's fundamental properties to uncover both past and future scientific phenomena. In his speech, Shri Vivek Bhasin, Director, BARC, while honoring the legacies of Prof. C.V. Raman and Dr. Homi J. Bhabha, highlighted materials development crucial for advancing India's nuclear program. Dr. Raghvendra Tewari, Director, Materials Group, focused on innovative applications of the Raman Effect in healthcare.

### Student Activities

Students participated in science exhibitions and enjoyed guided tours of BARC's prominent facilities, giving them firsthand exposure to cutting-edge research and technologies in nuclear science.

### Exploring Materials Science

The second day focused on deepening students' understanding of materials science and its applications. Dr. Gautam Kumar Dey, Former Director, Materials Group, delivered a talk on "The World of Materials" followed by an engaging Q&A session with students.

### Interactive Innovation

A new format was introduced where students submitted queries on general science and nuclear energy topics. Select questions were addressed by BARC's young and experienced scientists and researchers, creating a more interactive and responsive learning environment.

### Concluding Session

The final day continued the educational momentum with more expert presentations. Dr. R. Tewari, Director, Materials Group, presented "The Story of Mean and Materials," further exploring the crucial role of materials science in nuclear technology. The question-and-answer format initiated on Day 2 continued, allowing more student queries to be addressed by BARC scientists.

### Facility Tours and Exhibitions

Throughout the three days, students had the opportunity to visit several state-of-the-art research facilities at BARC: Dhruva Research Reactor, Nuclear Waste Management Facility, Robotics & Remote Handling Facility and Nuclear Agriculture, Food and Biotechnology Facilities.

### Educational Activities

The program featured multiple interactive elements designed to engage students: Souvenir with tailor-made information on

historical journey and the growth of research and development activities in materials, Scientific quizzes, Exhibitions on materials science highlighting its role in India's nuclear energy expansion, Audio-visual screenings about eminent Indian scientists and pioneers in nuclear materials science, Demonstrations of advanced nuclear materials manufacturing technologies, Working models showcasing latest innovations in the field.

### Program Leadership

The National Science Day 2025 celebration was spearheaded by the Materials Group of BARC, under the distinguished leadership of Dr. R.N. Singh, Outstanding Scientist, who served as Chairman of the NSD-2025 Program, and Dr. Sanjib Majumdar, Scientific Officer/H, who acted as the Program Convenor. The event's success was further enhanced through valuable collaborative efforts from the Nuclear Fuels Group and the Scientific Information Resource Division of KMG, whose contributions were instrumental in orchestrating this comprehensive educational program.

### Significance of the Event

The celebration served multiple important purposes, which include

- Honoring Sir C.V. Raman's discovery of the Raman Effect, which earned him the Nobel Prize in Physics in 1930
- Highlighting the significance of nuclear energy in India's transformation towards becoming self-reliant (Aatmanirbhar Bharat)
- Demonstrating how nuclear energy contributes to a clean, green, and sustainable future
- Emphasizing the role of advanced materials in successfully harnessing nuclear energy
- Inspiring the next generation of scientists and innovators who will drive India's scientific progress
- Fostering critical thinking and creativity among young minds

This immersive three-day program successfully combined theoretical knowledge with practical experiences, giving students a comprehensive understanding of nuclear science and advanced materials while inspiring them to pursue scientific inquiry and innovation.



## Awards & Honors

# BARC Scientist Honored



Dr. Anup Kumar Bera

**D**r. Anup Kumar Bera, Scientific Officer/F in the Magnetism Section of the Solid State Physics Division, has been honored with the Asia-Oceania Neutron Scattering Association (AONSA) Science Award 2025 for his exceptional contributions to neutron science. His groundbreaking experimental observations include the realization of "Bethe Strings" and the discovery of novel quasi-particle excitations such as "doublons" and "quartons," alongside his dedication to solving complex scientific challenges.

Dr. Bera joined BARC as a Scientific Officer in 2015 after earning his Ph.D. in Physics from the University of Mumbai in December 2011. He then conducted postdoctoral research at Helmholtz-Zentrum Berlin für Materialien und Energie, Germany, from December 2011 to June 2015.

His research interests encompass strongly entangled quantum spin systems, quantum phenomena in low-dimensional magnetic materials, quantum phase transitions, quantum spin-liquids, and energy materials for future technologies. Dr. Bera has authored over 90 research papers in leading international journals such as Nature, Nature Physics, and Nature Communications, along with 20 conference papers and two book chapters.

Among his notable achievements are the Young Scientist Award (2018) from the DAE, Government of India, and the Young Achiever Award by the DAE-Solid State Physics Symposium. He has been elected as a Young Associate of the Maharashtra Academy of Sciences and has delivered several invited lectures, including the Infosys Condensed Matter Seminar at TIFR, Mumbai. Additionally, he has received multiple best presentation awards at prestigious conferences.



# RPNST 2025

## Conference on Recent Progress in Nuclear Science & Technology & Commemorating the Birth Centenary of Dr. Raja Ramanna

The Recent Progress in Nuclear Science & Technology conference (RPNST2025) took place on January 27-28, 2025, at the DAE Convention Centre in Anushakti Nagar, Mumbai. This significant event celebrated the birth centenary of Dr. Raja Ramanna (1925-2004), former Chairman of the Atomic Energy Commission (AEC) and Secretary of the Department of Atomic Energy (DAE). It was organized by the Physics Group of the Bhabha Atomic Research Centre (BARC).

The conference commenced with an inaugural session featuring distinguished speakers such as Dr. V.S. Ramamurthy, Dr. S.S. Kapoor, and Dr. Ajit Kumar Mohanty, Chairman of the AEC and Secretary of the DAE. The session outlined the objectives of honoring Dr. Ramanna's legacy while discussing advancements in nuclear science and technology.

Day one included three technical sessions focused on Fission Physics and Technology, Fusion Physics and Technology, and Energy Security and Economic Growth. Dr. V.S. Ramamurthy presented on "Ramanna and his Legacies," while Dr. Mohanty discussed India's three-stage nuclear program aimed at self-reliance. Dr. R.K. Choudhury, former Director of IOP, shared insights on neutron-induced fission studies and research on superheavy nuclei.

Dr. Shashank Chaturvedi, former Director of the Institute of Plasma Research, discussed global approaches to nuclear fusion. Former AEC Chairman and DAE Secretary Dr. Anil Kakodkar addressed nuclear energy's role in economic security, and Shri V. Rajesh of NPCIL presented the current scenario of nuclear power generation in India.

The day concluded with special sessions, including "Physics of Music" led by Prof. Milind N. Kunchur from the University of South Carolina, followed by a cultural evening.

Day two began with a session on Physics with Mega Science Facilities, where Dr. S.M. Yusuf, Outstanding Scientist and Director of BARC's Physics Group, discussed multi-dimensional R&D activities within BARC's Physics Group. Professor V.C. Sahni covered the Indian accelerator landscape, while Dr. Jayaram N. Chengalur from TIFR explored radio wavelength studies of the universe.

The afternoon featured a session on Nuclear Technology for Societal Benefit, with Dr. Sudeep Gupta discussing DAE technologies' contributions to nationwide cancer care and Smt. Meera Venkatesh addressing radiation applications for improving quality of life.

A Basic Research & Developments session followed, where Dr. B.A. Dasannacharya reflected on "Ramanna: The Man



Dr. Homi J. Bhabha and Dr. Raja Ramanna interacting with the foreign scientific delegation at the Apsara Reactor during their visit to AEET (now BARC). Photo Courtesy: DAE.

and His Legacy." Presentations included neutrino physics research by Dr. Vishwajeet Jha from NPD, Physics Group, and a discussion on the proton accelerator program by Dr. Sista V.L.S. Rao from IADD, MRG.

The conference concluded with a panel discussion on "Future Challenges in Fission and Fusion Technologies," featuring notable figures such as Dr. V.S. Ramamurthy, Shri K.N. Vyas, Dr. R.B. Grover, and Dr. Shashank Chaturvedi. Shri K.N. Vyas delivered concluding remarks before Dr. S.M. Yusuf offered a vote of thanks.

RPNST2025 successfully brought together leading national and international experts to discuss advancements in nuclear science and technology while honoring Dr. Raja Ramanna's contributions to India's nuclear program. The conference underscored India's progress in fission and fusion technologies as well as societal applications of nuclear science, reinforcing the nation's commitment to sustainable energy development and scientific advancement.



# Inspiring Young Minds

## Outreach Programs by BARC in Madhya Pradesh

**B**eamline Development & Application Section (BDAS), Physics Group, BARC camped at RRCAT, Indore organized a series of outreach programs across three locations in Madhya Pradesh during January and February 2025. These initiatives aimed to educate and inspire students about nuclear science, radiation safety, and career opportunities within the Department of Atomic Energy (DAE).

The outreach initiatives were conducted at the following locations: a. PM Shri Shaskiy Kanya Uchhtar Madhyamik Vidyalay at Barela in Jabalpur during January 21–22, b. Shri Sitaram Jaju Govt Girls College, at Neemuch during February 18–19, c. Jawaharlal Nehru Smriti Govt. P.G. College at Shujalpur during February 24–25. The target audience included school students from grades 6 to 12, as well as undergraduate and postgraduate students and their teachers.

### Topics Covered

The sessions were designed to cater to diverse educational levels and included the following topics.

**Basics of Synchrotron Radiation** - An introduction to the nature of synchrotron radiation and its production.

**Applications of Synchrotron Radiation** - Real-world applications such as X-ray imaging of mosquitoes, analyzing gold jewelry composition, and experiments at the Indus synchrotron facility at RRCAT in Indore.

**Basics of Nuclear Reactors** - An overview of nuclear fission, reactor components like turbines and generators, and their role in electricity production.

**Radiation Safety** - Insights into radiation types, safety measures for public and workers, and monitoring protocols near nuclear facilities.

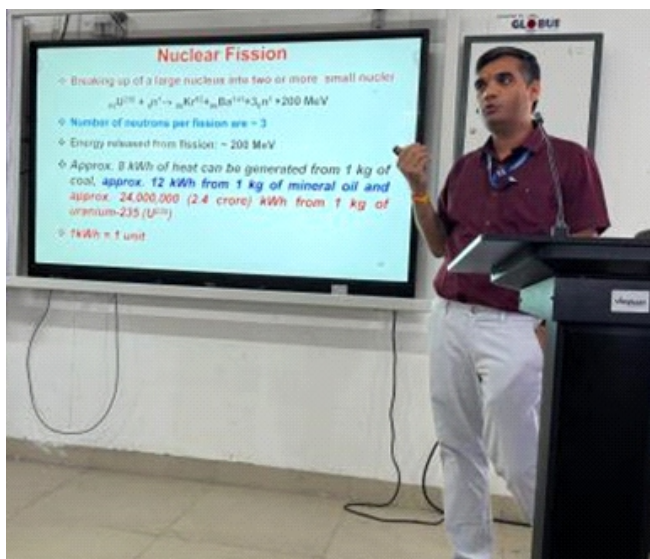
**Career Opportunities in DAE** - Guidance on eligibility criteria, qualifications required, and application processes for careers in DAE.

### Engagement Approach

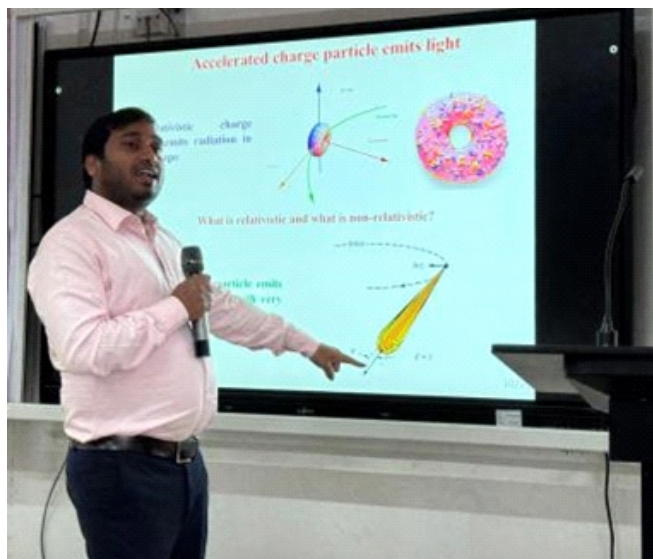
The programs were tailored to suit the audience's educational background. For school students (grades 6–12), sessions were simplified and delivered primarily in Hindi to ensure better understanding. For college students, a mix of Hindi and English was used with more advanced technical content. Interactive engagement methods were employed to engage students effectively. Simple questions were posed during lectures to encourage participation. Students were motivated to focus on their studies and consider careers in nuclear science.

### Speakers at the Programs

Four young officers from the ranks of Beamline Development & Application Section (BDAS), Physics Group, BARC camped at Indore led these sessions. Their relatable approach helped bridge the gap between complex scientific concepts and student comprehension.



Dr. Yogesh Kumar interacting with the students at Jawaharlal Nehru Smriti Govt. P.G. College.



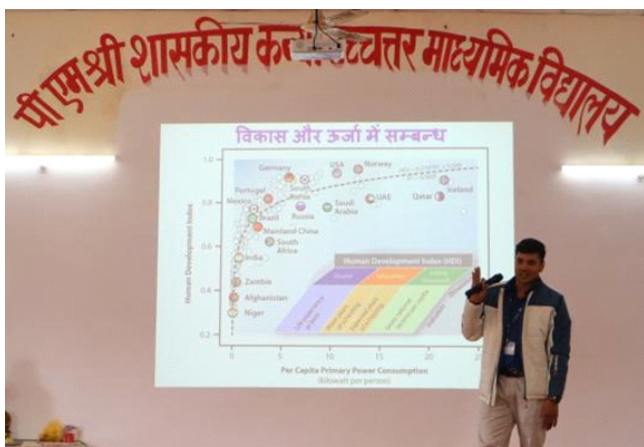
Shri Kiran Kumar Gorai speaks during an interactive session with the students of Jawaharlal Nehru Smriti Govt. P.G. College.

Reports from conferences, theme meetings, symposia, and outreach

Program Impact

These outreach programs served as a platform for fostering scientific curiosity among students from rural and urban areas alike. By addressing misconceptions about radiation safety and highlighting diverse career opportunities in nuclear

science, the initiative aimed to inspire the next generation of scientists and engineers. The Bhabha Atomic Research Centre and the Department of Atomic Energy continue to play a pivotal role in advancing nuclear science while simultaneously promoting public awareness through such outreach efforts.



Dr. Mangla Nand interacting with the students of PM Shri Shaskiy Kanya Uchhtar Madhyamik Vidyalay.



Dr. Shilpa Tripathi speaks during an interactive session with the students of Shri Sitaram Jaju Govt Girls College.



# Industry

## BARC's Nuclear

By Technology Transfer & Collaboration Division and SIRD Newsletter Editorial Team

BARC regularly transfers spinoff technologies from nuclear energy research to industry for commercialization. They provide comprehensive support to licensees through technology training, field demonstrations, consultancy, and detailed documentation (including procedures, flowcharts, diagrams, troubleshooting guides, and lists of raw materials, equipment, and suppliers). Between January and February 2025, Technology Transfer & Collaboration Development (TT&CD) continued its efforts to commercialize BARC technologies. A technology transfer ceremony was organized on February 7, 2025, at the HRDD complex in Anushakti Nagar, BARC. A brief summary of the proceedings of the ceremony is presented here.

### Technology Transfers

**A** technology transfer agreement was signed with M/s Relegare Agro Life Bioscience Pvt. Ltd., Sangamner, Maharashtra for the know-how transfer of a process for developing zinc fertilizer formulation from biosludge. Unlike chemically synthesized zinc fertilizers that have limitations in availability and are effective only at certain levels, zinc fertilizer derived from biosludge offers slow-release properties and increases crop yield at half the recommended dose. The process converts post-biomethanation distillery sludge, a waste material for distilleries, into high-efficiency zinc fertilizer for soil application. This improved fertilizer enhances zinc availability to plants while improving crop yield and soil conditions.

Another agreement was signed with M/s Kavitul Life Science Pvt. Ltd., Vadodara for the know-how transfer of shelf-stable oil-free potato chips in different flavors. With potato chips being a

fast-moving snack item globally with high growth potential, and increasing health consciousness among consumers, there is growing interest in tasty potato chips that don't use oil in preparation. The developed process creates oil-free potato chips/wafers in six different flavors with reduced sugar and starch content. This unique process utilizes induction heating, microwave, and hot air oven baking techniques, followed by appropriate packaging.

#### Agreements for the know-how transfer

- A rapid composting technology for decomposition of dry leaves, kitchen waste, and temple waste (transferred to M/s Kavitul Life Science Pvt. Ltd., Vadodara)
- Gluten-free multigrain premix (transferred to M/s Kavitul Life Science Pvt. Ltd., Vadodara)
- Composite metal membrane reactor for production/separation/recovery of high-purity hydrogen (transferred to M/s Dipesh Engineering Works, Mumbai)

#### Atal Incubation Centre - BARC

AIC BARC ANUSHAKTI FOUNDATION has been established to connect India's robust start-up ecosystem to the nuclear sector by setting up Technology Development cum Incubation Centers.

AIC-BARC signed a collaborative incubation agreement with M/s Ambetronics Engineers Pvt. Ltd., Mumbai for fabricating sensor electrodes for frying oil quality testing and dew point measurement applications. In alignment with the Government of India's Aatmanirbhar Bharat mission, Ambetronics Pvt. Ltd. aims to develop indigenous sensors with assistance from BARC's Chemistry division.



Officials of Food Technology Division and TT&CD in BARC exchanged the technology transfer agreement with Kavitul Life Science Pvt. Ltd. of Vadodara during the tech transfer ceremony organized on February 7, 2025.



# beckons



## Spin-off Technologies



BARC and PAN Science India signed an institutional collaboration agreement aimed at building and scaling up cutting-edge deep-tech and AI startups by leveraging industry expertise.

AIC-BARC extended its collaborative incubation agreement with Dipesh Engineering Works Pvt. Ltd., Mumbai for the Iodine Sulphur Thermochemical Process Plant for Hydrogen Production by Splitting Water. The original agreement was signed last year under the mentorship of the Chemical Technology Division. Following successful design and detailed engineering work, the one-year extension agreement was finalized.

AIC-BARC also signed institutional collaboration agreements with Hotel and Resort Association of Western India, M/s PanScience Innovations (PSI), and Foundation for Innovation and Social Entrepreneurship (FISE). As part of Atal Incubation Mission's community engagement program, AIC-BARC approached the Hotel and Resort Association of Western India (HRAWI) to implement BARC's solid wet and dry waste management technologies at their members' premises, with no financial implications for AIC-BARC.

The agreement with PanScience Innovations aims to build and scale cutting-edge deep-tech and AI startups with passionate entrepreneurs by leveraging deep industry expertise. Through hands-on operator support, strategic mentorship, and robust industry partnerships, PSI, working alongside BARC experts, will transform groundbreaking ideas into scalable, market-leading companies that solve real-world problems. PSI and BARC will host final pitching sessions with industry leaders, experts, and a BARC jury to evaluate startups.

Foundation for Innovation and Social Entrepreneurship (FISE), also known as Social Alpha, is a technology business incubator approved by the Department of Science and Technology, Government of India. This agreement aims to promote

technology-based innovation, incubation, and entrepreneurship development including research, training, consulting, and support for entrepreneurs, social enterprises, and startups with social impact. It will establish a center of excellence in social business, entrepreneurship, sustainability, and philanthropy with charitable objectives.

### AKRUTI Program

AKRUTI Kendra – Tarapur participated in an entrepreneurship development awareness program to showcase DAE-BARC technologies in Boisar on January 12, 2025. A kite festival was organized to increase attendance, attracting approximately 2,000 visitors who responded positively to products manufactured by KRUTIK Kendra (Vengani, Karajgaon) members.

AKRUTI Kendra – Tarapur, in collaboration with Pasthan Kala Krida and Sanskritik Mandal, Boisar, jointly organized an awareness camp and Pasthan Mela in Boisar. The event featured products manufactured using BARC technologies, generating interest among rural entrepreneurs in obtaining licenses for BARC technologies. A training workshop on dried food packaging and marketing was conducted at Gnyanjyoti Community College, Karajgaon, and in Vengani villages near Boisar. During this period, two bio-compost units were installed at TAPS Colony.

AKRUTI KENDRA – BMI (Brahmdevdada Mane Institute of Technology) Solapur participated in Krushi Pradarshan organized by Shri Siddheswar Devastan Trust, Solapur, presenting BARC technologies to approximately 100,000 attendees. As a result, 80 farmers and entrepreneurs expressed interest in acquiring BARC technology licenses.



A workshop on 'Foldable Solar Dryer' and 'Bio-Composting' technologies was conducted on February 10, 2025, at Gnyanjyoti Community College, Karajgaon.





Edited & Published by

Scientific Information Resource Division

Bhabha Atomic Research Centre, Trombay, Mumbai-400 085, India

BARC Newsletter is also available at URL:<https://www.barc.gov.in>